UNIVERSIDADE D
COIMBRA

António Pedro Ferreira Sampaio

Optimization of a device for deep-brain transcranial magnetic stimulation via simulations

Thesis submitted to the Physics Department of the Faculty of Sciences and Technology of the University of Coimbra for the degree of Master in Engineering Physics with specialization in Instrumentation, supervised by Prof. Dr. Paulo Alexandre Vieira Crespo.

February 2023

UNIVERSIDADE D
COIMBRA

António Pedro Ferreira Sampaio

Optimization of a device for deep-brain transcranial magnetic stimulation via simulations

Thesis submitted to the
University of Coimbra for the degree of
Master in Engineering Physics

Supervisors:
Prof. Paulo Alexandre Vieira Crespo

Fevereiro, 2023

This work was developed in collaboration with:

Laboratório de Instrumentação e Física Experimental de Partículas

Acknowledgments

Chegada a reta final do meu percurso académico, o momento é também apropriado para agradecer aqueles que fizeram parte desta caminhada, pois se há lição que a vida nos dá, é que não somos nada sem "os outros".

Começo por agradecer ao meu orientador, Professor Paulo Crespo, pela paciência, partilha de conhecimento, positividade, disponibilidade, e oportunidade que me deu em fazer parte deste projeto. A si, o meu muito obrigado! :)

Aos demais não tão próximos, mas que também fizeram parte daquilo que foi a minha vida neste período académico, acho que também lhes é devido um agradecimento. A vós, o meu obrigado por toda a partilha de conhecimentos, arte, cultura, ciência, etc. Que, de uma forma mais positiva ou negativa, tiveram impacto na pessoa que sou hoje, pelos interesses e novas portas que me foram despertando e abrindo. A Universidade de Coimbra, por motivos geográficos, demográficos, e de tradição, proporciona, sem dúvida, da minha perspetiva, uma experiência única de vida, onde temos a oportunidade de conhecer diversas personalidades das mais diversas origens e áreas de formação, que, muitas vezes, inconscientemente, e apenas através de partilhas singulares que duram horas ou minutos, acabam por indiretamente moldar parte do que seremos no futuro.

Mas mais importantes que os não tão próximos, são os mais próximos. Aqueles que já vinham de outras fases de formação e da "vida em geral", e aqueles que entraram na minha vida neste percurso universitário. Na memória ficam (sem dúvida) as noites académicas, os jantares, as viagens, as boleias, as idas ao Kurger Bing, a produção de músicas populares portuguesas, as muitas horas de trabalho, os *memes*, e muito mais... Com *vosotros* também aprendi muito, descobri novos interesses e outros mundos. Nos fracassos, nas vitórias, nas festas, nas ansiedades, nos momentos mais *hyggelig*, o meu muito obrigado pela vossa humanidade, maturidade, boa disposição, aleatoriedade, e, acima de tudo, partilha. A vida nem sempre é uma festa, mas eu

sei que sempre que pudermos vamos contribuir para que assim seja, porque como diria esse ilustre *alumnus* da Universidade de Coimbra: "O que faz falta é animar a malta..."

Ao meu board do NEXT Coimbra, um agradecimento especial, por toda a partilha de cultura e informação que esta organização tem vindo a fazer. Sem dúvida que temos algo singular e com impacto no mundo que nos rodeia. A nossa história mostra-nos que, *meme-a-meme*, e interjeição-a-interjeição, podemos mudar o mundo, seja qual for o nosso ponto geográfico.

Finalmente, umas palavras à minha família, pois eles são a base daquilo que sou. Com o nosso amadurecimento, apercebemo-nos da sorte, ou não, que tivemos à nascença. Porque a vida é sem dúvida uma roleta russa a partir do momento em que somos concebidos. Já nesta fase adulta, apercebi-me da sorte que tive no berço. Das pessoas humanas, empáticas, e bondosas que me deram e continuam a dar as bases para ser um ser livre e afortunado em muitos aspetos da vida. A vocês, o meu muito obrigado, também, pela vossa compreensão, paciência e, fundamentalmente, apoio, independemente da fase mais ou menos boa que possa ter vindo a passar neste percurso. Sei que sempre me tentaram e tentarão dar tudo o que necessite para ser feliz, e isso não tem preço.

"... the cosmos is also within us, we're made of star-stuff. We are a way for the cosmos to know itself."

CARL SAGAN

Resumo

Estimulação magnética transcraniana é o termo utilizado para descrever uma técnica não invasiva terapêutica e de diagnóstico, que tem por base a aplicação de campos magnéticos variáveis. Os campos magnéticos variáveis são adequadamente produzidos por um conjunto de espiras, com o propósito de induzir de forma não invasiva correntes no cérebro. A técnica foi introduzida há quase quatro décadas, sendo que desde então tem sido alvo de vários desenvolvimentos relevantes, com o propósito de proporcionar opções terapêuticas alternativas. Um dos principais desenvolvimentos foi a estimulação de zonas de cérebro profundo, consequentemente denominada Estimulação magnética transcraniana profunda. Vários pacientes com diversas doenças neuropsiquiátricas (e.g., depressão, transtorno obsessivo-compulsivo, tabagismo, entre outras) já beneficiam da aplicação desta técnica. Contudo, existe ainda incapacidade de estimular zonas de cérebro profundo com intensidades apropriadas para o entendimento dos benefícios ou falta dos mesmos em estimular diretamente estas zonas.

Neste projeto propusemo-nos a começar a implementação experimental de um sistema de estimulação magnética transcraniana profunda de 5 espiras, denominado Configuração Ortogonal, inicialmente proposto para ultrapassar as limitações das espiras representativas do estado da arte. Vários componentes importantes do sistema foram adquiridos e desenvolvidos (e.g., bomba de água, sensores de corrente), e uma solução com base em silicone e grande potencial de preencher os requisitos elétricos necessários para um modelo de crânio esférico, com base no modelo previamente simulado, foi encontrada. Simulações, com recurso ao software COMSOL Multiphysics® AC/DC, em que se considerou os fios elétricos da configuração ortogonal encapsulados num material isolador com 5 mm de raio proporcionaram resultados de estimulação em profundidade sem precedentes, atingindo-se uma estimulação no centro do cérebro de 71% do máximo de superfície. Esta abordagem aproximou o sistema simulado das futuras condições experimentais.

Finalmente, foi estudada a hipótese de melhorar a praticabilidade da con-

figuração ortogonal através duma redução das dimensões do contentor. Dois estudos foram conduzidos. O primeiro, no qual todas as dimensões do contentor variaram a mesma quantidade demonstrou resultados insignificantes para o que era pretendido. No segundo, em que apenas a largura do contentor variou, observou-se uma manutenção dos resultados de indução de densidade de corrente no centro do cérebro, relativamente ao máximo de superfície, de contentor para contentor, e mesmo comparativamente com os resultados do contentor original ($\approx 71\%$), variando apenas a intensidade das densidades de corrente induzidas. Ambos os estudos foram realizados através de simulações com recurso ao software COMSOL Multiphysics® AC/DC. Uma redução de 390 litros de água foi obtida entre o contentor mais pequeno do estudo e o contentor original, consequentemente implicando, também, uma redução de NaCl.

Palavras-chave: Estimulação magnética transcraniana (TMS), Estimulação magnética transcraniana profunda (dTMS), TMS cerebral total, COMSOL Multiphysics AC/DC.

Abstract

Transcranial magnetic stimulation (TMS) refers to a noninvasive therapeutic and diagnostic technique based on the application of transient magnetic fields. The transient magnetic fields are properly delivered by a set of coils, and have the purpose of noninvasively induce brain currents. The technique was first introduced almost four decades ago, and ever since has been under important developments with the main purpose of offering alternative therapeutic options. One of the main developments has been the stimulation of deep brain areas, termed deep Transcranial Magnetic Stimulation (dTMS). Many patients with several neuropsychiatric disorders (e.g. major depressive disorder (MDD), obsessive-compulsive disorder (OCD), smoking addiction, among others) already benefit from this technique. However, there is still a lack of capacity of stimulating deep brain structures with appropriate intensity to understand the benefits, or lack of them, in directly stimulating these regions.

In this project, we propose to start the experimental implementation of a new dTMS 5-coils system, named Orthogonal Configuration, initially proposed to overcome the limitations of deep stimulation other state of the art coils suffer. Many important components of the system were acquired and developed (e.g., water pump, current sensors), and a silicon-based solution, highly potential to fill the electrical requirements needed for a spherical skull-model based on previous simulations, was found. Simulations, via the COMSOL Multiphysics® AC/DC software, where we considered the orthogonal configuration electrical wires encapsulated in a 5-mm radius insulating material provided unprecedented stimulation-with-depth results of 71% the surface maximum at the brain center. This approach brought the simulation system closer to the real conditions.

Finally, we studied the hypothesis of improving the physical layout of the orthogonal configuration by means of reducing the container's dimensions. Two studies were conducted. The first, where all the dimensions of the container varied by the same amount showed no significant results. In the second, where only the width

of the container varied, the current density induction at the center of the brain, relative to the surface maximum, was approximately constant, and equal to that of the original container ($\approx 71\%$), independently of the width of the container, varying only the intensity of the induced current densities. Both studies were conducted with resort to COMSOL Multiphysics® AC/DC software. Between the original container, and the smallest of the second study, there is a 390 litres reduction of water, also implying a reduction in the NaCl amount to be used in the composition of a conductive liquid solution.

Keywords: Transcranial Magnetic Stimulation (TMS), deep-brain Transcranial Magnetic Stimulation (dTMS), whole-brain TMS, COMSOL Multiphysics AC/DC.

List of Abbreviations

AC Alternating Current

ACC Anterior Cingulate Cortex

AD Alzheimer's Disease

AEs Adverse Events

AP Action Potential

AUD Alcohol Use Disorder

BDNF Brain-Derived Neurotrophic Factor

B-field Magnetic field

CE Conformité Européene

CNS Central Nervous System

CS Conditioning Stimulus

CSF Cerebrospinal Fluid

cSP cortical Silent Period

CT Cognitive Training

cTBS continuous Theta Burst Stimulation

CUD Cocaine Use Disorder

DAT Dopamine Transporter

DC Direct Current

DLPFC Dorsolateral Prefrontal Cortex

dpTMS double-pulse Transcranial Magnetic Stimulation

dTMS deep-Transcranial Magnetic Stimulation

EEG Electroencephalogram

E-field Electric field

FDA Food and Drug Administration

fMRI functional Magnetic Resonance Imaging

H-coil Hesed-coil

HCA Halo Circular Assembly

HF High-frequency

HFA Halo figure-8

ICNIRP International Commission on Non-Ionizing Radiation Protection

IPG Implanted Pulse Generator

ISI Interstimulus Interval

iTBS intermittent Theta Burst Stimulation

LIP Laboratório de Instrumentação e Física Experimental de Partículas

LTD Long-Term Depression

LTP Long-Term Potentiation

MDD Major Depressive Disorder

MEG Magnetoencephalogram

MEP Motor Evoked Potential

mPFC medial Prefrontal Cortex

MR Magnetic Resonance

MS Multiple Sclerosis

MT Motor Threshold

OC Orthogonal Configuration

OCD Obsessive-Compulsive Disorder

PET Positron Emission Tomography

PFC Prefrontal Cortex

PNS Peripheral Nervous System

RI Relative current density Induction

RMT Resting Motor Threshold

rTMS repetitive Transcranial Magnetic Stimulation

SPL Sound Pressure Level

sTMS single-pulse Transcranial Magnetic Stimulation

SUDs Substance Use Disorders

TBS Theta Burst Stimulation

TES Transcranial Electric Stimulation

TI Temporal Interference

TMS Transcranial Magnetic Stimulation

TS Test Stimulus

VAS Visual Analog Scale

VNS Vagus Nerve Stimulation

VTA Ventral Tegmental Area

List of Figures

List of Tables

Contents

1

Introduction

1.1 Project objectives

This project's objectives had to suffer some mutations along the developed work. At the beginning, there were two main goals. One of the goals was to finish the development of an experimental setup of a new deep-Transcranial Magnetic Stimulation (dTMS) system, the orthogonal configuration, previously conceptualized and, respectively, studied via simulation in collaborative works. The other goal consisted on experimentally test the conclusion of previous collaborative work regarding the importance of the skull as a head-layer crucial for the unprecedented power-with-depth demonstrated with this new dTMS system.

Towards the practical implementation of this new system some work was successfully started. Still, the pandemic situation, which introduced some alterations to what once was the normality, had us changing our plans. Thus, we focused our work on understanding, via simulation, if it was sustainable to introduce some dimensional changes that would make the system more practical for a future clinical/academic application. We have also focused on finding appropriate materials for future experimental tests and turning the simulations' features closer to what will be the experimental setup.

1.2 Motivation and Foundations

Transcranial Magnetic Stimulation (TMS) is a noninvasive stimulating procedure proposed by Barker et al. (1985) about 37 years ago. The noninvasive nature of such a technique relies on the application of transient magnetic fields (i.e. rapidly time-varying intensity), which based on electromagnetic phenomena allows the induction of currents in the head tissues, especially in the brain, consequently changing the neural activity. Depending on the increase or decrease of activity in a specific brain region, the effects of TMS are cataloged as excitatory, or inhibitory,

respectively.

Throughout its history, TMS has been the subject of various studies concerning its potential applications. Diagnostic, mapping, and therapeutical purposes are some of these applications. Concerning the therapeutical applications of this technique, there are several neurological, psychological, and even metabolic disorders that may benefit from TMS therapy. For some disorders, there are already TMS protocols legally approved by the responsible health entities, in many different countries. In 2008, the first TMS protocol for the treatment of pharmacoresistant major depressive disorder (MDD) was approved by the US FDA (United States Food and Drug Administration), and ever since, by the same legal entity, dTMS protocols have been approved for, e.g., the treatment of pain associated with certain migraine headaches, in 2013, for the treatment of obsessive-compulsive disorder (OCD), in 2018, and for short-term smoking cessation more recently. Europe has also provided European CE (Conformité Européene) Mark approval for some devices and protocols regarding diagnostic and therapeutic clinical applications.

With the development of stimulators was introduced the repetitive application of TMS pulses, namely, repetitive TMS (rTMS). The difference between the rTMS protocols and the single-pulse protocols is concerned with the delivery time between pulses and their relative effect on the brain. In single-pulse protocols, the TMS pulses are delivered with a time interval large enough (5-8 seconds) so that there is no summation over time of the individual effects of each pulse. When it comes to rTMS, the purpose of such protocols is so that there is an accumulation of the individual effects, thus inducing a long-term effect. This long-term effect can either be excitatory or suppressive, being this mainly influenced by the frequency of the protocol. Typically, protocols with a frequency lower than 1 Hz have a suppressive effect, and protocols with a frequency higher than 1 Hz have an excitatory effect. These excitatory and inhibitory long-term effects are usually called long-term potentiation, and long-term depression, respectively. Nevertheless, there are other conditions that determine whether the effect of a specific protocol will be excitatory or inhibitory, as we will see in Section 2.7. The long-term effects introduced with rTMS protocols allow this modality to have therapeutical applications. As we have seen above, all the disorders we mentioned with a TMS therapeutical protocol FDA-approved benefit from this long-term therapeutical effect. However, there is one major physical limitation that might not allow other neurological and psychological disorders to benefit from this modality's effects. Standard TMS coils' applications are limited by the exponential decrease of the magnetic field (B-field) intensity along the brain depth, i.e., with distance from the coil. Therapeutical advantages in stimulating

deep brain targets have been over time hypothesized for certain disorders. This decrease in the magnetic field intensity with depth is also responsible for a decrease in the intensity of the induced current in the brain with depth. DTMS emerged as a modality with great clinical potential because of its capacity of stimulating deep brain targets. Over the years, many potential solutions have been introduced by researchers all over the world, with some already commercialized, as we will discuss in Section 2.8. The work we developed here is inserted in a bigger project where the main objective is to develop a dTMS system of coils capable of stimulating deep-brain areas with an unprecedented power-with-depth, in order to tackle this therapeutic opportunity.

In collaboration with ISEC (Instituto Superior de Engenharia de Coimbra) and IBEB (Instituto de Biofísica e Engenharia Biomédica), LIP (Laboratório de Instrumentação e Física Experimental de Partículas) has proposed an innovative dTMS system. The system, termed Orthogonal Configuration (OC), is constituted by a five-coil configuration immersed in a conductive liquid. The conductive liquid, among the dTMS systems that have been developed, is an innovation, and the main reason for the success achieved in previous simulations by Sousa (2014) and Santos (2015), with a 60% relative induction at the center of the brain (10-cm depth) achieved by Santos (2015) simulation work, after some alterations in the system. These alterations emerged to tackle the patient's and operator's safety, which were not fully guaranteed by Sousa (2014) simulations.

All this previously developed work needs experimental validation. This experimental validation requires the gathering of the appropriate materials in order to replicate the simulations' conditions as close as possible. In this work, we proposed to gather some of these materials, as well as to simulate the system's layout closer to experimental conditions (introduction of insulation around the electrical wires). Due to the pandemic, some work plans had to change, and we have decided to study potential future alterations regarding the dimensional practicality of the Orthogonal Configuration, given the significant amount of space and resources the previously studied system, by (Santos, 2015) and (Sousa, 2014), requires.

1.3 Dissertation structure

This dissertation is divided into seven chapters. In the present chapter, chapter 1, a brief introduction to several important concepts and work developed is made. The second chapter exposes some important moments concerning the history of brain stimulation, the physical and biological principles behind TMS stimula-

tion, TMS outcomes' influencing factors, and TMS' state of the art. In Chapter 3 we describe various disorders that already benefit from rTMS and/or dTMS, and some that may also do in the future (especially from dTMS), with multiple studies providing evidence of the beneficial effects of TMS protocols. Chapter 4 brings a contextualization of the major results achieved in previous collaborative work, and the inherited features and concepts of the system, from those works, in the one developed here. In Chapter 5 we detail the first part of the work developed in this project, with the presentation of the developments made regarding the experimental orthogonal configuration system, and the stimulation effect of introducing an insulating layer to the wires that make up the coils. Chapter 6 presents two simulation approaches with the main goal of improving the dimensional practicality of the system in future real applications. The closing chapter, Chapter 7, summarizes the general conclusions of this work and proposes some of the future directions this project should or could take.

2

TMS evolution, principles, and state of the art

2.1 TMS

Transcranial Magnetic Stimulation is a safe technique for electrically stimulating the human brain in a non-invasive way (Burke et al., 2019). This technique fits various purposes of diagnosis or treatment. In terms of diagnosis, TMS allows the recording of Motor evoked potentials (MEPs) in order to perform functional mapping of muscle representation within the motor cortex, as well as the assessment of brain circuits' excitability or plastic changes affecting these circuits. The last two assessments are accomplished via various types of paired-pulse configurations.

For treatment-related applications, TMS applied in repetitive trains, repetitive Transcranial Magnetic Stimulation (rTMS), may have excitatory or inhibitory effects in cortical networks, being these effects maintained for a certain amount of time after the stimulation. Therefore, rTMS opens exciting perspectives as a potential therapeutic alternative to standard treatments (that may not be effective enough) (Lefaucheur, 2019).

2.2 History and evolution of brain stimulation

The history of brain stimulation goes back to the Roman empire. Circa 46 AD, Scribonius Largo, the physician of the Roman emperor Claudius, suggested in his text *"Compositiones medicamentorum"* the use of electric ray fish on the cranial surface as a remedy for headache (Sironi, 2011). Other conditions such as depression, seizures, and pain were later treated with these fishes, as this resource was kept in function late until the eighteenth century (Sironi, 2011).

The history of brain electrical stimulation and the understanding of brain functioning go hand in hand. In the early nineteenth century, Giovanni Aldini performed

electrical stimulations over his own head and the exposed human cerebral cortex of recently decapitated prisoners (Vidal-Dourado et al., 2014) (Sironi, 2011). He concluded that the cortical surface could be electrically stimulated, supporting the idea that electricity could have therapeutic effects in the treatment of several neuropsychiatric disorders. Aldini's investigations are considered a landmark in electrical stimulation for the treatment of psychiatric disorders, leading to the investigation of brain stimulation to understand brain functioning, and of brain stimulation techniques for therapeutic purposes (Vidal-Dourado et al., 2014) (Sironi, 2011).

Regarding studies of brain function, Gustav Fritsch and Eduard Hitzing's observations were crucial to putting to rest the general belief (for over two millennia) that the brain is a homogeneous mass without discrete function (Schwalb and Hamani, 2008). Fritsch and Hitzig published in 1870 the results of a series of experiments on dogs at Hitzig's home, where they found that they could elicit graded motor responses to tonic-clonic seizures based on the amount of current applied and that by stimulating specific cortical areas it is possible to evoke muscle contractions (Schwalb and Hamani, 2008) (Sironi, 2011).

In 1874, Robert Bartholow reported, for the first time, findings from studies of electrical stimulation of the cerebral cortex in an awake human. The experiments consisted of the application of alternating current (AC) electrical stimulation in the exposed brain of a patient with a parietal epithelioma. At first, the experiments went well, with contralateral movements being induced, but the last set of experiments induced seizures, becoming these recurrent in days after and leading to the patient's death (Vidal-Dourado et al., 2014) (Sironi, 2011) (Schwalb and Hamani, 2008).

Alberto Alberti also made a major contribution to brain mapping research via electrical stimulation. In an experiment lasting 8 months, Alberti mapped the brain of a patient suffering from epileptic seizures, reporting that speech, coughing, crying, and abdominal and limb muscle contractions could be evoked by direct current (DC) cortical stimulation (Vidal-Dourado et al., 2014) (Sironi, 2011).

Regarding magnetic stimulation of the brain, Oersted had already observed at the beginning of the nineteenth century (1819) that a magnetic needle could be deflected by the influence of an electric current, thus hypothesizing that there are magnetic fields in the space surrounding the electric currents (Vidal-Dourado et al., 2014). The concept that electricity and magnetism were interactive phenomena was conceived between 1820 and 1822, by Faraday, Arago, Andre-Marie Ampére, Jean-Baptiste Biot, and Felix Savart, but it was almost a decade later (1831) that Faraday announced the discovery of the capacity of time-varying magnetic fields to induce electric currents. Faraday and Henry reported the electromagnetic phenom-

ena of induction as "a brief electric current in copper coil generating a time-varying magnetic field which induces a new electric current in nearby conductors" (Vidal-Dourado et al., 2014). In 1833, Heinrich Lenz observed that "the direction of the electric currents induced by the magnetic field is opposite to the electric current flow that produces it", in what is called the "Lenz's law" (Vidal-Dourado et al., 2014).

Still in the nineteenth century, Jacques d'Arsonval reported the effects generated by AC magnetic fields in the human nervous system. In 1893, d'Arsonval employed time-varying magnetic fields of high-frequency with different types of coils. d'Arsonval experience with magnetic stimulation of the brain was reported by the self to the French community in 1896, having d'Arsonval and others placed their heads inside the coils and reporting that phosphenes and vertigo can be triggered in anybody (Vidal-Dourado et al., 2014). Until the late twentieth century, non-invasive magnetic stimulation focused on visual phenomena, being the greater development reported attributed to electrical stimulation of the brain, when compared to that of magnetic stimulation (Vidal-Dourado et al., 2014).

Late in the twentieth century (1976), Anthony Barker and colleagues started to investigate magnetic stimulation of the brain, until in 1985 Transcranial Magnetic Stimulation (TMS) of the motor cortex was presented by Barker at the London Congress of the International Federation of Clinical Neurophysiology. A demonstration of TMS by Anthony Barker is depicted in Figure 2.1. TMS was described by Barker and others as a contactless and non-invasive neurophysiological tool, where a pulse of electric current flows a magnetic coil placed on the scalp, generating a time-varying magnetic field, and consequently inducing an electric current flow in cortical neurons, consistent with Faraday's and Lenz's law. These currents produce a sufficiently powerful ion flux across the membrane of cortical axons to depolarize the membrane and trigger an action potential with potential inhibitory or excitatory neural responses (Vidal-Dourado et al., 2014).

TMS arose as a potential alternative to diagnostically measure motor conduction times in patients with multiple sclerosis, typically measured by physicians in the late 1970s with resort to Transcranial Electric Stimulation (TES). The advantage of TMS was that this technique, via single-pulse stimulation, allowed physicians to perform similar motor conduction time tests in a safer and less painful manner (Horvath et al., 2011). This historical context determined the physicians' interest regarding the application of TMS to be, at its first stages, essentially in the domain of diagnostics and investigation (Horvath et al., 2011).

Nevertheless, TMS studies concerning interventions with repetitive protocols soon began to emerge, allowing researchers to conduct more refined studies of cog-

nitive function and neural interaction. After study reports such as that by Pascual-Leone et al. (1994), where post-stimulation lasting cortical effects by rTMS protocols were mentioned, TMS started to be considered as a conducive tool regarding the field of therapeutic medicine (Horvath et al., 2011). Proof-of-principle studies regarding therapeutic applications of TMS started to emerge, and in 2007, O'Reardon et al. (2007) conducted a multisite randomized controlled trial in which 301 patients with major depression, who had failed to respond to at least one previous adequate antidepressant trial, were subject to stimulation of the left dorsolateral prefrontal cortex (DLPFC) with the Neurostar TMS device (Horvath et al., 2011). The employed treatment protocol led to statistically significant improvement in several secondary outcome measures (Horvath et al., 2011). This study's results led to FDA approval for the treatment of specific forms of medication-refractory depression with the specific protocol of stimulation employed in the study and the NeuroStar TMS device (Horvath et al., 2011).

The application of TMS, either for investigation, diagnostic or therapeutic purposes has been evolving with the development of new coil designs, new stimulation protocols, and the knowledge of the "normal" and the "diseased" brain physiological processes. Nowadays, there are already several approved therapeutic applications of distinct TMS protocols and coil designs, for different conditions, in various, or in particular regions of the world, with some of these applications and coils to be further discussed in Section 2.8 and Chapter 3.

2.3 Physics behind TMS

The fundamentals of TMS are based on several physical processes leading to currents being induced in the brain in a non-invasive way. These currents are induced in the cerebral tissue as a consequence of a varying magnetic field that is generated in a coil/configuration of coils, placed above the human head. The magnetic field is capable of penetrating the human head (the scalp and skull) (Santos, 2015), thus reaching the brain and inducing there a varying electric current that flows in the same or opposite direction of the current in the coils (eddy currents), as depicted in Figure 2.2.

2.3.1 Physical Principles

TMS is a technique based on several important laws of electromagnetism. Everything starts with the physical processes induced by the passage of current in the

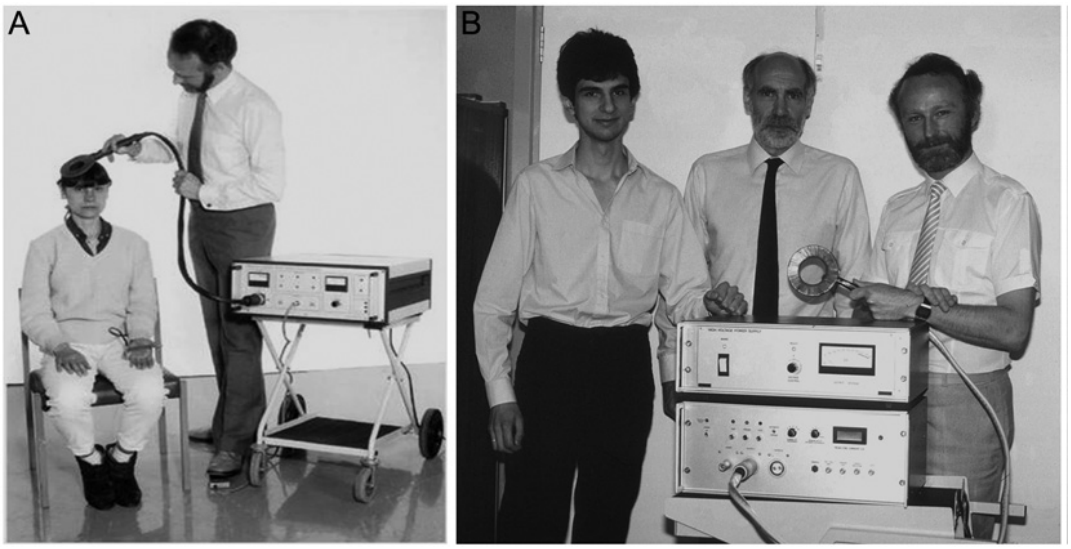

Figure 2.1: **A:** Demonstration of transcranial magnetic stimulation being performed by Anthony Barker in London, 1985. **B:** Reza Jalinous (left), Ian L. Freeston (middle), Anthony Barker (right) exhibiting their TMS device, 1985. Adapted from Vidal-Dourado et al. (2014).

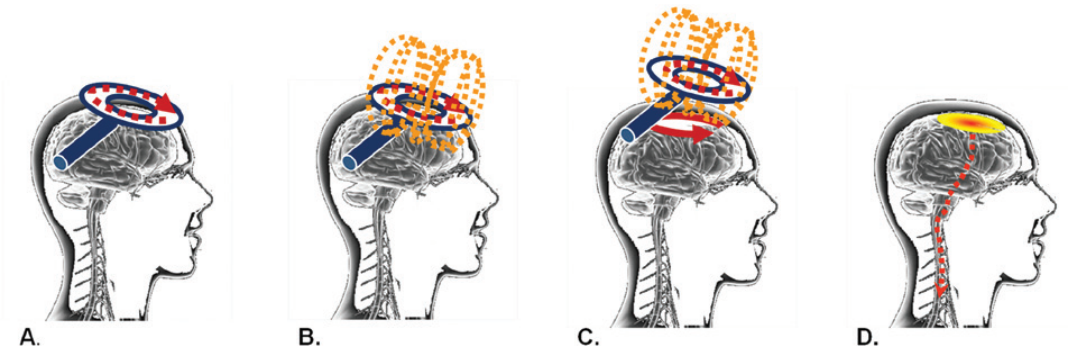

Figure 2.2: Brain current induction and consequent cortical activation schematics. **A:** Time-varying electric current flowing in a circular coil. **B:** Time-varying magnetic field induced by the electric current in the coil. The magnetic field is induced in a perpendicular plane to that of the coil. **C:** Induced electrical current in cortical layers, parallel to the coil. **D:** Activated cortical area and corticospinal tract as a result of neurons depolarization after TMS. Adapted from Vidal-Dourado et al. (2014).

coils. The currents flowing through the TMS coils are generated by charging large capacitors and then quickly discharging them. These currents are, typically, very large, ranging from 5 to 50 kA. As a consequence of these currents flowing in the coils, a varying magnetic field is induced beneath the coils, according to Ampére's Law(Rutherford, 2018):

$$\nabla \times \vec{B} = \mu_0 \left(\vec{J} + \frac{\epsilon_0 \partial E}{\partial t} \right) \tag{2.1}$$

In this equation, B is the magnetic field in tesla (T), J is the current density, E is the electric field, μ_0 is the permeability of free space and ϵ_0 represents the permittivity of free space. The value of this magnetic field is possible to calculate with resort to the Biot-Savart law. Biot and Savart's law allows to determine the magnetic field, $\vec{B}$, at any given point in space, produced by a current in a complete circuit (Santos, 2015), and is expressed as follows:

$$\vec{B} = \int_{AB} d\vec{B} = \frac{\mu_0}{4\pi} \int_{AB} \frac{I\vec{dl} \times \hat{r}}{r^2} \tag{2.2}$$

where dl are infinitesimal segments of a wire with an arbitrary form with the same direction as I, the current passing through the wires, r represents the distance between the B-field source, dl, and the field point, dB, where it is being calculated. As seen previously, μ_0 is the magnetic permeability of free space (Santos, 2015).

Regarding TMS, a particular application of the Biot-Savart law is the magnetic field produced by a circular coil. This particular case can be mathematically solved considering the circular loop in Figure 2.3 b), and the magnetic field produced at a particular point of the loop axis. Considering Figure 2.3 b) geometry, we have that all the projections of $d\vec{B}$ perpendicular to the axis of the loop will be canceled in pairs. The total magnetic field produced by the loop will then have the direction of the loop axis. Given that the position vector, $\vec{r}$, and the current element, $\vec{dl}$, are perpendicular, $\vec{dl} \times \hat{r} = dl$. In addition, considering the angle ϕ between the loop axis and $d\vec{B}$ depicted in Figure 2.3 b), each current element contributes with

$$|d\vec{B}| = \left(\frac{\mu_0}{4\pi} \frac{I}{r^2} \right) \cos\phi dl \tag{2.3}$$

Looking at Figures 2.3 a) and b) it is possible to see that $\cos\phi = \frac{R}{r}$. In order to calculate the total magnetic field produced, $\vec{B}$, one must integrate over the whole perimeter of the loop. The total magnetic field is thus given by

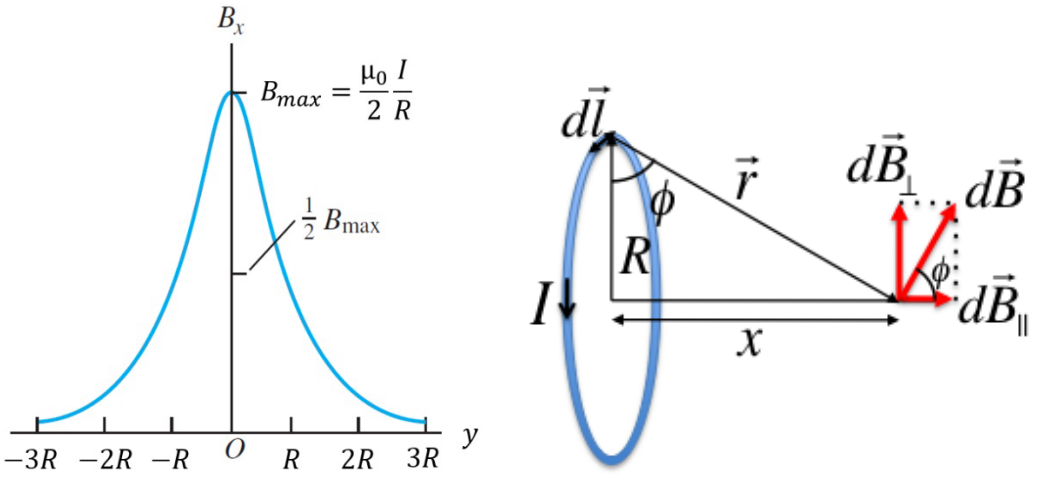

(a) **(b)**

Figure 2.3: **a)** Representation of the induced B-field along the axis of a circular loop. The $|\vec{B}|$ is maximum at the center of the loop (point O) when y=0. R is the loop radius, and y is the distance from the point where the B-field is being measured to the loop center. **b)** The $\vec{B}$ is split, being possible to observe that all the projections of $d\vec{B}$ perpendicular to the axis of the loop will be canceled in pairs. Adapted from (Young et al. (2004), Sousa (2014)).

$$\vec{B} = \int_0^{2\pi R} \frac{\mu_0}{4\pi}\frac{IR}{r^3} = \frac{\mu_0}{2}\frac{IR^2}{r^3} \tag{2.4}$$

Considering a circular coil with N turns, the total magnetic field at a particular point of the coil axis will, thus, be N times the field produced by a single loop, assuming that the turns are closely placed and the distance between the center of each loop and the axial point is approximately the same (Santos, 2015).

According to Faraday's law, this changing magnetic field produced by the current in the coils will then produce an electrical current in a nearby circuit, being this circuit, in our case, the human brain (Santos, 2015). Faraday observed, with a permanent magnet and an electrical circuit, that when there was a variation of the B-field passing through the circuit (by moving it relative to this circuit), an electric current was then induced in the circuit (Santos, 2015). This electromagnetic induction is a result of the variation of the magnetic flux, ϕ_B, through a surface delimited by the circuit. But Faraday also realized that, in order to induce and maintain an electric current flowing through the circuit, an electromotive force needed to exist. It can also be assumed that this variation of the magnetic flux, responsible for the induction of the current in the circuit, is also responsible for the emergence of an electromotive force $\varepsilon = RI$ (Santos, 2015). The relationship between this induced

electromotive force and the variation of the magnetic flux, ϕ_B, was deduced by Faraday, and is expressed as:

$$\varepsilon = -\frac{d\phi_B}{dt} \tag{2.5}$$

being this equation widely known as Faraday's law of induction. Focusing our attention on the negative sign of the equation, we get to Lenz's law. This law states that the direction of the current induced by a changing magnetic field is such as to oppose the effect of this magnetic field.

As described previously, in our real system of TMS we will have the coil with a changing current passing through it inducing a changing magnetic field. Looking at Faraday's law, we see that this changing B-field will, then, be able to induce an electric current in the head tissue, and, more importantly, in the brain tissue, being the brain, thus, in this case, the stationary conductor. The induced current will then be, assuming R as the resistance of the conductor (brain), $I = \frac{\varepsilon}{R}$ (Santos, 2015).

The movement of the charged particles (ions existing in the brain) within the stationary conductor (brain) will be due to an induced Electric Field (E-field) which is induced by the transient magnetic flux. This E-field will apply a force $\vec{F} = q\vec{E}$ on the charged particles within the brain, making them flow at a constant velocity in the direction of the E-field, thus, constituting a current. These induced currents are known as eddy currents and these are the currents able to stimulate the brain tissue and, so, modulate the neural activity. Modulation of the neural activity is a consequence of the eddy currents producing changes in the transmembrane potential of the neural cells, given the movement of the ions, inducing, therefore, action potentials (Santos, 2015). Eddy currents form closed loops and circulate in a perpendicular plane to that of the changing B-field, as depicted in Figure 2.2.

In our work we will drive our analytical focus to the eddy currents density, as we will see in Chapters 5 and 6, as it is believed that these are better described when expressed as current density, $\vec{J}$. Being the divergence of $\vec{J}$ equal to zero, and this physical quantity proportional to the E-field, $\vec{E}$, induced in the brain, according to Ohm's law:

$$\vec{J} = \sigma\vec{E} \tag{2.6}$$

with σ the electrical conductivity of the tissue, the current density emerges as a crucial quantity for the calculation of the E-field in the brain. The current density

represents the amount of charge per unit of time that flows through a certain cross-sectional area, thus, its units are amperes per square meter (A/m^2) (Santos, 2015).

2.3.2 Brain's physiological principles and TMS

2.3.2.1 The nervous system

The human nervous system is extremely complex, both structurally and functionally. Almost everything behind our unique experience of life is collected and processed in this system. From the maintenance of the body's autonomous functions to the complex processes of cognition and behavior, everything is controlled by the nervous system. The main task of the nervous system is, therefore, to ensure that our organisms adapt optimally to the environments we are living in (Brodal, 2010). Because of the detailed reasons, a lot is still to be learned before major progress in fundamental questions is done.

The nervous system can anatomically be divided into two major parts: the central nervous system (CNS), and the peripheral nervous system (PNS). The CNS consists of the brain and the spinal cord, whereas the PNS represents the nervous system part that connects the CNS to sense organs that react to sensory information or stimuli (receptors), and to the muscles and glands (effectors) (Brodal, 2010).

Furthermore, the PNS can be subdivided into two systems: The autonomic nervous system, and the somatic nervous system. The autonomic nervous system is responsible for controlling the activity of involuntary muscles (e.g., heart muscle cells) and gland cells. This nervous system can also be subdivided into two other subsystems, the sympathetic and the parasympathetic, the former responsible for mobilizing body resources when the demands increase, and the latter committed to the daily maintenance of the body. The somatic nervous system is provided with the responsibility of receiving the information coming from the sense organs (e.g., vision, receptors in the skin) and controlling the activity of our voluntary muscles (Brodal, 2010).

2.3.2.2 Nervous system's cells

Neurons

The building blocks of the nervous system consist of two kinds of cells. The first we are addressing are the nerve cells, also called neurons, which are responsible for the unique functions of the nervous system, with electric discharges as the means for transporting information between these special cells. These are composed of a

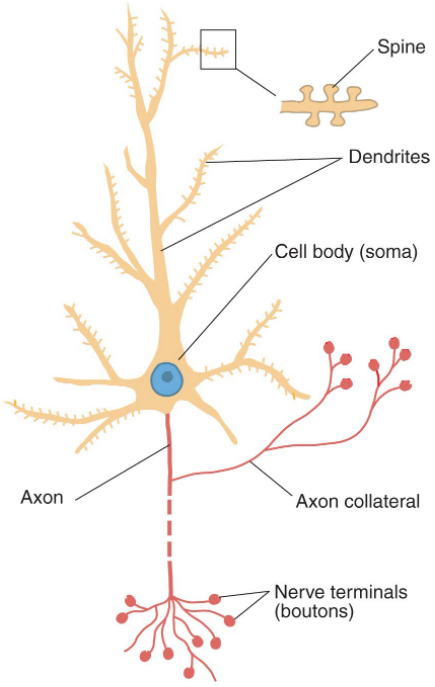

Figure 2.4: Representation of a neuron's main constituents, with the cell body and the signal emitting (axon) and receiving (dendrites) ramifications depicted. Adapted from Brodal (2010).

cell body called the soma, by multiple dendrites, which are extensions of the cell body that mostly receive stimuli from other neurons, and a single axon, responsible for conducting nerve impulses from the cell body to other neurons or muscle cells (Brodal, 2010), as it can be seen in Figure 2.4. Even though for each neuron there is only one axon, this axon can have many ramifications, enabling the parent cell to influence many other cells. Particularly for dendrites, even though a neuron may have several of these, these extensions of the cell body usually branch into several separate small spikes, called spines, represented in Figure 2.4, increasing the number of contact sites with other neurons, and consequently increasing the complexity of information flow within each neuron (Brodal, 2010).

The conduction of information between nerve cells is characterized by nerve impulses fastly conducted over short or long distances. These electrical discharges cross the axon length until they reach the synaptic cleft, where a neurotransmitter is released from the axon terminal conveying a chemical signal to the next neuron, where the information is transmitted, being this process called a synapse. This is a process where no direct propagation of the nerve impulse from one cell to the other occurs. The signal molecules (neurotransmitters) released at the synaptic cleft are the chemical signals that are going to influence the other cell (Brodal, 2010).

Glial cells

The other type of cells that constitute the nervous system are the glial cells. These are in a larger number than neurons in the brain, and their major purpose is to allow the proper functioning of the neurons. These cells are grouped into three categories: astrocytes, oligodendrocytes, and microglial cells. Each of these categories of glial cells is different structurally and functionally than the others (Brodal, 2010).

Astrocytes are cells with major importance regarding the maintenance of balance in the processes occurring outside the neurons, which will influence the processes of the neurons. This kind of cell is in intimate contact with neurons, capillaries, and the cerebrospinal fluid (CSF), meaning that they are in a unique position to control the extracellular fluid of the brain. Major concern processes like the control of the extracellular concentrations of ions and neurotransmitters, the extracellular osmotic pressure control, and the control of many potentially harmful substances from entering the brain are ensured by the astrocytes (Brodal, 2010).

Oligodendrocytes are responsible for a very important insulating layer along the axons of the neurons: the myelin sheath. This insulating layer allows for a faster and more efficient current conduction along the axon, reducing the loss of current from the axon to the surrounding tissue fluid. As illustrated in Figure 2.5, this myelin sheath consists almost exclusively of numerous layers of the oligodendrocytes cell membrane. Oligodendrocytes are responsible for this insulating layer along axons in the CNS, whereas Schwann cells are the responsible ones in the PNS. Beyond this important effect in electric conduction along the human nervous system, oligodendrocytes and Schwann cells' affecting diseases produce axonal loss additionally to the loss of myelin (Brodal, 2010).

The third kind of glial cells are the microglial cells. These cells are designated to conserve homeostasis, i.e., they act to minimize damage and protect neurons. They are believed to constantly scan their "surroundings" for foreign material and sick or dead cellular elements.

Although it is not their main purpose, glial cells can also send electric impulses which will influence many neurons, helping their synchronization of activity within a certain group. These electric impulses are produced given the opening of membrane channels for Ca^{2+}, evoked by the binding of neurotransmitters to protein receptors in the astrocytes membrane (Brodal, 2010).

Action potential generation

We have seen the two major cellular components of our nervous system and

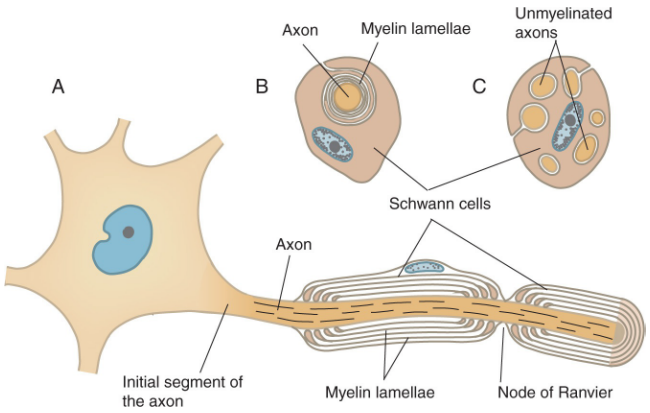

Figure 2.5: Myelinated and unmyelinated axons. A) Neuron with myelinated axon. The myelin lamellae are composed of glial cells (oligodendrocytes) membrane, where each cell produces one segment of myelin. A node of Ranvier consists of a point of contact between two myelin segments. Nerve impulses are generated in the segment closest to the cell body, and jump from one node of Ranvier to the next. B) Cross section of an axon in the process of being wrapped by a glial cell, thus becoming myelinated. C) PNS unmyelinated axons. Adapted from Brodal (2010).

some of their functional purposes and structural features. Along one of these nervous system's major components, the neurons, electric discharges with information are conducted in the axons. The question is: How do these electric discharges are generated in these cellular structures? To understand this, we have to look at what are some of the "normal" conditions of the neurons and their surroundings' ion concentrations, that, when altered, induce an electrical discharge in the neurons' axons.

Neurons have inside their cellular tissue, at a particular time point, a certain concentration of charged particles: ions of different elements and charges. Outside the neurons, in the extracellular fluid, there is also a certain concentration of ions of different elements and charges. But these concentrations are unequally distributed between the inside medium and the outside and are subjected to variations, depending on several variables (Brodal, 2010). Given this unequal distribution of positively and negatively charged particles, an electric potential between the interior and the exterior of the cell appears, also termed membrane potential. For this potential to change, the concentrations of ions in the interior and the exterior of the cell have to change. These concentrations can, actually, vary, given the presence of ion channels in the membrane of the cell, where these ions can enter or leave the neuron. The ion channels are more or less selective for the passage of particular ions, meaning that some ions pass more easily through a particular channel than others, being their opening controlled by neurotransmitters binding to the channel, or by the magni-

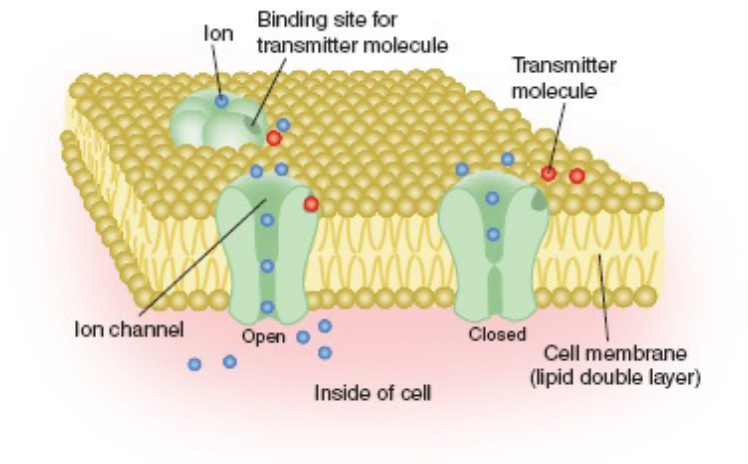

Figure 2.6: Representation of a cell membrane with interspersed ion channels. The ion channels are represented in different states, where the transition between close and open is depicted via neurotransmitter binding. Adapted from Brodal (2010).

tude of the membrane potential. The passage of these ions through these channels is dependent, when they are opened, on the concentration gradient and the voltage gradient across the cell membrane (Brodal, 2010). Figure 2.6 depicts accurately the mentioned dynamics between the exterior and the interior of the nerve cell, as well as the state of the ion channels.

Typically, the nerve cell potential across the membrane, in the resting state, is stable at approximately 60 mV, with the interior of the cell having a small surplus of anions. Given this small surplus of negatively charged ions inside the cell, it has been arbitrarily decided to define this potential as a negative one. This is known as the resting potential, and its typical value is -60 mV (Brodal, 2010). Figure 2.7 a) depicts the distribution of the ions particularly relevant for the membrane potential and their concentrations for a resting potential of -85 mV. In terms of the cations, it is possible to see a greater concentration of K^+ rather than Na^+ inside the membrane. In the resting state, the cell membrane is selectively permeable to the K^+ ions, being almost impermeable to the other ions depicted in Figure 2.7 a). This means that the resting membrane potential can accurately be explained focusing on the concentration gradients and flow of the K^+ ions.

Given the higher concentration of K^+ inside the cell, compared to the exterior, an outflow of K^+ ions will occur, making the interior negative, compared to the exterior. However, given the electrical gradient, these ions will be over the action of a force driving them to the interior of the cell. When the two forces are equally strong, the outflow and the inflow of K^+ ions will be equal, and the cell will reach the equilibrium potential. This potential is about -75 mV, but given that the cell

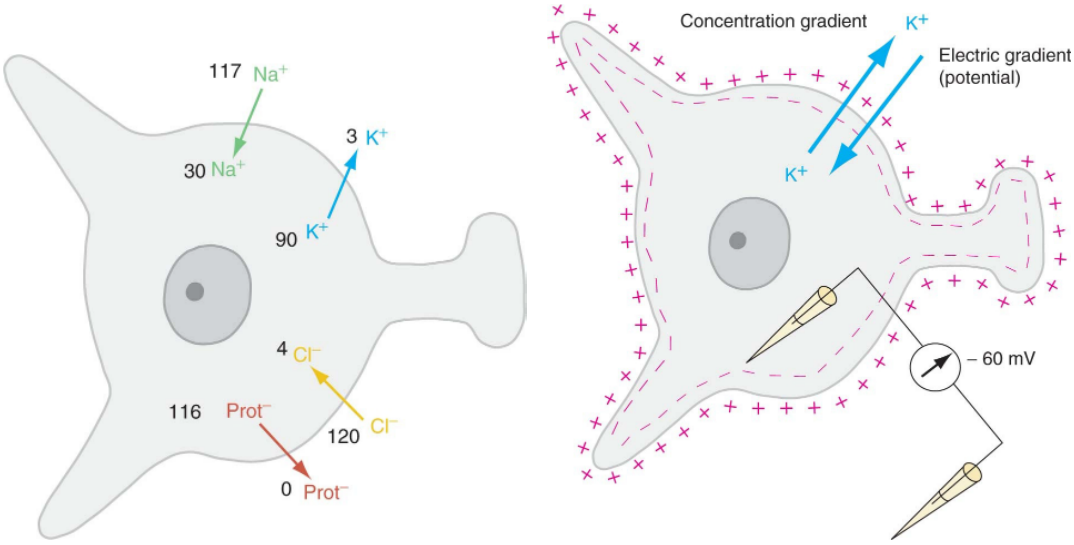

(a) **(b)**

Figure 2.7: **a)** Distribution of the ions particularly important for the membrane potential and their respective concentrations for a resting potential of -85 mV. **b)** Equally strong forces acting on the K^+ ions. The outflow and inflow of K^+ ions are the same, and the cell has reached the equilibrium potential. In this case, this potential is being measured by two electrodes as -60 mV. Adapted from Brodal (2010).

membrane is slightly permeable to Na^+ ions, and given the concentration gradient for these cations, an inflow of these ions will make the interior of the cell less negative than the equilibrium potential for K^+, and, for most of the neurons, the typical value is equal to -60 mV (Brodal, 2010), as illustrated in Figure 2.7 b).

Even though the discussed cations are the most important ones for the membrane potential, there are as many cations as anions. The major anions are Cl^- and negatively charged protein molecules. An uneven distribution across the cell membrane is also the reality for the negatively charged particles. The concentration gradient tends to drive the Cl^-, and the membrane is somewhat permeable to these ions. The protein molecules, however, have a different concentration gradient, with a higher concentration inside the cell, but given their large size, they cannot pass through the membrane. So, for the resting potential of the neurons, the Cl^- ions are the negatively charged particles that contribute to the membrane potential. Given the two main forces acting on these molecules, the membrane potential driving these particles out, and the concentration gradient driving them in, their net flow is small. Distinctively, these ions also have an equilibrium potential close to the resting potential of most neurons (Brodal, 2010).

We have seen so far that neurons have a resting state where they are not generating electric discharges. But the main purpose of our project is to generate or inhibit these electric discharges in order to potentially improve several health conditions. These electric discharges are specifically called action potentials, and their induction is related to the above-mentioned ions and their variations of concentration inside and outside the cell. We have seen that these concentrations can change, given the membrane of the nerve cells also being composed of ion channels, which allow the passage of several or particular ions. But these channels are not constantly opened. Two types of ion channels are present in the neurons' membrane: Transmitter-Gated Ion Channels, and Voltage-Gated Ion Channels (Brodal, 2010). In order for an action potential to be generated, the ion channels in charge are the Voltage-gated ones, especially the voltage-gated Na^+ channels. The opening of the voltage-gated channels happens given the depolarization of the membrane, and this depolarization can occur in artificial or natural conditions. The artificial conditions can include electrical stimulation by TMS. Depolarization is the name given to the reduction of the membrane potential magnitude.

In terms of the action potential, the basis of the phenomenon is found in the presence of voltage-gated Na^+ channels, which, as said previously, are opened by depolarization of the membrane. These channels are only opened when a certain potential threshold value is achieved, the threshold for producing an action potential. The inflow of Na^+ ions to the cell will depolarize more the membrane, opening more voltage-gated channels. This Na^+ ions current stops when the membrane is depolarized to +55 mV, when the equilibrium potential for the Na^+ ions is achieved. Once the equilibrium potential is achieved (peak in Figure 2.8), the membrane becomes impermeable to Na^+ ions. After this peak of the action potential, and given the positive potential of the membrane, the two forces acting on the K^+ ions will act on an outflow flux of these ions, turning the interior of the cell negative, because the Na^+ ions cannot enter the cell. Repolarization is this period of time depicted in Figure 2.8 where the membrane returns to its resting potential. When the membrane is sufficiently depolarized, voltage-gated K^+ channels open, and this leads to more K^+ ions leaving the cell, becoming the membrane potential more negative than the resting potential, a process illustrated as the latest phase of an action potential in Figure 2.8 and called hyperpolarization. The action potential consists of this process of depolarization and repolarization, caused by the flux of ions inwards and outwards the neurons (Brodal, 2010).

As mentioned earlier, the action potential flows through the axons until the next nerve cell. But the action potential is locally induced and there has to be a

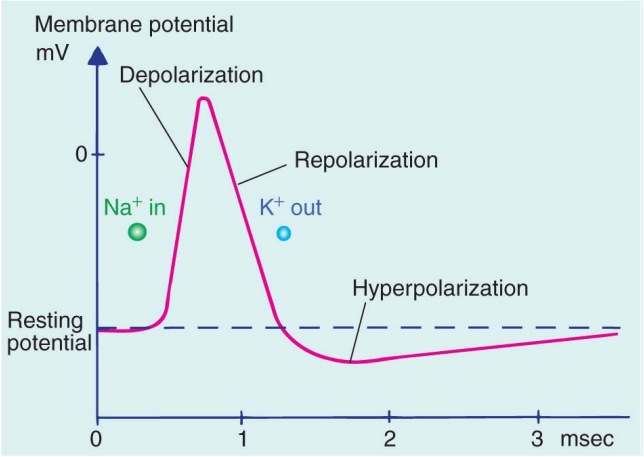

Figure 2.8: Action potential processes. Adapted from Brodal (2010).

way for this process to turn into an electrical discharge along the axon body. The action potential usually arises in the first part of the axon, because that is where the density of voltage-gated Na^+ channels is higher, and then is spread along the axon length. Action potentials can also be elicited in dendrites, but their threshold is usually much higher, given the lower density of voltage-gated channels (Brodal, 2010). The axon is a poor conductor, with enormous internal resistance, and charged particles are lost from the interior of the axon as the current passes along its length, because the axon is not a perfect insulator. According to these physical properties of the axon, if the propagation of the action potential along the axon occurred only by passive, electrotonic movement of charged particles, it would only travel a short distance before it "vanishes". In reality, what happens is that the action potential is regenerated as it moves along the axon, occurring, this way, the action potential propagation with undiminished strength from the cell body to the nerve terminals (Brodal, 2010).

As above explained, the action potential is produced by positive charges penetrating to the interior of the axon, becoming the axon, at that point, positive relative to more distal parts. This way, inside the axon, an electrical gradient is created along its length, which makes the positive charges start moving in the direction of the gradient. This movement of positively charged particles in the distal direction of the axon depolarizes the membrane as the charges move along, and this depolarization induces the opening of enough voltage-gated Na^+ and K^+ channels to produce a new action potential. This way, the action potential is regenerated along the axon, and the electric signal is not lost to the surroundings of the axon, reaching the termination of the nerve (Brodal, 2010). An easier understanding of the process is possible by visualizing it in Figure 2.9 a).

An additional feature is important for this process to be successful. The axons attain a certain electrical capacity, which allows this structure to store charged particles, the same way a battery does. This electrical property allows the membrane to be charged, an important feature before there can be a net flow of charges through it. When the action potential is propagated along the axon, the membrane enters a refractory state, for some milliseconds, where no action potentials can be generated, preventing the action potential from spreading backward, toward the cell body. This ensures that, in normal conditions, the action potential propagation is unidirectional.

As seen previously, axons myelinated and unmyelinated exist. The latter explanation of the propagation of the action potential over the axon length suits the unmyelinated axons. For the myelinated axons, the main difference comes in the regeneration of the action potential only happening at each node of Ranvier, as depicted in Figure 2.9 b), thus being the regeneration of the action potential, not a slow and "continuous" process, but instead a fast and "jumpy" process from one node of Ranvier to the other (Brodal, 2010).

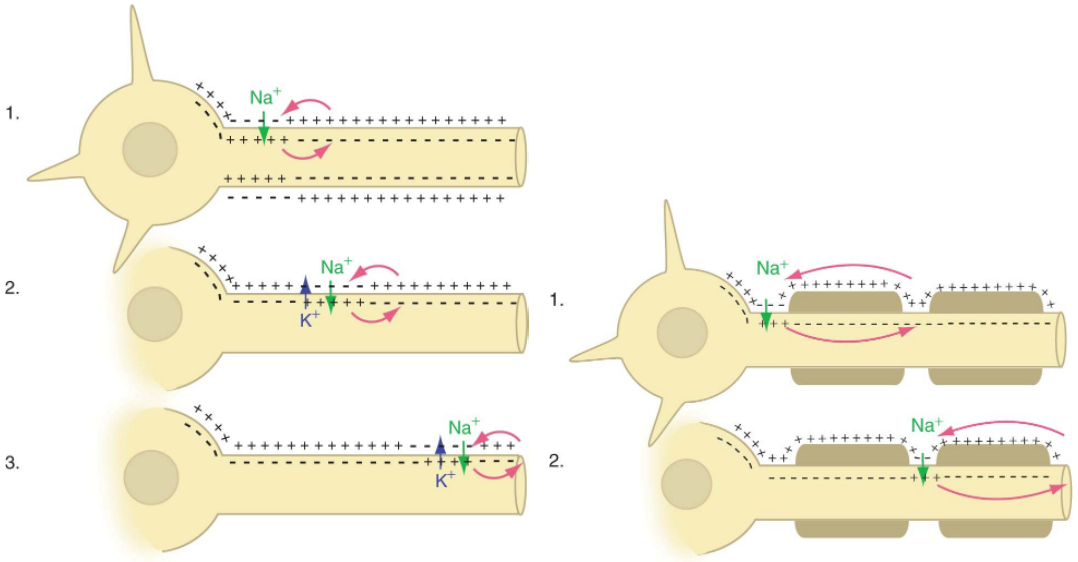

(a) **(b)**

Figure 2.9: **a)** Electric nerve impulse conduction in unmyelinated axon. The conduction happens via a renewal of the action potential along the axonal membrane given the electrical gradient created along its length. **b)** Electric nerve impulse in a myelinated axon. The action potential regeneration only happens at each node of Ranvier, with very rapid impulse propagation between nodes. Adapted from Brodal (2010).

2.3.2.3 Rheobase

As previously mentioned, action potentials can be induced by artificial stimulation, like TMS. It is, therefore, important to understand the temporal characteristics of the neuronal response to TMS pulses. There is an electric field threshold to attain neuronal response, but this neuronal response is also dependent on pulse duration. What is observed is that, as the pulse duration is extended, the electric field threshold to reach the neuronal response decreases. Figure 2.10 depicts this strength-duration curve for the human motor cortex that represents the relationship between the electric field magnitude and pulse duration (Roth and Zangen, 2012), which can be translated to a relationship between the current density and the pulse duration of the same form, given the proportionality between the E-field and the current density previously discussed in Section 2.3.1, as:

$$J_{th} = J_0 \left(1 + \frac{\tau_e}{t}\right) \tag{2.7}$$

where J_0 and τ_e are two biological parameters termed rheobase and chronaxie, respectively. Rheobase is the threshold of stimulation at infinite pulse duration, which means that any stimulus below the rheobase magnitude is ineffective, with no action potential (AP) generation. Chronaxie is the pulse duration at which the threshold of stimulation is twice the rheobase. These biological parameters depend on many biological and experimental factors, such as, for example, the myelination or not of the axons (Roth and Zangen, 2012).

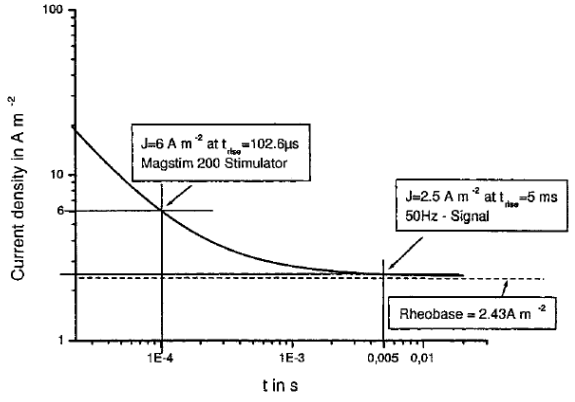

Figure 2.10: Current density strength-duration curve for the human motor cortex area, by Kowalski et al. (2002).

Kowalski et al. (2002) conducted a simulation study where the current density threshold for stimulating the motor cortex area of the brain was determined. At a frequency of 2.44 kHz, the determined threshold current density for the motor cortex

area was 6 A/m^2. Conversion to lower stimulation frequencies was addressed given the strength-duration curve in Figure 2.10 and the Equation 2.7, since it was not possible for the used stimulator to produce strong pulses in the low-frequency range of 50 Hz. The rheobase was determined assuming the threshold current density of $J_{th} = 6$ A/m^2, $t = 102.7$ μs (the pulse rise time applied by Kowalski et al. (2002)) and $\tau_e = 150$ μs, the motor cortex time constant, being the result obtained $J_0 = 2.43$ A/m^2. Knowing these constants value, and the frequency value of the pulse to be applied, one can calculate the threshold current density for stimulating the motor cortex with other stimulation frequencies, with t, the rise time, being $\frac{1}{4}$ of the induced current period. For a 50 Hz pulse, $J_{th} = 2.5$ A/m^2 (Kowalski et al., 2002).

2.3.2.4 TMS Modulatory effects

Ever since its introduction in 1985 by Barker et al. (1985), TMS has been used for basic neurophysiology research as well as for rehabilitation and therapy across several studies regarding neurologic and psychiatric conditions (Noh, 2016). It has been observed that the TMS modulatory effects remain even after the stimulation period. The widespread assumption behind this stimulation aftereffects is that the application of certain TMS protocols is able to induce plasticity mechanisms in the patients' nervous systems (Thomson et al., 2020).

Plasticity is known as the self-reorganization capacity of the brain in order to improve the function of its own networks, enabling the short- and long-term remodeling of neural interaction that outlasts experimental manipulation. The goal of these processes is to improve the function of the brain networks. The phenomenon of plasticity can occur at several levels of brain organization, ranging from the ultrastructural to the synaptic level (Noh, 2016), (Hoogendam et al., 2010).

Regarding TMS long-lasting effects, there are pharmacological, physiological, and behavioral studies providing lines of evidence that these long-term effects are produced through alterations in synaptic plasticity, and this has been assumed as the driving force of sustained TMS aftereffects (Huang et al., 2017). Namely, the induced changes after TMS in brain activity have been described as LTP (long-term potentiation)- and LTD (long-term depression)-like. LTP and LTD are excitatory and inhibitory, respectively, long-lasting changes induced in the synaptic efficacy and strength. This means that a long-lasting increase in synaptic strength is commonly referred to as LTP, with an illustration of a typical full process illustrated in Figure 2.11, whereas a long-lasting weakening of synaptic strength is commonly referred to as LTD. These long-lasting plasticity phenomena can last for days, weeks, or even months after the stimulation protocol was applied (Hoogendam et al., 2010).

However, more direct and conclusive evidence of synaptic plasticity mechanisms in humans following TMS is still needed, given that most of the evidence comes from studies in animal models (Thomson et al., 2020) (Huang et al., 2017).

Some progress has already been made and Thomson et al. (2020) developed an *in vitro* human neuron model, in order to assess protocol-specific effects of intermittent Theta Burst Stimulation (iTBS) and continuous Theta Burst Stimulation (cTBS) on plasticity markers of gene expression (associated with synaptic plasticity) and neurite outgrowth. They have focused on investigating changes in the Brain-derived neurotrophic factor – tyrosine kinase receptor B (BDNF-TrkB) signaling cascade - because of its importance in plasticity mechanisms, and previous animal studies have shown an rTMS-induced effect on protein expression in this pathway (Thomson et al., 2020). A significantly enhanced expression of plasticity genes 24h after iTBS compared to sham TBS was observed, providing support for the widely assumed plasticity mechanisms underlying iTBS on human cortex excitability.

Although TMS modulatory aftereffects share many similarities with LTP and LTD, and this has been, generally, the major line of thought regarding the TMS residual effects (as previously mentioned), there is, yet, no direct evidence for such association in humans, even though strong indirect links were already found, and LTP and LTD processes were already confirmed in subcortical neurons as TMS aftereffects in animal rTMS studies (Noh, 2016) (Tang et al., 2017). But given that TMS affects different neuronal and non-neuronal processes (e.g., neuromodulators production, growth factors such as brain-derived neurotrophic factor (BDNF), early gene proteins, among other non-neuronal processes, as cerebral blood flow and glucose metabolism), it is unlikely that the stimulation outlasting effects fall simply over synaptic plasticity, with other mechanisms such as altered membrane excitability, or breakdown of cortical inhibition being also potential drivers of these modulatory aftereffects (Noh, 2016) (Tang et al., 2017). It is also hard to exclude evidence showing that TMS affects different cell types, with different excitability properties, leading this stimulation, in different brain areas, to different outcomes, as well as study results where cortical oscillations induced by TMS were found not to be correlated with MEPs amplitudes (an indirect measure of synaptic plasticity) (Noh, 2016) (Tang et al., 2017). The reality is that the subject of TMS aftereffects in animals and humans, even though with some strong lines of thought supported by several studies, has still to be deeply studied in order to get to specific conclusions.

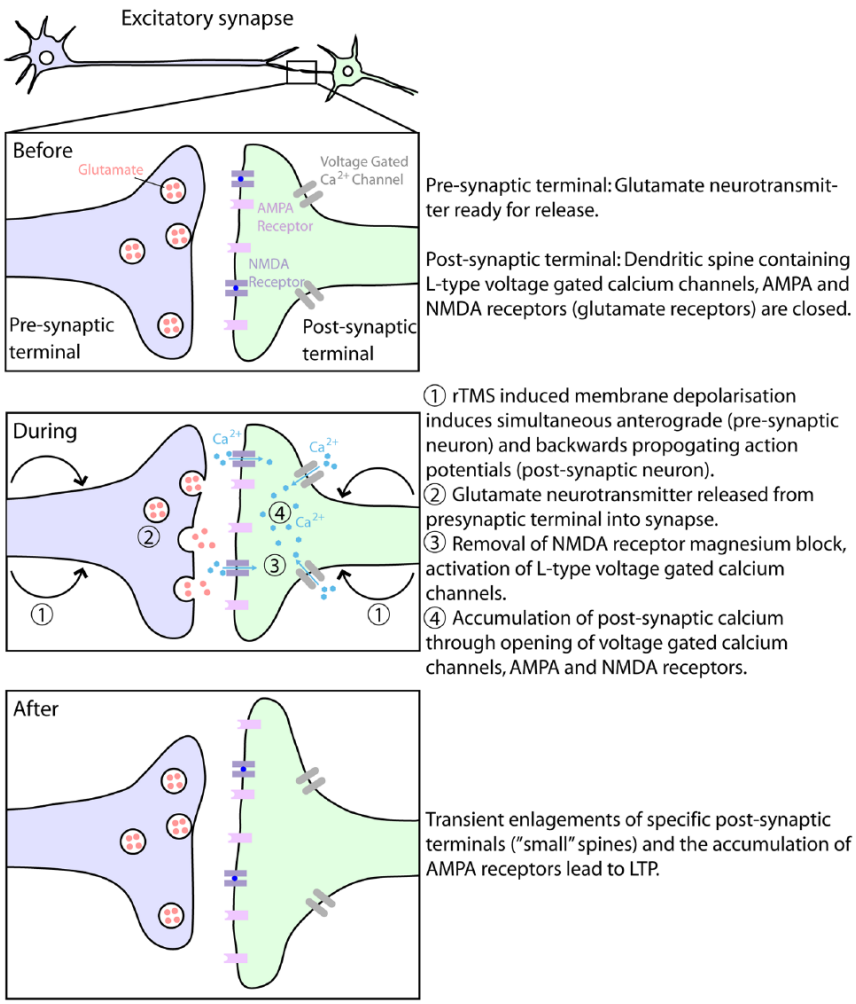

Figure 2.11: Proposed rTMS-induced LTP mechanism at an excitatory synapse in the hippocampus. rTMS induces LTP by simultaneously activating the pre- and post-synaptic cells. Voltage-gated Ca^2+ channels and NMDA receptor dependent on the calcium influx facilitate the process. The result is an enlargement of the dendritic spine and accumulation of AMPA receptors in the postsynaptic cell. These effects last 2-6 hours poststimulation. Adapted from Tang et al. (2017).

2.4 Stimulation protocols

Nowadays, TMS can be easily recognized as a broad concept that, ever since its conceptualization, has been developing into a range of protocols of stimulation that typically surpass the complexity of their first predecessor. These protocols have been developed over the shoulders of knowledge that has been mounting regarding the TMS effects and the brain's anatomy and neurophysiology. From protocol to protocol, the most recognized variables influencing the effects of stimulation are stimulus intensity, stimulus frequency, the total number of stimuli, duration of the

application period, and the shape of the magnetic pulse (Hoogendam et al., 2010). We will review some of the main protocols' applications and features.

2.4.1 Single-pulse TMS

Single-pulse TMS (sTMS) is the "simplest" pattern of TMS. It consists of the discharge of single pulses (with a duration of $\approx 250 - 750\mu s$ for standard biphasic pulses) separated by time intervals long enough so there is no summation over time of the individual effects of each pulse (typically 5-8 s). Single-pulse TMS is a versatile pattern of stimulation in terms of its purpose of application since it can be used for diagnostic purposes, mapping, and assessment of changes produced by alteration of the activity of several brain areas (e.g., characterization of motor or visual cortical excitability changes, via the estimation of changes in MEP or phosphenes threshold; map causally the spatial distribution and somatotopic/retinotopic representations of muscles and visual receptor fields; assess changes produced by physical activity, psychoactive drugs, or the impact of long trains of rTMS, among others). Delivering sTMS pulses at different time intervals during the performance of a visual perceptual task can also be used to elucidate the time course of a complex neural process (Valero-Cabré et al., 2017).

2.4.2 Double-pulse TMS

Double-pulse TMS (dpTMS), or paired-pulse TMS, is a modality consisting of two different TMS stimuli: a conditioning stimulus (CS), and a test stimulus (TS), being the stimuli delayed by an interstimulus interval (ISI). The CS precedes the TS. The applications of dpTMS rely, essentially, on the assessment of intracortical modulatory mechanisms or interregional interactions between two regions in close or distant areas of the same or opposite hemispheres. The TS and CS intensities are different, and, typically, the TS intensity is set above the individual motor threshold (MT), while CS intensity is set up below. However, this is not always the case for all the modalities of dpTMS, as we will see ahead. The ISI intervals, like the stimulus intensities, influence the outcome of this protocol (Valero-Cabré et al., 2017).

Extensive research using a large variety of short ($<$ 7ms), intermediate (7-15 ms), and long (50-200 ms) ISIs has revealed in the primary motor cortex (M1) up to 5 intracortical modulatory phenomena: Intracortical facilitation (10-15 ms ISI; CS subthreshold and TS suprathreshold), short interval intracortical inhibition (1-4 ms ISI, CS subthreshold, TS suprathreshold), short interval intracortical facilitation (1-4 ms ISI, CS suprathreshold, TS subthreshold), long interval intracortical

facilitation (100 ms ISI, CS subthreshold, TS suprathreshold), and long interval intracortical inhibition (50-200 ms, CS suprathreshold, TS subthreshold). The aim of these paired-pulse protocols is to explore inhibitory and excitatory intracortical mechanisms mediated through specific populations of interneurons. The outcomes are always normalized relative to the isolated TS effects, in order to assess the change in outcomes compared to a single stimulus (Valero-Cabré et al., 2017).

The other application of paired pulses is the assessment of interregional interactions, especially between two regions. Here, two pulses are discharged on pairs of distinct cerebral sites, where the pulses are separated by a variable ISI. The outcomes of this application are the determination of the presence or absence of connectivity and an estimation of the conduction time between the two regions (that can be close or distant, and in the same or in opposite hemispheres). This way, this modality of dpTMS allows studying not only the timing but also the modulation direction of the interactions between two regions of the brain. The outcomes of the interactions are addressed by the characterization of the changes that a CS on cerebral area "1" exerts on the sensory, electrophysiological, or behavioral output of cerebral area "2" (Valero-Cabré et al., 2017).

2.4.3 Repetitive TMS

Repetitive TMS (rTMS) is a TMS modality that englobes a wide range of stimulation patterns. It refers to any combination of more than two pulses separated by a time interval equal to or smaller than 2 seconds. The diverse stimulation patterns of rTMS are capable of inducing different outcomes than single pulses, with these effects changing from pattern to pattern. Typically, what differs between the various rTMS patterns of stimulation is their frequency and distribution of pulses (Valero-Cabré et al., 2017). This means that there are several possible stimulation patterns. We will see ahead that, for a specific modality of rTMS there is, typically, an expected outcome. But this cannot be taken as an absolute truth. Given the differences in the cytoarchitectural, neurochemical and neurophysiological organizations across cortical areas, or differences in the activity of the stimulated area at the time of stimulation, it is precarious to assume the effects of a given combination of parameters region-, time-, and activity-invariant (Valero-Cabré et al., 2017).

The main feature of rTMS patterns is that when delivered in long trains and in consecutive daily sessions, these protocols have the potential to induce plastic mechanisms that will modulate function long-lastingly. This long-lasting modulation potential raises certain rTMS protocols as potential therapeutic alternatives for a

wide range of psychiatric and neurological conditions, with some already, not only, but also, FDA-approved for certain conditions, as we will see in Chapter 3. However, these long-lasting effects are not the only ones induced by rTMS, being the main differences between the effects the moment they are induced, and the time interval they are kept. There are three types of rTMS effects on cognition and behavior: Online effects, offline effects or after-effects, and long-term effects (Valero-Cabré et al., 2017).

Online effects occur as an immediate consequence of stimulation. These effects interfere with the brain's neuronal discharge patterns, leading to changes in behavioral performance. The silent period is a TMS motor phenomenon that illustrates well the TMS online effects. In this event, electromyographic signals are suppressed during an ongoing voluntary hand muscle activation, induced by a TMS pulse applied over the primary motor cortex, until the cortico-spinal descending activity recovers back. This phenomenon represents the ability of TMS patterns to impact cortically- and spinally-driven processes during its application (Valero-Cabré et al., 2017).

Offline effects are the outlasting effects on cerebral processes posteriorly to the delivery of an rTMS protocol. When applied in long patterns of individual pulses with a defined frequency (rTMS), evidence shows that cortical activity remains altered for an average period of 30 minutes, being this value affected by the protocol of stimulation, with some extending for up to 60 minutes post-stimulation. Nevertheless, the duration of these rTMS after-effects depends on several variables, such as the rTMS parameters and the specific behavioral (task performance, reaction times), hemodynamic and metabolic (fMRI, PET), or electrophysiological (MEPs, EEG, MEG, etc) read out measures engaged. The intensity of these offline effects is always weaker than the observed in the online effects (Valero-Cabré et al., 2017).

With long-term TMS effects, we enter the therapeutic potential field. Typically, as it has been widely demonstrated, a periodic repetition of stimulation sessions, with intervals between sessions shorter than 24 hours and modulations of the cortical activity being induced in a single direction, can generate long-term effects. This means that these lasting neuromodulatory effects have the potential to translate into meaningful therapeutic interventions. However, if the intervals between sessions exceed the 24 hours period significantly (days or weeks), the lasting neuromodulatory effects may not occur effectively, having been widely demonstrated that these long intervals between sessions are too long to lead to cumulative effects. It has also been shown that reducing the time interval between sessions can strongly enhance the magnitude of the rTMS effects and their duration (Valero-Cabré et al., 2017).

In sum, the effects of a specific protocol of stimulation tend to be associated with the parameters of the protocol. However, the responses to the protocols of rTMS can be variable, depending the patients' response on several factors. This subject will also be addressed further in the next section.

2.4.3.1 rTMS protocols

Low-frequency rTMS

rTMS protocols known as low-frequency are composed of patterns of pulses repeated with a frequency, typically, smaller or equal to 1 Hz, as represented in Figure 2.12. The effects of these protocols are, typically, inhibition or suppression of excitability within the targeted cortical areas. This inhibition or suppression results in a weakened intrinsic level of activity, reduced efficacy of the outputs of the cortical target, or even silencing the contribution to cognitive processes in which the cortical targets are involved (Valero-Cabré et al., 2017). However, these suppressive or inhibitory effects are not always the case observed. Facilitatory effects have also been observed in some studies when applying 1-Hz rTMS. This variability of response might have several causes, such as the large interindividual variability, or the level of excitability of the cortical area stimulated, among others to be detailed in Section 2.7. Regarding the levels of excitability of the target area, it has been observed, in motor areas, that when the muscle being stimulated is at rest, MEPs become suppressed, whilst when it is under voluntary contraction, no suppression occurs. In addition, when primed protocols are applied with high-frequency stimulation preceding the low-frequency protocol, the ability of the subsequent 1-Hz protocol to induce depressing effects greatly increases (Hoogendam et al., 2010).

High-frequency rTMS

Typical high-frequency protocols are characterized by patterns of TMS pulses with frequencies above 1 Hz (typically equal to or above 5 Hz), being represented in Figure 2.12 by a protocol of 5 Hz. Contrarily to low-frequency protocols, the effects of high-frequency rTMS tend to be facilitatory, i.e., increases in activity and excitability of the targeted area are observed, meaning improvement of the processes related to intracortical activity or networks related to the stimulated area (Valero-Cabré et al., 2017). Nevertheless, as mentioned regarding the low-frequency protocols, the facilitatory effects are not always the results observed when it comes to high-frequency protocols. Among factors such as those pointed to low-frequency rTMS, like priming, the excitability of the cortical target, and interindividual variability, it has been observed that for high-frequency rTMS protocols the aftereffects depend heavily on the intensity of stimulation. This idea is supported by studies

reporting a decrease in excitability after high-frequency rTMS at low intensities, and an increase in excitability after high-frequency rTMS at higher intensities, meaning the outcome is not always the same, but tendentially dependent on the intensity of stimulation (besides the other mentioned factors) (Hoogendam et al., 2010).

Theta burst stimulation

Theta burst stimulation is a patterned form of rTMS. This protocol is based on the naturally occurring theta rhythm of the hippocampus. Its application in humans arises as an adaptation form of the theta-burst protocol used in animal experiments, already proven to induce synaptic plasticity (Hoogendam et al., 2010) (Valero-Cabré et al., 2017). TBS protocols consist of bursts of 3 pulses with a frequency of 50 Hz repeated every 200 milliseconds (i.e. 5 Hz), being the latter the frequency of the theta rhythm. The outcomes of the TBS protocols depend on the pattern of stimulation.

The two main TBS protocols are continuous Theta burst stimulation (cTBS) and intermittent Theta burst stimulation (iTBS). The cTBS protocols tend to induce inhibitory effects in the cortical activity of the targeted area, whilst the iTBS protocols tend to induce facilitatory effects. The protocols differ in the way the applied TMS bursts are spread in time. cTBS, as the name denounces, consists of a continuous stimulation protocol, without time intervals with an absence of stimulation, whereas iTBS consists of stimulation periods separated by a certain time interval. The representation of both protocols in Figure 2.12 allows seeing this difference in the distribution of the bursts. This time difference between protocols is one of the possible reasons for the different aftereffects of the two protocols. Comparatively to traditional rTMS patterns, theta burst stimulation protocols appear to induce longer-lasting and more powerful effects after a short period of 20-190 seconds of stimulation (Valero-Cabré et al., 2017).

Other protocols

The previously mentioned protocols are the most studied and acknowledged by the scientific community in terms of their application and respective therapeutic potential. Nevertheless, more recent protocols have been developed and studied, with some of these protocols already showing promising results.

Multi-coil TMS is one of these novel protocols. This group of protocols is derived from the double-pulse protocol, and most of the applications are similar. Some of these applications concern the determination of connections between brain areas, the timing of the interregional communication between the connected areas, or even the modulation of the activity within the target area. These multi-coil protocols

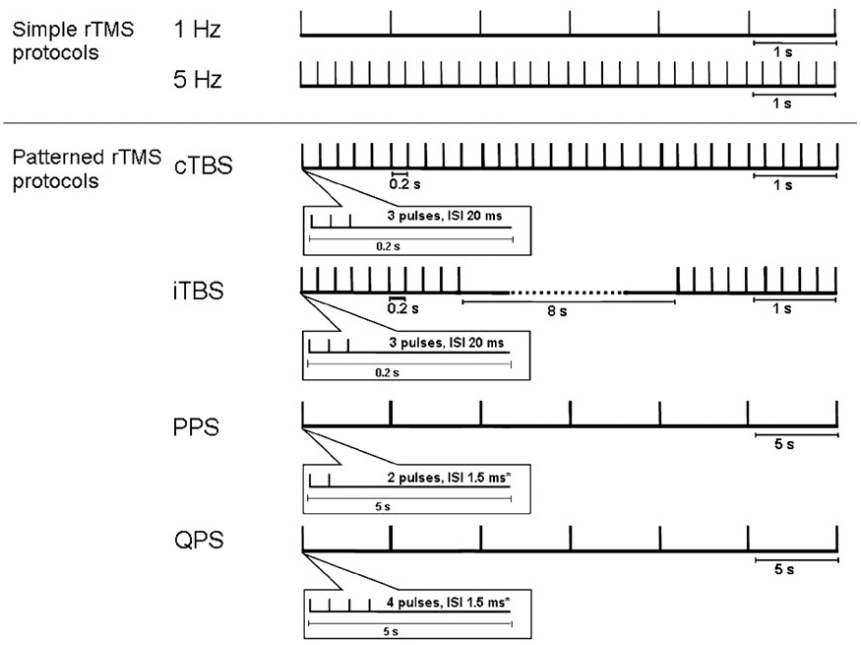

Figure 2.12: rTMS protocols. The simple protocols depicted are defined as low-frequency (<=1 Hz), or high-frequency (>=5 Hz). Tendentially these are, respectively, seen as inhibitory or excitatory protocols. Patterned protocols are characterized by having different ISIs. Continuous theta-burst stimulation (cTBS) is characterized by long uninterrupted trains of TBS (e.g., 40 s, with an ISI of 20 ms). In intermittent theta-burst stimulation (iTBS) shorter trains of TBS are delivered with a defined interval between trains of TBS (e.g., the depicted protocol is a 2-second train with an ISI of 20 ms, repeated every 10 seconds). In paired-pulse stimulation (PPS) there is a conditioning stimulus and a test stimulus. These stimuli are separated by an ISI, and the procedure is repeated every, e.g., 5 s. In quadripulse stimulation (QPS), there are 4 pulses being applied with a specific ISI. These pulses can be delivered over different areas of the brain to probe any influence between these areas (like in PPS). The features of these protocols that influence the outcomes are their frequency, ISIs, and intensity. Adapted from Hoogendam et al. (2010).

also allow the achievement of two different goals within the same study, such as, for example, a three-coil protocol where the connection between two stimulated areas is being probed, and the other area under stimulation is only being manipulated in terms of its activity (Valero-Cabré et al., 2017). To our knowledge, the protocols already studied used a maximum number of 4 TMS independent coils. In one study regarding, precisely, 4 stimulation coils (quadripulse stimulation) it was shown higher effectiveness in increasing the MEP size than with a dpTMS protocol with the same ISI (Hoogendam et al., 2010). The aftereffects of quadripulse stimulation seem to depend on the ISI interval, as in the dpTMS case, with facilitatory effects

tendentially observed with short ISI, and inhibitory effects observed with long ISI, as it was observed by Hoogendam et al. (2010).

Paired Associative Stimulation (PAS) is another stimulation protocol involving TMS already with some promising results regarding motor deficits recovery. This protocol differs from the typical TMS protocols given its inclusion of electric stimulation. That is right, this protocol seizes both electric and magnetic stimulation together. However, the different stimulation techniques are not delivered at the same time, or at the same spot. This protocol is based on the Hebbian concept of spike-timing-dependent plasticity[1]. Given the Hebbian basis of the protocol, the temporal order of the presynaptic and postsynaptic spiking is important for the stimulation outcome. Typically, the electrical peripheral stimulation of the nerve precedes the TMS over the cortex, and the temporal order of the ISI between these two stimuli will rule whether the effects are LTP or LTD-like. What is commonly observed is that when the ISI is slightly longer than the necessary time for the afferent pulse to reach the motor cortex, the modulatory effect is facilitatory, i.e., this area excitability increases. On the contrary, when the ISI is slightly shorter than the necessary for the afferent pulse to reach the motor cortex, the effect is inhibitory, and the excitability of the motor cortex tends to decrease (Hoogendam et al., 2010).

2.5 Waveforms and current direction

When stimulating the brain with TMS, a matter of relevance relies on the waveform nature of the pulses produced in the stimulator that will flow through the coils and induce the magnetic fields that will stimulate the brain. Nowadays, the "offer" in terms of the waveform nature is, naturally, bigger than it was at the beginning of the TMS investigation and application. The first TMS stimulators produced monophasic pulses of electric current, where the current only flows in one direction, as depicted in Figure 2.13 - left. Nowadays, the most widely used TMS stimulators produce the pulses depicted in Figure 2.13 - right, i.e., biphasic pulses, where a current flows in both directions, being the pulses terminated after a single sinusoidal cycle (Roth and Zangen, 2012) (Marcolin and Padberg, 2007). Other pulse waveforms such as half-sine pulses, also depicted in Figure 2.13, where the current flows in both directions and terminates after the "negative" phase of the pulse (not completing a full sinusoidal cycle), and polyphasic pulses, where the oscillation does not terminate after a single sinusoidal cycle, but instead the signal

[1] biological process where the strengthening or weakening of a synapse is dependent on the relative timing between the pre-synaptic and post-synaptic action potentials (spikes).

alternates for many cycles until it is almost zero, are less frequently used in TMS (Roth and Zangen, 2012).

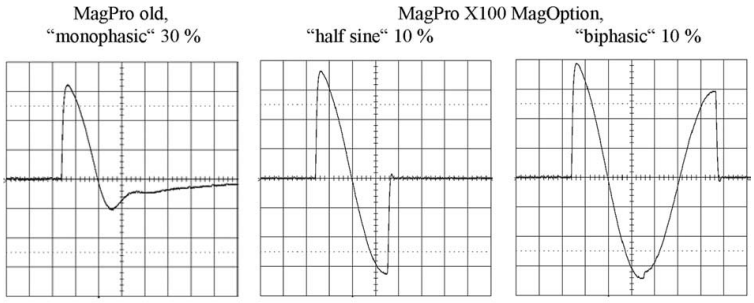

Figure 2.13: Common TMS waveforms induced by a circular probe coil, and two different stimulators. On the left, a monophasic waveform is depicted, as induced by a MagPro stimulator. In the center and right images, a half-sine waveform, and biphasic waveform stimulus are depicted, having been induced by a MagPro X100 MagOption stimulator, and recorded by an oscilloscope. The percentages represent "how much" of the maximum stimulator output is being delivered. Adapted from Sommer et al. (2006).

The application of either monophasic or biphasic pulses has technical and physiological arguments. Compared to monophasic pulses, biphasic pulses have higher energy efficiency (part of the energy returns to the capacitor at the end of the cycle, shortening the recharging time and enabling to save energy), less coil heating, and the threshold for neuronal activation is generally lower (Marcolin and Padberg, 2007). Maccabee et al. (1998) reported a biphasic waveform to be more effective than a monophasic waveform regarding the threshold of excitation and response amplitude (Sommer et al., 2006). The potential explanations given by Maccabee et al. (1998) relied on the influence of the phases of the pulse waveform on processes such as the depolarisation and hyperpolarisation of an action potential (Sommer et al., 2006). Given that a significant portion of the energy returns to the capacitor at the end of the cycle, which enables the shortening of the recharging time, biphasic pulses are typically used in stimulators intended for rTMS (Roth and Zangen, 2012).

The interaction with the neural substrate is also affected by the waveform. However, this is not the only current feature important for the results of the stimulation. The direction of the induced current also seems to influence the interaction of the pulses with the neurons (Davila-Pérez et al., 2018). The subject of waveform and current direction as pulse parameters influencing the stimulation outcomes has been studied, majorly with resort to single- and paired-pulse protocols, through the assessment of the influence of these parameters in typical neurophysiological measures, such as Resting Motor Threshold (RMT), Motor Evoked Potentials (MEPs), corti-

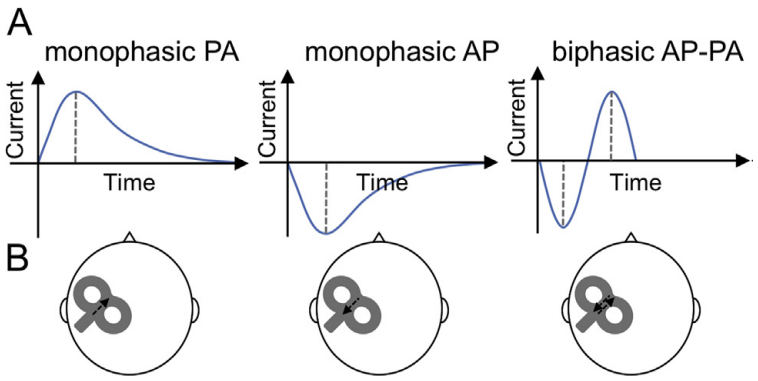

Figure 2.14: Pulse waveforms and current directions in a study by Davila-Pérez et al. (2018). **A:** Monophasic pulse with posterior-to-anterior direction (left), monophasic pulse with anterior-to-posterior direction (middle), biphasic pulse with an anterior-to-posterior and posterior-to-anterior directions (right). **B:** Location of the TMS coil over the left primary motor cortex, with arrows depicting induced currents' direction in the brain. Adapted from Davila-Pérez et al. (2018).

cal silent period (cSP), MEP latency, among others. Over the years, investigators have been studying this influence of direction and waveform in neurophysiological markers and trying to find the proper justifications. The main evidence is based on the recording of TMS-induced descending volleys sampled with epidural. Following a series of experiments performed on patients with epidural electrodes implanted at the cervical spinal cord, Di Lazzaro and Rothwell (2014) proposed that different waveforms and current directions interact with stimulation intensity to evoke distinct patterns of D- and I-waves[2] (Davila-Pérez et al., 2018). These distinct patterns of waves are evoked by selective recruitment of particular neural components of cortical layers, as concluded by Di Lazzaro and Rothwell (2014) and Davila-Pérez et al. (2018). As a comparative example, from the experiments of Di Lazzaro and Rothwell (2014), monophasic pulses in a posterior-anterior (PA) direction at threshold intensities elicited early I-waves (I1), whilst monophasic anterior-posterior (AP) pulses tended to evoke late I-waves, that are more dispersed and have longer latencies, and biphasic pulses elicited more complex patterns of D- and I-waves (Davila-Pérez et al., 2018). These directions and waveforms applied in the study are depicted in Figure 2.14, in addition to a biphasic waveform not mentioned in the example above detailed. Given that the cortical folding impacts the axonal orientation, resulting in different susceptibilities of the targeted cortical neurons, the different waveforms

[2]Recorded corticospinal tract electrical activity when the primary motor cortex or brain areas with projections to the primary motor cortex are stimulated. D- stands for direct, as these volleys are thought to be caused by direct stimulation of corticospinal axons, while I- stands for indirect, as these are volleys recorded later along the corticospinal tract, and thought to be induced by indirect, synaptic activation.

may also affect different neuronal populations (Wessel et al., 2019).

2.6 Safety

Regarding TMS safety, three evidence-based safety guidelines for clinical practice and research were already published: the first in 1996, the second in 2008, and the third in 2021 (Kim and Paik, 2020) (Rossi et al., 2021). In order to ensure the safety of both the patient and the operator of the TMS device, many factors should be taken into consideration, by different entities, at different instants of time. TMS is generally considered safe, but there are some precautions that should be taken into account before the application of the technique. The renewal of the guidelines concerns new potential discoveries regarding the safety of previous, considered safe, used coils, waveforms, stimulators, protocols, etc. but also the application of new stimulators, coils, waveforms, protocols, etc. Adverse events (AEs) have been registered over time with the application of TMS protocols, and potentially harmful interactions of the induced fields with specific biological tissues (brain, heart, etc.), other electronic devices, or suppressive drugs of the patients' conditions being taken at the time of stimulation, are important to study and report. Although not often mentioned, safety guidelines for operators are also important.

Concerning the patients' safety, typical adverse events induced by TMS protocols have different degrees of severity and frequency. The less severe side effects of TMS administration are also the most regular, according to Rossi et al. (2009). In protocols of single-pulse, paired-pulse, rTMS, and TBS, transient headache and local pain are possible and even frequent in the case of rTMS protocols (Rossi et al., 2009). These side effects are undesirable, albeit them being less severe than other potential adverse events, such as prolonged hearing impairments or even seizures. The number of reported seizures, compared to the number of rTMS sessions conducted is very low, which led Rossi et al. (2009) and Rossi et al. (2021) to conclude that the risk of rTMS inducing seizures is very low. Most of the seizures reported to date happened before the first safety guidelines by Wassermann (1998). The reports about seizures are not connected to a single protocol of stimulation, but rather to various stimulation protocols, such as single-pulse, paired-pulse, and rTMS (low and high frequency) (Rossi et al., 2009) (Rossi et al., 2021). Even though a low rate of seizures is observed, before the administration of TMS to any healthy subject or patient, it is important to evaluate several conditions that can lower the seizure threshold of the patient, such as medical conditions, pharmacologic substances intake, and even kinship. If multiple factors that potentially lower the seizure threshold are present,

postponement of the TMS session should be considered (Rossi et al., 2021).

However, despite this theoretical risk of certain pharmacological drugs and kinship to, in conjunction with TMS, trigger convulsive events, a practical clinical risk has not been observed (Rossi et al., 2021). The rate of seizures can even be lower than the data reports, given that some of the seizures reported are potential convulsive syncopes. Other risk factors like sleep deprivation and stress/anxiety have been proven to increase the risk of seizure induction, with sleep deprivation, in studies combining TMS with EEG, being associated with increased cortical excitability. Careful should also be taken with first-time exposure to TMS since in a survey by Lerner et al. (2019), higher percentages of seizures were induced either in the first exposure or within the first three exposures. Deep H-coils also seem to have a higher seizure rate, potentially given their lack of focal stimulation (Rossi et al., 2021).

When the TMS stimulating coil is energized, it produces an intense broadband acoustic artifact that may exceed 140 dB of sound pressure level (SPL), as a consequence of the rapid mechanical deformation of the coil (Rossi et al., 2009). This sound pressure level exceeds the permitted noise exposure limit for impulsive noises (Rossi et al., 2021). Measurements concerning the SPL of frequently used protocols, such as single-pulse and rTMS have revealed values for both protocols exceeding the safety SPL thresholds, even though different studies have revealed different peak SPLs (a consequence of the different acoustic artifacts that measure the sound waves, their features, the features of the coil and stimulus, and the position and distance of the coil from the measurement microphone) (Rossi et al., 2021). Typically underestimated by conventional sound measurements is the sound conducted through the skull bone and consequent risk (Rossi et al., 2021). Nevertheless, there are no reports of hearing sensitivity change, after TMS, across studies, when hearing protection was used (Rossi et al., 2021) (Rossi et al., 2009). Regarding otoacoustic emission, small declines in amplitude were observed by Tringali et al. (2012) in a subset of participants for whom hearing protection was less effective, but this decline was resolved in the subsequent hour, suggesting a temporary effect. However, this is not the case for the degeneration of afferent auditory nerve fibers, which has been shown to be long-term (Rossi et al., 2021). TMS for patients with pre-existing noise-induced hearing loss or having concurrent treatment with ototoxic medications should be applied only after careful consideration of the risk/benefit ratio. Patients with cochlear implants should not undergo TMS, and for patients with hyperacusis present in concurrence with tinnitus and auditory hallucinations, the risk of increased auditory symptoms should be considered (Rossi et al., 2021).

Given the spectrum of psychiatric and neurological conditions, TMS can be

applied as a potential therapeutic alternative, risk assessment concerning the interaction of the magnetic field induced by the TMS coils and nearby electronic devices, implants, and stimulating/recording electrodes has been studied by the scientific community. When TMS is operated in conjunction with magnetic resonance imaging (MRI) or magnetic resonance spectroscopy (MRS) scanners, to probe acute changes in human brain function, the TMS coil must not contain ferromagnetic material and must be able to cope with the increased Lorentz forces the static magnetic field of the MR scanner creates on the coil windings (Rossi et al., 2021). The currently approved TMS coils for use in the MR scanner are only approved for scanners that induce a static magnetic field of 3 Tesla or less (Rossi et al., 2021).

With a typical temperature increase of less than 0.1 ℃, the heating produced in the brain tissue by TMS is considered to be safe. Even so, when skin electrodes and implants, and brain implants, are present in the patients' biological tissues, care should be taken. Skin burns can be caused by temperatures of 50 ℃ for 100 seconds or 55 ℃ for 10 s. Higher electrical conductivity of electrodes made of silver and gold can lead to substantial heat up, potentially leading to skin burns (Rossi et al., 2021). Regarding the brain tissue, a temperature increase over 43 ℃ can cause irreversible damage (Rossi et al., 2021). The magnetic field produced by the TMS coils can also exert attractive or repulsive forces on ferromagnetic or non-ferromagnetic head implants, respectively. As a consequence, displacement of these objects might occur, or proper functioning put at harm. Implants incorporating magnets could be moved or demagnetized, and materials like makeup or scalp tattoos containing ferromagnetic materials can lead to discomfort, but with no risk of inducing any serious adverse event (Rossi et al., 2021).

The magnetic pulses produced by the TMS coils can induce high voltages and currents in nearby wires and electronic devices. When administered concurrently with EEG, the wires connecting to the surface electrodes should be arranged to minimize loops that are coupled to the magnetic field and result in electromagnetically induced voltages and currents, by putting them close to one another, or twisting them together (Rossi et al., 2021).

Electronic implants such as systems for deep brain stimulation or spinal and cranial nerve stimulators, e.g., devices for vagus nerve stimulation (VNS), have either intracranial electrodes connected to wires under the scalp or subcutaneous wires, respectively (Rossi et al., 2021). In these electrode wires, electrical currents can be induced during the delivery of TMS, regardless of whether the implant is turned on or off, increasing the potential for the production of unintended stimulation in the central or peripheral nervous system (Rossi et al., 2021). These electrical currents are

typically induced between a pair of electrode contacts or a pair of lead wire contacts that connect to the implanted pulse generator (IPG) and between an electrode and the IPG case or the IPG side-connector of the lead (Rossi et al., 2021). When too close to electronic implants, there are reports of *ex vivo* studies where the TMS coil at a distance of 2-10 cm could cause malfunction of a deep brain stimulation (DBS) IPG, and at distances equal to or smaller than 2 cm could lead to permanent damage of the IPG (Rossi et al., 2021). On the contrary, there was a study that reported no damage on a VNS IPG caused by the TMS pulses (Rossi et al., 2021).

Regarding cochlear implants, no reports on TMS being performed in people with these implants exist, and the fact that most cochlear implants are not compatible with MRI led Rossi et al. (2021) to conclude that, unless additional safety evaluation showed that there are no AEs, TMS should not be used to stimulate patients with these specific implants. With regards to electronic implants, the studies show that TMS with the figure-of-8 coil is safe in individuals with cardiac pacemakers, VNS systems, and spinal cord stimulators, as long as the TMS coil is not activated closer than 10 cm to electronic components, such as the IPG (Rossi et al., 2021). TMS can also be delivered in subjects with implanted electrodes in the central and peripheral nervous system that are not connected to an IPG, with special caution regarding potential induced currents in connections to external devices (Rossi et al., 2021).

2.7 Outcomes' variability

As the knowledge regarding the consequences of the application of a certain TMS protocol in a certain population is developing, several setbacks may come along the way when comparing the results from different studies. By setbacks, we mean different outcomes from study to study, with the constants between studies being the condition or not of the attendants and the protocol of application. This means that something has changed between studies, in a significant way. There are several factors, to our knowledge, that (most) can be controlled and that may influence the outcomes of identical studies. We will review these in the next pages.

Coils

In order to conduct a TMS study, it is important to be aware of the features related to the coils' operation and, in case of having one, to the control group coil management. TMS coils generate a brief but intense clicking noise, capable of activating the auditory system and a scalp-taping sensation where the magnetic pulse is delivered. The clicking noise is capable of activating the auditory system even if earplugs or headphones are used. This phenomenon has its origin in the

high-intensity and short-duration electrical currents (that generate the magnetic field) when passing through the wire loops shocking against each other, and against the plastic casing of the coil. These sensory effects can potentially distract patients' attention, interfere with the activity of the cerebral networks being probed causally, or even impact task execution. Thus, it becomes important for the success of a TMS study to control these sensory effects in order to achieve success without loose ends (Valero-Cabré et al., 2017).

Last, but not least, regarding the physical processes involving the TMS coils that may condition the outcomes of the studies, long trains of rTMS may heat up the coil and increase the scalp temperature, bringing up discomfort to the participants. This typically requires a coil change in the middle of the experiment. However, there have already been developed water- or oil-cooled rTMS coils to keep the temperature low, allowing for long rTMS procedures (Valero-Cabré et al., 2017). Regarding this constraint, our built-in-house device (Orthogonal Configuration), even though for other reasons, is already water-cooled.

Interindividual variability

As mentioned previously, several TMS studies involving the same protocol, type of population, and other main features, tend to fail when it comes to replicating the results. This leads to a lot of frustration, especially when the results from small studies are unable to be replicated in larger-scale trials. The reasons behind this failure can be related to the fact that non-invasive neurostimulation is a technique for which a large level of interindividual variability occurs. The sources of such variability have already been identified and will be next addressed, as well as whether it is possible to control their effects or not.

Age and gender

The debates on whether gender and age are factors capable of producing changes in rTMS effects remain open for study. However, it has already been observed, in single and paired-pulse TMS studies, that inter-hemispheric inhibition tends to decrease with aging (Valero-Cabré et al., 2017). In terms of gender-related TMS effects, differences in plasticity between men and women still remain controversial. Nevertheless, Pitcher et al. (2003) suggested influences of hormonal rhythms in female participants, given the significant differences in excitability levels following rTMS across the menstrual cycle.

These mentioned factors should and could be taken into account at the time of recruitment for TMS studies, while further, more conclusive studies on these subjects should also be taken in the future (Valero-Cabré et al., 2017).

Scalp thickness and Scalp-to-cortex distance

From patient to patient, there are anatomical differences, specifically in the thickness of the scalp, and in the scalp-to-cortex distance. The electric field generated by the TMS coils on the head layers drops off rapidly with distance from the coil. This means that these anatomical differences in patients will impact more positively or negatively the amount of current reaching the cortical tissue. These differences between patients might explain variations in MEP amplitude or even disparities in clinical effectiveness for the treatment of depression in adults (Valero-Cabré et al., 2017).

Nevertheless, there have already been developed simple metrics that take into account the decay of TMS intensity with depth, as well as differences in scalp-to-cortex distance, in order to estimate the compensatory increases of intensity throughout the scalp.

Individual excitability and neurophysiological traits

Besides scalp thickness and scalp-to-cortex distance, a high variability of intrinsic excitability is observed across individuals, as demonstrated by the characterization of motor and visual excitability markers. The reasons behind this variability possibly rely on the regional neurochemical and cytoarchitectural organization of cortical cell layers, their relative orientation, and their individual coordinated/spontaneous/evoked firing patterns. Nevertheless, these traits are difficult to document with the current neuroimaging techniques. For non-motor/non-visual regions, the strategy among researchers relies on preliminary testing of TMS cognitive tasks at different intensities, or on previously published intensity levels effectively employed in the same region using a similar task. Despite the mentioned strategies, more recently, standardized atlases indexing cortical excitability estimates were developed by recording TMS-evoked cortical potentials throughout the brain regions with EEG (Valero-Cabré et al., 2017).

A neurophysiological trait that has been on the rise, when it comes to TMS application, is the natural frequencies of oscillation related to specific brain regions. TBS protocols, which are based on the naturally occurring theta rhythm of the hippocampus, as mentioned previously, tend to emulate better therapeutic outcomes when compared with other conventional rhythmic protocols. What happens is that, when studying rhythmic TMS applications, optimal increases of power at a specific frequency band by phase resetting or entrainment are achieved when the frequency of the stimulation source matches these natural frequencies of a given region, characteristic for each participant (Valero-Cabré et al., 2017). Nevertheless, this is a

TMS subject with future studies yet to happen in order to be a reference when it comes to the application of this non-invasive technique.

White matter connectivity

The human nervous system is extremely complex. An important feature of neuronal structures, that affects our knowledge of the potential outcomes of TMS stimulation is that, even though we know a certain region of the brain is responsible for the processing of a specific function, some of the neurons of this region can have connections to neurons of other regions with different functions, making everything more complex. What we have is that by modulating the activity of the "first neuron", many others related to different functions, and part of the network of this neuron are potentially affected. This means that TMS spreads its local effects across networks, being dependent, this way, on the richness and sign of structural white matter pathways.

According to some studies, a significant inverse correlation between inter-individual microstructural properties of white matter pathways and the impact of single pulse or rhythmic TMS patterns on specific tasks has been observed for different tasks and pathways (Valero-Cabré et al., 2017). This evidence has led Quentin et al. (2015) to suggest that white matter connectivity could be used to predict the participants' behavioral response to stimulation (Valero-Cabré et al., 2017).

Genetic phenotypes

As seen until this part, there are many factors conditioning the potential outcomes of TMS application. rTMS applications are intended for long-term modulation of brain regions working in a disabling manner. As seen previously in Section 2.3.2.4, the "speculation" about whether these long-term modulations induced by TMS are due to synaptic plasticity processes already has some study results in humans that point in that direction. However, these synaptic plasticity mechanisms, such as LTD and LTP rely on the expression of activity-dependent genes. The importance of these genes falls on their coding for several physiologic "constituents" involved in synaptic plasticity, such as proteins, voltage-dependent receptors units/subunits, and neurotransmitters, among others, by unmasking existing "silent" connections, or via the germination of dendritic spines and axonal branches (Valero-Cabré et al., 2017). What is being discussed are the individual differences in terms of the expression of these important specific genes. It has been observed in non-invasive stimulation studies that these differences might play a role in predicting the modulatory effects of rTMS. One particular case is the Brain-Derived Neurotrophic Factor. This is a protein that influences memory and learning, by

having an action on dendrogenesis, synaptogenesis, neurotransmitter signaling, and regulation. It has been reported that, in participants carrying a specific allele of this protein gene, inhibitory and facilitatory offline effects of rTMS protocols were approximately absent, leading to the conclusion that people carrying this allele of this gene are less susceptible to the rTMS effects than people carrying other alleles. Thus, there seems to be here an open door to, by determining the BDNF polymorphisms in saliva or small blood samples of the studied population, at a post-hoc approach, identify and exclude from main analyses potential outliers (Valero-Cabré et al., 2017).

State dependency

All of the previously mentioned control conditions were either of physiological or anatomical nature. State dependency is also of a physiological nature, but this condition can be manipulated by the study operators in order to achieve a specific goal, i.e., the nature of the study is not adapted to this condition, but this condition can be adapted to the nature of the study. State dependency is a term that refers to the dependency of the direction and magnitude of the modulatory TMS and rTMS effects on the level of ongoing activity at the site of stimulation. It has been observed that areas of the brain with low excitability levels at the time of receiving excitatory rTMS stimulation protocols are more likely to suffer lasting excitatory effects, whilst areas with high excitability levels are more likely to suffer lasting inhibitory effects at the time of receiving inhibitory TMS stimulation protocols. Studies have even shown, in an extreme case, that excitatory TMS patterns can lead to inhibitory effects when the stimulated brain region was already at a high excitability state, and inhibitory TMS patterns of stimulation can lead to excitatory effects when the stimulated neuronal cluster is at a low excitability state, previous to stimulation. That is, an inversion of the expected direction of modulation is observed (Valero-Cabré et al., 2017).

With state dependency comes an opportunity for researchers to improve the expected outcomes of their study. By priming the stimulation sessions with specific tasks, prior to or during the stimulation session, researchers can condition the neuronal population activity to get the best outcomes. However, this priming may not only rely on specific tasks but also on other stimulation protocols applied previously to the stimulation session, conditioning the neuronal population to a best-suited pattern of activity previous to the stimulation session (Valero-Cabré et al., 2017). Thus, a well-suited manipulation of neuronal activity may allow researchers to shape the direction, selectivity, and magnitude of the neurostimulatory effects on small and complex regions, which raises even the possibility to overcome the limitations

in spatial resolution of TMS approaches in the human brain (Valero-Cabré et al., 2017).

2.8 Coils

Coils are a crucial element of a TMS device. Through these structures flow the currents that will induce the magnetic fields responsible for inducing the eddy currents in the brain. Several physical characteristics of these structures, such as, e.g., their shape and size will determine the spatial pattern and distribution of the induced E-field in the brain. It is important for researchers and physicians to be aware of the best-suited coil type, in terms of induced E-field, for the brain region they want to stimulate. In these sections, we will address the state-of-the-art coils, including deep stimulation coils, and their features, as well as the recent developments and studies regarding new coil types or stimulation techniques with promising clinical outputs.

2.8.1 TMS coils

Circular coil

The circular coil is the simplest TMS coil. Classical circular coils are composed by high-density circular wire windings covered by a plastic case, as exemplified by the commercial coil depicted in Figure 2.15 a). The induction capacity of circular coils mainly relies on superficial cortical regions, having this type of coils a dramatic induced electric field drop when deep brain regions are concerned (Roth et al., 2002). The maximum induced electric field, in the brain, given the coils structure, has an annulus-shaped distribution, making it lacking focality (Valero-Cabré et al., 2017) (Siebner et al., 2009), as it is depicted in Figure 2.15 b).

The problem with stimulating deep regions with this type of coils is that neither their geometry, nor size, are the most adequate, and an increase in stimulation intensity at the source would be needed. However, this approach endangers the patient's safety, possibly leading to undesirable effects. As it was demonstrated by Bagherzadeh and Choa (2019), increasing the size of the coil could lead to a smaller induced field decay rate. Nevertheless, when it comes to dTMS, only increasing the size of a single circular coil has not been the followed approach to improve stimulation with depth. But these coils must not be completely discarded, given the current state and needs of TMS study and applications, since, e.g., these coils have useful applications regarding the measurement of the excitability of specific cortical

(a) **(b)**

Figure 2.15: **a)** Magstim circular coil. **b)** Simulation model of a Magstim circular coil, and corresponding electric field distribution in the brain. Adapted from (Bagherzadeh and Choa (2019), Deng et al. (2014)).

areas.

Figure-8 coils

Figure-8 coils arose from the necessity of a more focal stimulation. Developed by Ueno et al. (1988), these coils had the purpose of fulfilling the gap of a non-focal stimulation left by the first TMS coils developed, and previously analyzed, the circular coils (Wei et al., 2017). Geometrically represented by two side-by-side circular coils, each with currents that flow in opposite directions, these coils are capable of inducing a positive overlap of the induced fields at a central junction, as depicted in Figures 2.16 a) and b), given that at this region of space the currents point towards the same direction (Koponen et al., 2017) (Rastogi et al., 2017). This current distribution will lead to a summation of the induced electric fields under the junction, becoming this region where higher intensity induced fields are registered (approximately double the induced field at the edges of the wings), thus inducing the desired focal stimulation (Valero-Cabré et al., 2017) (Siebner et al., 2009). Therapeutic application in depressive patients is marked with FDA approval for depression treatment (Deng et al., 2014). Over the years, this coil design has led other researchers to develop different coils with similar designs (some of them to be addressed posteriorly), but typically with different coils' orientation ($\neq 180^o$), and size, with the main purposes of these alterations in geometry being an increased focality of stimulation (Rastogi et al., 2017), or an increased penetration depth but smaller focality. Thus, we can state that this coil design has been a major reference in TMS studies, either for therapeutic applications, diagnostic, or development of other coils (Wei et al., 2017). To this date, this coil design is still a reference when it

comes to the ratio between focality and depth of penetration. None of the many coils designed over the last twenty years has shown significant improvements compared to the figure-8 in their focality capacity while maintaining the required field intensity to stimulate areas at the surface of the brain (Rastogi et al., 2017).

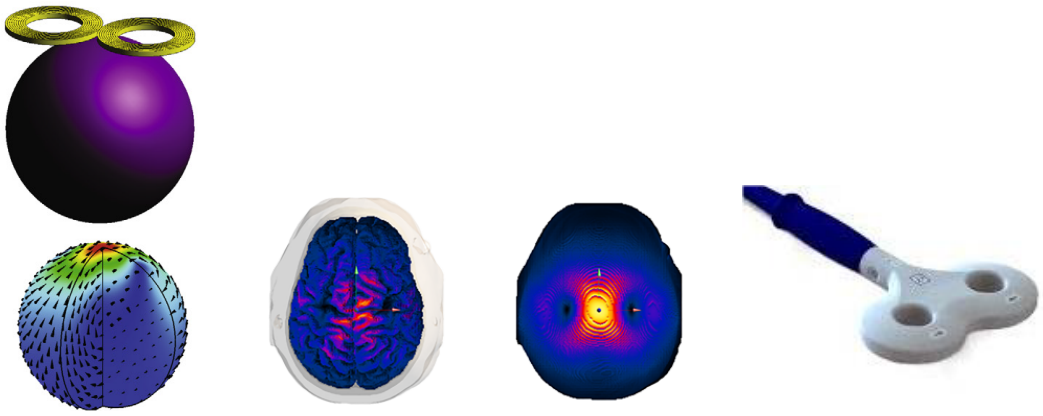

(a) **(b)** **(c)**

Figure 2.16: **a)** Simulated model of a Magstim 70 mm figure-8 coil with corresponding electric field distribution in the brain. **b)** Induced electric field on the scalp and gray matter of a figure-8 coil over the vertex. **c)** Magstim figure-8 coil. Adapted from (Deng et al. (2014), Rastogi et al. (2017), Bagherzadeh and Choa (2019)).

2.8.2 Deep TMS coils

The study of neuropsychiatric disorders has given researchers evidence regarding some neurophysiologic traits behind each specific disorder. It has been observed and reported that for many disorders the affected regions are located not only in cortical tissues but also in non-superficial brain areas (Wei et al., 2017). This evidence led modulatory therapies fields of study, such as TMS, to adapt and develop new stimulators and coils capable of stimulating these deeper brain areas. As a result, dTMS coils started to be developed and consequently studied by researchers, with a focus on their field induction capacity, safety, and therapeutic potential for several disorders. The challenge was to develop coils capable of stimulating deeper than the previous TMS coils (figure-8 and circular coils), as a function of the distance from the coil (Roth et al., 2002). Nowadays, there are already, in some countries and continents, heavily studied and legally approved dTMS coils as therapeutic tools for several neuropsychiatric disorders.

The accumulating evidence suggesting that the nucleus accumbens plays a fundamental role in mediating reward and motivation, as well as the association of other

deep brain areas, such as the amygdala, and the ventral tegmental area, among others, with reward circuits, led Roth et al. (2002) to develop the Hesed-coil (H-coil). The main purpose of Roth et al. (2002) was to develop a coil capable of stimulating deep brain regions, especially the nucleus accumbens and the nerve fibers connecting the prefrontal cortex with the nucleus accumbens, without increasing the electrical field intensity in the superficial cortical regions. With this goal in mind, the basic concept behind this new coil design relied on generating a summation of the electric field with depth by generating electric fields with a common direction in several locations around the head. At the time of its development, the double-cone coil was the main reference for stimulating deep brain regions, but it could not stimulate the aimed areas by Roth et al. (2002) without putting at risk the patients from suffering pain sensations and other side effects (Roth et al., 2002). Nowadays, the family of H-coils turned into a vast family of coil designs, aiming at the stimulation of different networks and brain areas, with the main purpose of treating different disorders (Tendler et al., 2016).

The H1-coil is likely the most acknowledged and tested ever since its FDA clearance for the treatment of treatment-resistant unipolar depression patients. This turned out to not be the only legal clearance in the world by this coil. In Europe, the H1-coil is legally cleared for the treatment of unipolar and bipolar depression, negative symptoms of schizophrenia, and post-traumatic stress disorder, thus increasing the number of therapeutical applications of this coil (Tendler et al., 2016). Concerning its stimulation pattern, the H1-coil has as its main targets the left, right, and medial prefrontal cortex areas, with a left hemisphere preference. Figure 2.17 a) depicts colored field maps indicating the absolute magnitude of the electric field for the H1-coil, making, thus, possible, the previously mentioned stimulation pattern to be seen. Besides the H1-coil, other designs of the H-coils family are cleared in Europe for the treatment of different conditions, such as Alzheimer's, chronic pain, smoking cessation, Parkinson's, stroke rehabilitation, and multiple sclerosis (Tendler et al., 2016).

Nevertheless, the family of the H-coils might not be the only dTMS therapeutic alternative for patients with neuropsychiatric disorders. Other coils' and stimulation protocols' therapeutic efficacy and safety have been, and are being studied. The double cone coil is a larger figure-8 coil with a fixed angle of 95 degrees (toward the patient's head) between the two wings, as depicted in Figure 2.18, typically capable of stimulating regions at a depth of 3-4 cm (leg motor area) and commonly involved in dTMS studies, either simulations or experimental (Lu and Ueno, 2017a)(Rossi et al., 2021).

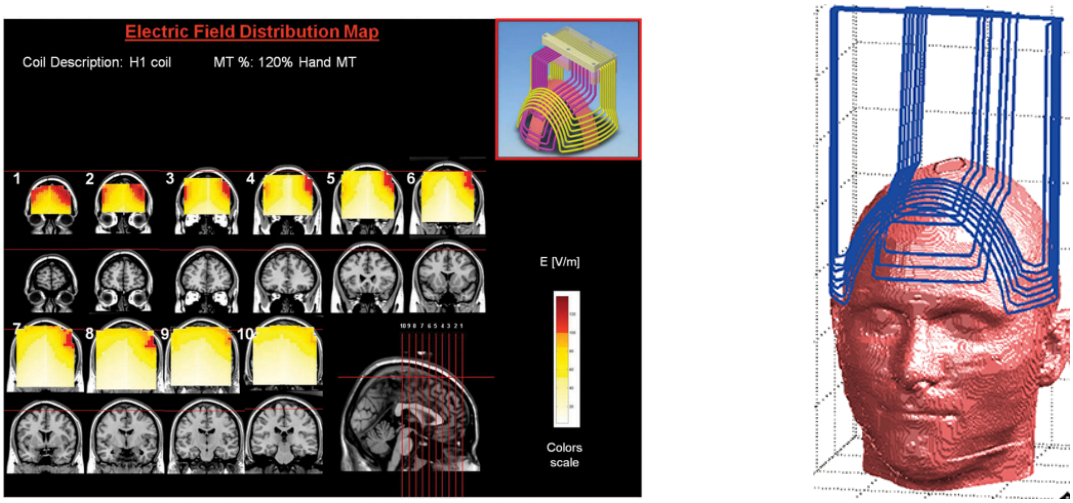

(a) **(b)**

Figure 2.17: **a)** Colored field maps for the H1-coil. 10 coronal slices are depicted, and each pixel depicts the absolute electric field at 120% motor threshold stimulation. Red pixels represent an intensity above the threshold for neuronal activation. **b)** Simulation model of an H-coil. Adapted from (Tendler et al. (2016), Lu and Ueno (2017a)).

In a study by Deng et al. (2014) concerning TMS coil designs for deep stimulation, the double cone coil was the second most energy efficient and, even though when stimulating deep targets (6 cm deep) the scalp stimulation was 10-20 times the threshold, Deng et al. (2014) considered this as a suitable coil for some dTMS studies given its high energy efficiency and balance between stimulated volume and superficial strength (Deng et al., 2014). Among the evaluated coils by Deng et al. (2014), the conventional double cone coil was the one with the highest focal capacity capable of stimulating deep targets within the energy limit of standard TMS devices. Nevertheless, the therapeutic potential of the double cone coil is still under study, and no legal clearance report was found for any therapeutic application regarding this coil.

Another state-of-the-art family of coil designs is the Halo coils. Figure 2.19 represents a simulation model of the original Halo coil, a large circular coil intended to be placed around the human head. This large circular coil was developed to stimulate the brain in-depth (Lu and Ueno, 2017b). Given its simple design and consequent room for improvement, the Halo coil design has been suffering various mutations with different purposes. One of the mutations of the Halo coil is the Halo circular assembly (HCA) coil. This coil design consists of two circular coils, a bigger circular coil around the head (Halo coil), and a smallercircular coil on top of the

(a) **(b)** **(c)**

Figure 2.18: **a)** Simulation model of a double cone coil, and respective induced electric field distribution in the brain. **b)** Magstim double cone coil. **c)** Simulation model of a double cone coil over a realistic head model. Adapted from (Deng et al. (2014), Bagherzadeh and Choa (2019), Lu and Ueno (2017a)).

head. Similar to this design, the Halo figure-8 (HFA) assembly coil was introduced by Lu and Ueno (2015). This design is essentially the same as the HCA, except the circular coil on top of the patient's head is replaced by a figure-8 coil. Both these updates of the Halo coil design had a simple main intention: to improve the stimulation in depth. These coils' performance has been assessed in several studies, and even new updated designs have been proposed and studied. Figure 2.20 depicts these two coil designs, where they are represented by the simulation models studied in Wei et al. (2019) and Lu and Ueno (2015) investigations. In a group-level analysis of the induced electric field in deep brain regions by different TMS coils, Gomez-Tames et al. (2020) concluded that the HCA and HFA coils induced the highest electric fields in all deep brain regions with respect to the cortical electric fields. Of all the assessed coils these are the coils that might require the lower stimulation output of the TMS stimulators in order to target specific deep brain regions. In particular, the HCA was the coil that produced the highest penetration, but also the wider field spread, followed by the HFA coil (Gomez-Tames et al., 2020). This wide-field spread of the HFA coil led Lu and Ueno (2017b) to study an alternative coil design inspired by the HFA coil, but capable of inducing a more focal stimulation. By shifting one of the wings of the figure-8 coil on top of the head away from the head, Lu and Ueno (2017b) found that a smaller depth of stimulation was induced, but a more reasonable focality was achieved, proposing this way the design depicted in Figure 2.21 as a suitable alternative for the stimulation needs of some specific study/therapeutical application looking for focality and penetration depth.

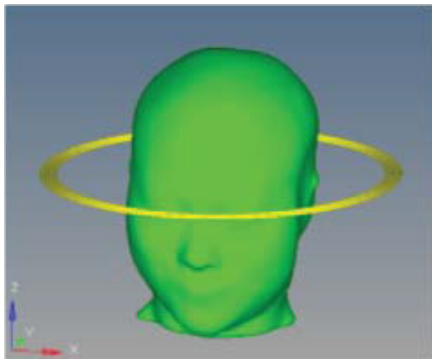

Figure 2.19: Simulation model of a Halo coil over a realistic head model. Adapted from Wei et al. (2019).

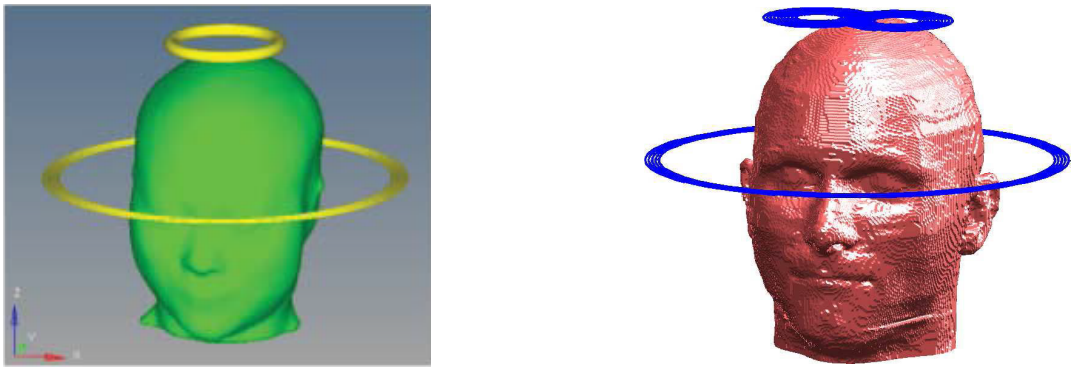

(a) **(b)**

Figure 2.20: **a)** Simulation model of an HCA coil over a realistic head model. **b)** Simulation model of an HFA coil over a realistic head model. Adapted from (Wei et al. (2019), Lu and Ueno (2015)).

Wei et al. (2019) studied via simulation the induced magnetic and electric fields in a realistic head model by four different coils. The four coil designs were variations of the Halo coil, being one of those coils the Halo coil itself. The other studied coils were the HCA coil and the other two were designated as the HPC and the HMTC coil. The HPC coil design is essentially an HCA coil with two parallel to the head circular coils on both sides of the ears. The HMTC shares the same geometric distribution as the HPC, but instead of the inner parts of the coils surrounding the head being empty, they are occupied by five small circular coils, which are tangent to each other. An easier understanding of the geometry of these coils is possible with the depicted designs in Figure 2.22. The two coils were designed for different purposes. The HPC coil was designed to get a better stimulation effect, whilst the HMTC coil was designed in view of the brain safety requirements under high-intensity electric fields (Wei et al., 2019). The study results show that the

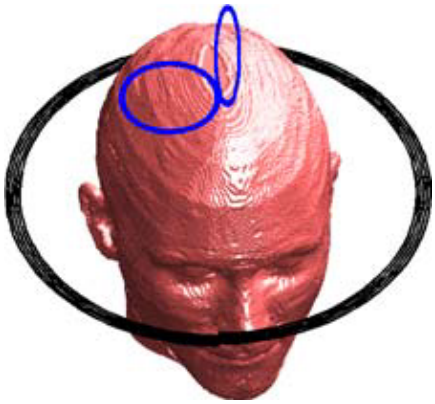

Figure 2.21: Simulation model of an HFA coil with the figure-8 coil having the right wing bent 80 degrees, over a real head model. Adapted from Lu and Ueno (2017b).

induced electric fields at two specific depths (30 mm and 60 mm) were larger both in the periphery and center parts of the brain for the HCA, HPC, and HMTC coils when compared to the electric fields induced by the Halo coil. The overall brain distribution of the electric field for the HPC and HMTC was very similar, but it was the HCA and HPC coils that induced the maximum values of the electric field in deeper regions. Nevertheless, the HPC and HCA coils also induced higher E-fields on the skin, muscles, eyeball, and optical nerve. Given that the HMTC coil induced very similar intensities and distribution of the electric fields in deeper brain regions to the ones induced by the HPC coil, but reduced electric field strength on tissues prone to discomforts, such as muscle, eyeball, and optical nerve, this was considered by the authors the best solution of these family of coils for the stimulation of deep brain regions (Wei et al., 2019). To our knowledge, this coil only exists as a simulation design, and, as a consequence, needs further study for its potential physical development.

Significant developments in dTMS stimulation protocols have also been made not concerning simply the coil design, but instead focusing on optimizing the way the electric fields are induced in the brain to achieve a deeper and/or more focused stimulation. Sorkhabi et al. (2020) introduced a temporal interference (TI) concept to achieve focal and steerable stimulation in the brain. Temporal interference is a stimulation method that works by inducing two high-frequency electric fields (induced by two independent coils), with a slight frequency difference. The purpose of the method is that the neurons at the intersection of the two electric fields "follow" the frequency difference between the two fields. This frequency difference phenomenon, also called beat frequency, can be easily visualized in Figure 2.23.

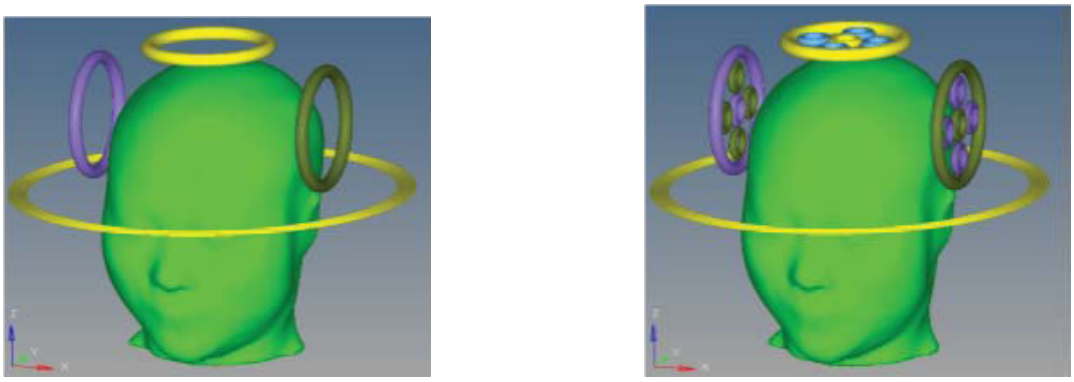

(a) **(b)**

Figure 2.22: **a)** Simulation model of an HPC coil over a real head model. **b)** Simulation model of an HMTC coil over a real head-model. Adapted from Wei et al. (2019).

Based on the recognized intrinsic nonlinear nature of the nerve fibers, acting as low-pass filters, neurons are prevented from directly following high-frequency sinusoidal fields. As observed by Grossman et al. (2017), in an animal model study, neurons, when stimulated by two identical high-frequency electric currents, have shown to be unable to follow any of the currents. However, when the two high-frequency currents are slightly different, the nerves are able to follow the frequency difference, typically called beat frequency (Sorkhabi et al., 2020). This phenomenon is recognized as temporal interference, and the purpose of Sorkhabi et al. (2020) was to study, for the first time, the concept of temporal interference for TMS with different coil orientations via simulation.

Sorkhabi et al. (2020) studied the performance of three different TI-TMS scenarios, and two commercial coils (single circular and figure-8 coils). The three different TI-TMS scenarios consisted of two single circular coils equally distanced in all arrangements, with one scenario having the coils at a 90-degree angle from each other, targeting the center of the brain, the other having the two coils with a 90-degree angle from each other targeting the primary motor cortex, and lastly a 180-degree angle with the center of the brain as the target. The study results show that the TI-TMS method coils are able to quantitatively stimulate deeper and more focal regions, compared to the single circular and figure-8 coils. Among the simulated protocols, the TI-TMS approach results obtained the best trade-off between depth and focality. However, for a stimulation depth of 1.4 cm from the top of the head, the energy consumption of the TI-TMS method was twice the energy consumption of the figure-8 coil, given the need for two stimulation pulses. Nevertheless, when compared to other coil designs for deep stimulation, the energy consumption of the

TI-TMS method was smaller.

The other main result of this study was the possibility to steer the stimulation target from the center of the electric field interference by varying the ratio of the stimuli amplitudes while holding the voltage sum constant. This approach leads to a shift of the stimulated area towards the coil with the lower voltage, enabling the coil design to shift the stimulated area without the need for movement from robotic systems, or even the need for an accurate placement (Sorkhabi et al., 2020).

One of the potential downsides of this stimulation method is that, even though the neurons are not expected to follow the high-frequency stimuli, they might be activated in a different way, leading to what was observed via simulation as an activation, when initially turning on the stimulation, and no further reaction (Sorkhabi et al., 2020).

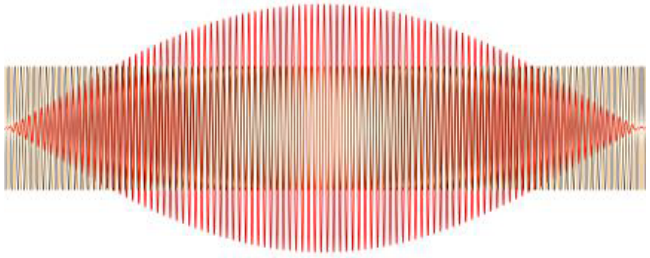

Figure 2.23: Shape of the individual coils' waves, with frequencies f and f+δf, and their interference pattern, the beat frequency. Adapted from Sorkhabi et al. (2020).

It was shown that the rate of change of the tangential electric field induced in a certain brain area leads to changing the membrane potential of the neurons. Following this, Jafari and Abdolali (2019) conducted a simulation study where the main criterium for the coils array design was to maximize the rate of change of the tangential electric field along the nerve cells fibers while minimizing the absolute value of the electric field in the target region as well as in the whole brain. Supported by an advanced brain imaging technique named tractography, the authors were able to detect the direction of part of the nerve fibers of the cingulum section of the brain, the target area, as depicted in Figures 2.24 a) and b).

In order to maximize the rate of change of the induced tangential electric field, the coil array was designed in such a way that every two coils cancel each others' absolute value of the electric field. Based on a proof-of-concept design consisting in a two-coil array, a 20-coil system was designed and its performance was compared with that of an HFA coil, being both the coil arrays pictured in Figure 2.24. With the ability to rotate the larger coil of the HFA coil, the best results for the induced electric field along the nerve fiber in the cingulum section were obtained when the

larger coil suffered a 40 degrees rotation, as depicted in Figure 2.24 d). The goal of the simulated 20-coil system was to achieve a rate of change of the tangential field equal to that of the HFA coil in the same brain section.

The results show that the same performance was achieved by the 20-coil system in the cingulum section nerve fibers as well as by the HFA coil, with the advantages of the 20-coil system desirably stimulating a much smaller volume of the brain and requiring less current source for the same stimulation goal (Jafari and Abdolali, 2019).

This approach can lead to different future DTMS and TMS system designs, based on more accurate mapping of the direction of the neurons and on potentially desired more focused stimulations with smaller electric fields induced in other brain areas (Jafari and Abdolali, 2019).

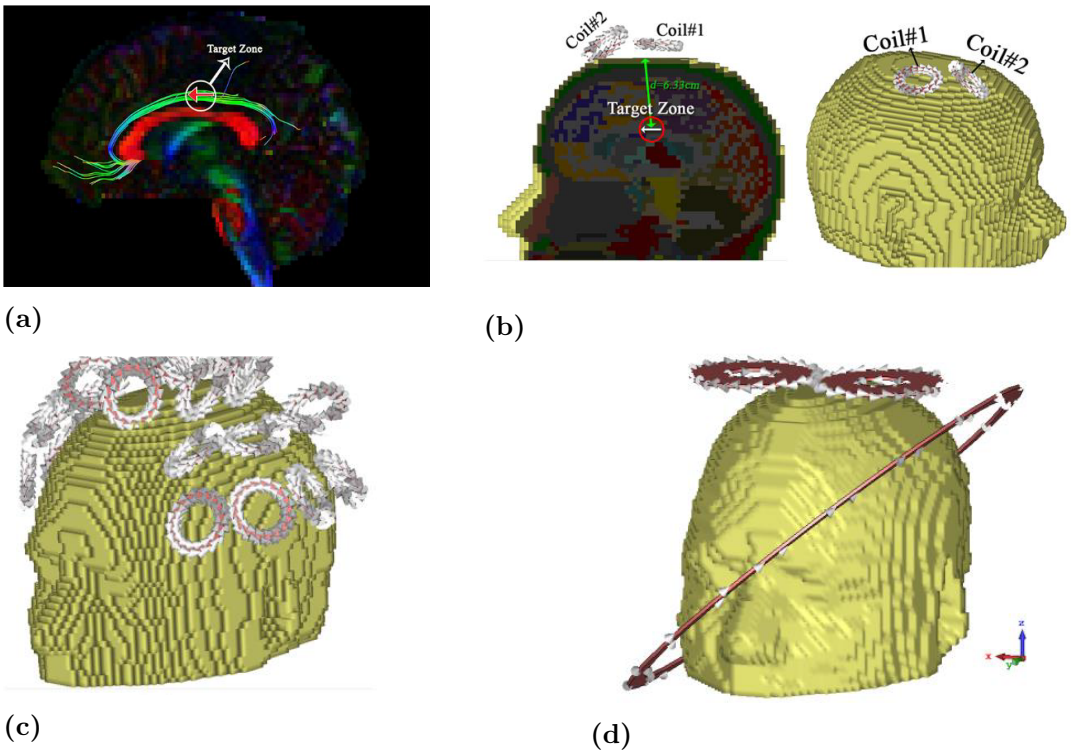

Figure 2.24: **a)** Based on the tractography imaging technique, the target zone's (cingulum section) nerve fiber direction is detected. **b)** Sliced HUGO model at the plane of the target zone and representation of the 2 stimulation coils array. **c)** Simulated 20-coil array around the HUGO head-model. **d)** Representation of the 40^o rotated Halo figure-8 coil studied around the HUGO model. Adapted from Jafari and Abdolali (2019).

3

Potential and effective clinical applications of TMS (simulated, studied and legally approved)

TMS has been studied as a potential therapeutic intervention for several psychological and neurological conditions. The number of conditions that can possibly benefit from Transcranial Magnetic Stimulation has been increasing with the increase of studies concerning TMS over the last few years. In this chapter, we present these conditions, some studies that show the TMS therapeutic potential for the conditions, and in some cases ending with some final notes on what still has to be done for the stimulation protocols to become certified therapeutic interventions, as well as the potential best ways each condition can benefit from TMS.

3.1 Substance use disorder (SUDs)

Substance use disorders (SUDs) are at the forefront of the worldwide causes of morbidity and mortality. The potential of rTMS in SUDs therapy is related to this technique's capacity of influencing neural activity in the short and long term, thus, possibly affecting behaviors related to drug craving, intake, and relapse (Diana et al., 2017). More precisely, dTMS seems to be the most appropriate application for drug craving, since the growing literature suggests that the craving-related brain structures include the prefrontal cortex (PFC), the anterior cingulate cortex (ACC), the insula, the hypothalamus, the amygdala, the hippocampus, the nucleus accumbens and the ventral tegmental area (VTA) (Fiocchi et al., 2018). Most of these areas are located deep in the brain, as depicted in Figure 3.1, therefore making it impossible to stimulate them with standard rTMS coils (Fiocchi et al., 2018). However, some studies with rTMS coils have already presented beneficial results in terms of intake and craving for people with this disorder.

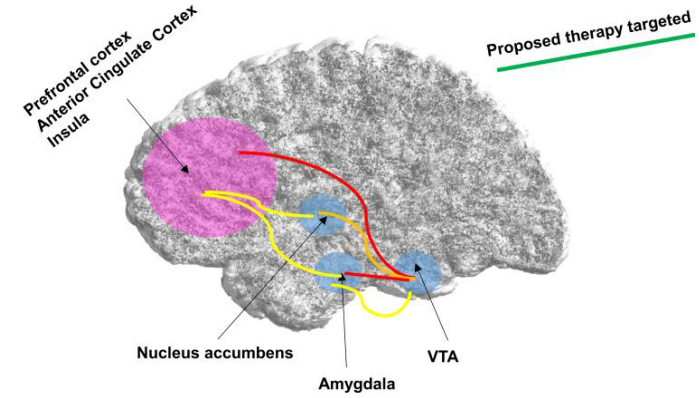

(a)

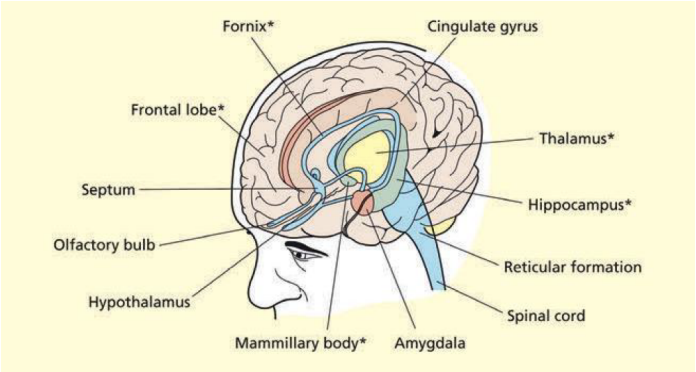

(b)

Figure 3.1: Representation of some of the brain areas associated with craving-related disorders, and respective connections between these areas. Despite other areas being identified, the areas of interest in **b) are the hippocampus, amygdala, and hypothalamus**. Adapted from (Fiocchi et al. (2018), Ward (2015)).

3.1.1 Alcoholism

Alcohol dependence has a global prevalence of 2.6%. There are documented treatments with beneficial effects for this disorder, but their effect sizes are limited and relapse rates are high (Perini et al., 2020).

Addolorato et al. (2017) studied the effect of dTMS over the dorsolateral prefrontal cortex (DLPFC) on Dopamine Transporter (DAT) availability and alcohol intake in fourteen Alcohol Use Disorder (AUD) treatment-seeking patients. Dopamine is a known neurotransmitter for playing a key role in the neurobiological mechanisms underlying chronic abuse and dependence. DAT is a plasma membrane protein that translocates the released dopamine from the extracellular space into the presynaptic neuron. Alterations in genes coding for DAT genes are a risk factor for developing

AUD (Addolorato et al., 2017). Previous studies to that of Addolorato et al. (2017) have shown the effect of rTMS on the excitability of mesolimbic and mesostriatal Dopaminergic pathways, suggesting, that way, the use of this technique as a potential therapeutic alternative in psychiatric disorders associated with abnormal dopaminergic activity and altered cortical excitability. The hypothesis of Addolorato et al. (2017) was to study the alcohol intake in AUD patients submitted to rTMS, alongside, for the first time, with the study of the striatal DAT availability. The selected stimulating area was the DLPFC. This is a known brain area for increasing dopamine release in the striatal pathway, after rTMS stimulation. This way, boosting the dopamine system may have therapeutic effects in reducing alcohol intake (Addolorato et al., 2017).

In the end, the study consisted of eleven patients randomized into two groups: real and sham stimulation. Five patients received high-frequency (10 Hz) stimulation and six patients were submitted to sham stimulation, 3 sessions per week, for 4 weeks, in a total of 12 rTMS sessions. For this study an H-coil was considered, allowing, already, deep stimulation of the brain. The patients underwent baseline Single Photon Emission Computed Tomography (SPECT) assessment of striatal DAT availability, 24 hours after their last drink. After the 4 weeks of rTMS sessions, these patients underwent the same SPECT assessment of striatal DAT availability, also 24 hours after their last drink. It was considered, from a normal SPECT database, a healthy subjects control group for comparison of the striatal DAT availability between the groups. This healthy controls data was collected via the same SPECT procedure as on the AUD patients.

Regarding the study results, state anxiety levels reached a significant reduction in the real group, but not in the sham group. Trait anxiety and current depression suffered no significant variations in both groups. Regarding alcohol intake, a significant increase in terms of abstinence days, as well as a significant decrease in terms of the number of drinking days was only achieved by the real group. In addition, the number of drinks per drinking days, and total drinks, significantly decreased in the real group, but both parameters did not change in the sham group. Comparing the DAT availability in both the real and sham groups to that of the healthy subjects group, an increased DAT availability in the caudate and putamen bilaterally was observed, previous to treatment, in the two treatment sample groups. However, after the 4-week rTMS treatment, the striatal DAT availability in the real group decreased to levels similar to the healthy subjects group, whilst the sham group striatal DAT availability remained unchanged. These positive results suggest that rTMS produces neurobiological effects in areas distant from the appli-

cation site, strengthening the hypothesis that cortical stimulation can also modulate sub-cortical activity and functions (Perini et al., 2020).

Another study, by Girardi et al. (2015), assessed the effect of add-on dTMS stimulation in patients with dysthymic disorder comorbid with AUD. The aim of the study was to assess the response of the AUD patients to an add-on dTMS treatment, comparatively to the response to standard treatment. During the study, 10 patients received add-on dTMS treatment, and 10 other patients received standard treatment. 20-Hz dTMS stimulation was delivered to the add-on dTMS treatment patients. The stimulation was delivered bilaterally over the DLPFC, given the knowledge of this area as dysfunctional in mood and substance disorders (Girardi et al., 2015). Patients in the add-on bilateral dTMS (dTMS-AO) underwent 20 sessions of dTMS, 5 sessions a week, for a total of 4 weeks. All the patients from both groups were abstaining from alcohol for, at least, 1 month before the first dTMS session, and undergoing standard detoxification treatment was kept throughout the study for both groups, with the addition of dTMS sessions for the dTMS-AO group.

The study results have shown a faster improvement of depressive and craving symptoms for the patients involved in dTMS-AO treatment. This improvement was significantly greater by the end of the treatment (after the 4 weeks) in the dTMS-AO group, comparatively to the standard treatment group. However, by the time of the 6-month follow-up assessment, this dTMS-AO group advantage, comparatively to the standard treatment group, disappeared for mood and general psychiatric conditions, while it was maintained significantly greater for craving and functioning.

These results suggest a possible utility of add-on dTMS for the treatment of patients with comorbid dysthymic disorder and AUD, with the important result of a significantly greater improvement when undergoing this add-on dTMS treatment, comparatively with that of standard treatment for craving symptoms, after the treatment and at the follow-up assessment. However, given the small sample, and the lack of a sham group, the results must be considered with caution (Girardi et al., 2015).

3.1.2 Tobacco

Tobacco smoking is considered by the World Health Organization (WHO) one of the biggest public health threats the world has ever faced. It kills more than 8 million people around the globe each year, given that 7 million of those deaths are the result of direct tobacco smoking intake, while around 1.2 million are non-smokers

exposed to second-hand smoke (Tobacco, 2021).

Like with many other substances, a lot of tobacco smokers become addicted, and even acknowledging the negative consequences of tobacco intake, it is hard for them to control compulsive drug-seeking behavior. Many smokers express a desire to reduce or stop tobacco intake, given their recognition of these negative consequences. However, the relapse rate is high among those who attempt to quit without assistance, with a value of approximately 85% (Dinur-Klein et al., 2014). Numerous successful, in terms of short-term effects, tobacco dependence medications exist, but their long-term positive outcomes are relatively low (Dinur-Klein et al., 2014). Tobacco smoking addiction comes primarily from the effects of nicotine on the central nervous system. Nicotine stimulates the mesolimbic dopamine system, which is a system that has projections to reward-related brain areas, like the prefrontal cortex (PFC) and the nucleus accumbens. Besides nicotine's effects on the central nervous system, this drug "also alters the capacity of gamma-aminobutyric acidergic pathways to inhibit dopaminergic activity". Chronic nicotine intake induces long-lasting neuroadaptations and altered cortical excitability (Dinur-Klein et al., 2014).

Tobacco smoking is, thus, as exposed above, a public health problem with no long-term significant available therapy. Knowing the capacity of rTMS for inducing lasting changes in neural excitability and dopamine release, this technique emerges as a potential alternative therapy to this addiction.

Dinur-Klein et al. (2014) conducted a study where 115 adults who smoked at least 20 cigarettes/day and failed previous treatments were recruited. Previous studies from these study authors, in animal models, and humans, suggest that "repeated activation of cue-induced craving networks followed by electromagnetic stimulation of the dorsal prefrontal cortex can cause lasting reductions in drug craving and consumption". It was hypothesized by the authors that disrupting these circuitries by stimulating the PFC and insula bilaterally with dTMS could induce smoking cessation.

The PFC is a brain reward-related area that is part of the mesolimbic dopamine system. The suggestion of the obtained results from previous studies to the one being discussed was that high-frequency rTMS stimulation of the DLPFC can attenuate nicotine consumption and craving. The problem arises from the limited intensity and duration of these effects (Dinur-Klein et al., 2014). The insula is a lateral deeper area of the PFC, as depicted in Figure 3.2, and the evaluation of changes in cigarette smoking after brain damage revealed that damage to the insula is significantly more likely to induce smoking cessation than damage that does not affect the insula. This is also a finding consistent with the crucial role of the insula in other drugs and food-

related cravings (Dinur-Klein et al., 2014). Since previous studies were performed with a standard TMS coil, like the figure-8, which only allows stimulation of more superficial and smaller brain areas, thus not stimulating deeper brain areas, like the insula, Dinur-Klein et al. (2014) decided to study the effects of a deeper and bilateral stimulation of the PFC, including, therefore, the stimulation of the insula. The study design consisted of a double-blind, placebo-controlled, randomized clinical trial. The study authors decided to study the effects of smoking cues prior to the treatment in order to understand if this cue exposure enhances the treatment efficacy. This way, the study participants were randomly allocated to 6 experimental groups. There were 3 stimulating TMS conditions (high-frequency, low-frequency, and sham) and 2 smoking cue conditions (cue, no cue) for each of these TMS stimulation conditions, making a total of 6 groups. Of the 115 treatment subjects, only 77 completed the whole study. The treatment frequencies for the high-frequency and low-frequency protocols were, respectively, 10 and 1 Hz. Each participant in all the treatment groups received 10 daily treatments within 2 weeks and 3 non-consecutive treatments in the third week. The cues were presented to the patients prior to the rTMS session. This study also allowed patients to smoke until one hour previous to the beginning of the treatment.

With regard to the study results, the analyzed parameters within the studied population were cigarette dependence, craving, and consumption. These parameters were assessed previous to the beginning of the study and throughout other assessment stages during the treatment, being cigarette consumption the only parameter analyzed at a 6-month follow-up. Cigarette dependence and consumption were significantly reduced at the end of the treatment in the high-frequency group, but not in the low-frequency and sham groups. However, craving was not significantly reduced in the high-frequency group, possibly due to the population of the group that smoked their last cigarette almost an hour previous to the beginning of the treatment, in this group, being unequally distributed relatively to the other groups. At the 6-month follow-up, the reduction in daily consumption of cigarettes was significantly greater in the high-frequency than in the sham groups, but not significantly greater than in the low-frequency groups. In terms of abstinence, a trend toward higher rates was observed in the 10 Hz groups. The smoking cue exposure allied to the dTMS high-frequency treatment enhanced the reduction in cigarette consumption, leading to abstinence rates, at the end of the treatment, and at the 6-month follow-up, of 44% and 33%, respectively.

This study's positive results of stimulating the PFC and insula bilaterally were later supported by a pivotal multi-center double-blind randomized controlled trial,

where 262 chronic smokers received three weeks of active or sham dTMS with a Brainsway H4-coil over the bilateral PFC and insula, followed by once-a-week dTMS for three weeks, where each session was preceded by a cue-induced craving procedure. This study led to FDA clearance for Brainsway's dTMS H4-coil treatment as an aid for short-term smoking cessation (Zangen et al., 2021), (Brainsway, ndg).

Figure 3.2: The insula is an island of cortex that lies in a lateral deeper area of the PFC. Stimulation of the insula might induce smoking cessation in addicts. Adapted from Ward (2015).

3.1.3 Cocaine

Cocaine use disorder (CUD) is a substantial public health problem (Cocaine, 2021). Associated with this drug dependence comes risk-taking behavior and an unhealthy lifestyle, leading to several medical, psychological, and social problems, like the spread of infectious diseases, the increase of crime and violence, and neonatal drug exposure. Cocaine lifetime use has rates of typically 1-3% in developed countries, with the highest rates in the United States and in the producer countries (Cocaine, 2021).

Current treatment for CUD includes pharmacological drug treatment, but this therapeutic alternative showed limited success for cocaine dependence. Somatic treatment and psychotherapy are nonpharmacological potential treatment tools in treating drug use disorders, however, their value is still not well-defined (Rapinesi et al., 2016). With recent neuroimaging studies that have provided insights into the neural networks affected by and involved in drug abuse and use, non-invasive and invasive brain stimulation of these dysfunctional neural circuits emerge as poten-

tial valuable therapeutic alternatives (Rapinesi et al., 2016). Particularly, imaging studies on CUD have shown that this disorder is associated with alterations in activation or connectivity in the dorsal attention, executive control, and salience networks, which include the DLPFC, the medial prefrontal cortex (mPFC), and the Anterior Cingulate Cortex (ACC), which are are relatively close to one another, as depicted in Figure 3.3 (Martinez et al., 2018). dTMS is a non-invasive technique capable of stimulating the above-mentioned areas, and some studies regarding dTMS over these areas were already conducted with promising results for CUD-related symptoms and behavior.

Rapinesi et al. (2016) conducted a study aiming to assess the effect of high-frequency dTMS on craving in patients with CUD. This study enrolled seven patients with CUD in dTMS sessions, three times per week, on alternate days, for a total of 4 weeks and 12 sessions. 20 Hz dTMS stimulation was delivered bilaterally to the DLPFC with preference to the left hemisphere. All patients were on medications for at least one month, for which they were unresponsive, keeping the medication intake throughout the entire study.

During the add-on treatment, the craving-related VAS scores reduced significantly from baseline to all the other time points of craving assessments (two weeks, four weeks, and eight weeks (follow-up)). From the two weeks time-point to the four weeks time-point there was a reduction in the visual analog scale (VAS) scores, however with no statistical significance. At the follow-up assessment, there was a significant increase in the craving-related VAS scores relatively to the four weeks assessment, but relatively to the baseline VAS scores, there was still a significant reduction in the craving-related VAS scores at this time point.

This study's results show a progressive cocaine craving reduction during the dTMS treatment. This was an add-on dTMS treatment and it could be argued that the results obtained could be partially explained by the pharmacotherapy results. However, Rapinesi et al. (2016) believe that this is not the case, since the pharmacotherapeutic drugs used were heterogeneous and mainly given to ease temporary anxiety, impulsivity, and insomnia. Additionally, all of the patients enrolled in the study had been taking these drugs for some time with no satisfactory response. Thus, the positive outcomes of the study might be related to the stimulation of deep brain tracts, which exert negative control over the striatum and which are deficient in various substance use disorders, including cocaine (Rapinesi et al., 2016).

These findings suggest that dTMS performed according to the parameters applied in the study conducted by Rapinesi et al. (2016) may provide a valid therapeutic alternative for cocaine craving and use disorder. However, looking at the

one-month follow-up significant worsening of the craving-related VAS scores, recall sessions could be useful to maintain craving improvement (Rapinesi et al., 2016). In this study it was not considered a sham group, therefore making the previous results needed to be considered with caution.

Bolloni et al. (2016) conducted a double-blind experimental design study, where 10 patients with cocaine use disorder were randomly assigned either to active or sham rTMS. The chosen stimulation site was the PFC, the stimulation being administered bilaterally to this area, which is known for being hypoactive in addicts. Thus, the active rTMS group received high-frequency 10-Hz stimulation. The study consisted of a total of 12 rTMS sessions throughout 4 weeks, with 3 stimulation sessions per week, for both groups of patients under active or sham stimulation. Cocaine intake was assessed at baseline, at the end of treatment (1 month), and at 3 and 6 months after the end of the treatment, as a follow-up. The cocaine intake was assessed by hair analysis, an indirect measure of drug intake that provides long-term information about drug consumption, with higher sensitivity and specificity than urine analysis (Bolloni et al., 2016). The study results indicate that no significant difference between the active and sham treatment protocols exists in terms of the patients' cocaine intake with time. However, a significant reduction of cocaine intake with time was found in the active group, but not in the sham group, with significant reductions in cocaine intake from baseline to the 3-month follow-up assessment, and to the 6-month follow-up assessment. In addition, a reduction in cocaine intake was observed from the 3-month follow-up to the 6-month follow-up, only in the active group, having the cocaine intake increased in the sham group between these time points. These promising results, although coming from a small sample test group, indicate that bilateral dTMS of the PFC may induce a long-lasting reduction in cocaine intake in patients with CUD.

A different study regarding the assessment of cocaine self-administration by patients was conducted by Martinez et al. (2018). This study had the goal of investigating the effect of dTMS on cocaine self-administration in the laboratory. The approach embraced by the researchers was, at the self-administration sessions, to give the hypothesis to the CUD patients to choose between two alternatives, cocaine and money, with money being an alternative reinforcer. This way, the cocaine-seeking behavior could be directly measured by the researchers.

For this study, 18 patients were divided into three dTMS groups: high-frequency (10 Hz), low-frequency (1 Hz), and sham. The participants were equally divided throughout the groups, meaning that each group was composed of 6 participants. dTMS was delivered over a time course of 3 weeks, during weekdays, for a total

of 13 dTMS sessions. The brain targets stimulated in this study were the mPFC and the ACC, brain regions which have demonstrated, in previous imaging studies, alterations in their activation and connectivity in CUD (Martinez et al., 2018). Three cocaine self-administration sessions occurred throughout the study. The first session occurred at baseline, the second after 4 days of treatment (in the first week of treatment), and the third at the end of the total 13 dTMS sessions, at the end of the third week of treatment. dTMS was not delivered on the same days as the cocaine self-administration sessions, as a safety concern regarding the possible interaction between dTMS and cocaine. In each cocaine self-administration session, the primary outcome variable was the number of doses of cocaine chosen during the session, with a minimum of 0 and a maximum of 9. This means that, throughout each session, the patients had 9 separate decisions to take, with two possible choices: 12 mg of cocaine or \$5. Each decision-making process was separated by 14 minutes. The second outcome variable was the craving scores, ranging from 0 to 100.

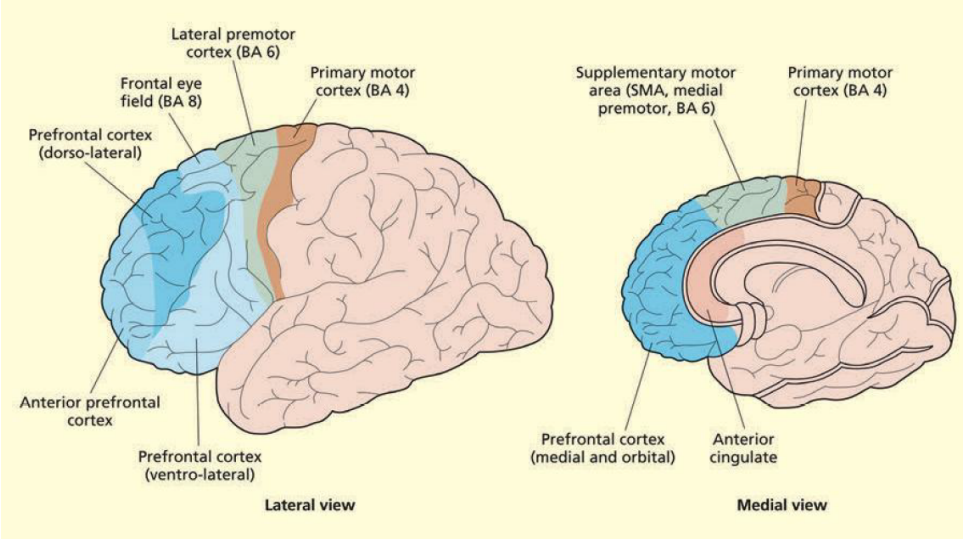

Figure 3.3: Anatomical division of the frontal lobes of the brain allows to locate stimulation targets important, not only, but also, for cocaine addiction, like the DLPFC, mPFC, and ACC. Adapted from Ward (2015).

The results of the study show a very small change in cocaine self-administration for the sham and low-frequency groups, throughout the 3 sessions. In all the groups, an increase in cocaine choices, in the cocaine self-administration sessions, occurred from baseline to the second session. However, in the high-frequency group, the number of choices dropped in the third session. By the time of the last session, a comparison of the number of cocaine choices between the high-frequency and the low-frequency groups showed a significant difference, with lower values coming from

the high-frequency group. Comparing the high-frequency and the sham groups, an almost significant difference was achieved. Regarding the craving assessment, even though for all three groups the craving scores at session 3 were lower than at session 2, the authors concluded that craving scores were not affected by the dTMS treatment.

Looking at the obtained results, we see that the study data suggest a beneficial effect of high-frequency dTMS in reducing cocaine choices after the 3-week treatment, comparatively to the low-frequency and sham groups (Martinez et al., 2018). A large reduction of cocaine choice was observed in the high-frequency group, comparing the assessments in the first and the third week, but not in the other two groups. The craving results show no effect for any of the treatment groups. However, as it is mentioned by the authors of the study, the large differences at baseline between the groups, regarding the craving scores, make the data hard to interpret (Martinez et al., 2018).

Overall, the results obtained in the studies previously described, show that, particularly, high-frequency dTMS over areas of the PFC regards potential as a future alternative therapeutic intervention for CUD. Future studies with larger sample sizes emerge as necessary to prove this alternative therapeutic intervention as a feasible and safe treatment alternative for patients with CUD (Martinez et al., 2018).

3.2 Alzheimer

Alzheimer's disease (AD) is an irreversible condition characterized by cognitive and behavioral disturbances, as well as by a decline in activities of daily life, varying as a function of time since the onset of the degeneration process (Avirame et al., 2016) (Zhang et al., 2019). It is the most common cause of dementia in older adults, and currently has no cure, with treatment alternatives being very limited, and having currently available drugs for treatment only the capacity of treating the disease's symptoms (Zhen et al., 2017) (Zhang et al., 2019).

Alzheimer's disease leads to memory decrease and cognitive deficits, and TMS has been long used to enhance performance on tasks involved in attention, memory, and language. Given the current lack of effective treatment alternatives for AD, nonpharmacological treatments arise as a very important potential alternative therapy (Zhen et al., 2017). rTMS is known for its positive outcomes in various psychological and neurological disorders, and some studies concerning this technique as a potential treatment alternative for AD were also already conducted.

Zhang et al. (2019) conducted a study where high-frequency rTMS treatment

was given in conjunction with cognitive training (CT) treatment. The objectives of the study were to "assess the effect of rTMS-CT on cognition, the activities of daily life (ADL), neuropsychiatric behavioral symptoms, and metabolite levels beneath the stimulated areas of the brain" of the patients (Zhang et al., 2019), while also investigating the correlation of metabolic changes with clinical outcomes after the treatment. Therefore, thirty patients with mild or moderate AD were randomly divided into one of two treatment groups: high-frequency rTMS with CT, and sham with CT. However, only 28 patients completed the whole treatment, since 2 patients in the sham group withdrew. The stimulated areas were the left DLPFC and the left lateral temporal lobe (LTL) for 20 minutes each day, five days a week, during 4 weeks. The assessment time-points distribution was: baseline, immediately after treatment, and four weeks after treatment. An optical navigation system guided the rTMS stimulation by marked coordinates, providing the features of tracking the coil and visualization of the stimulation sites. The real rTMS protocol consisted of 10 Hz stimulation. During each session, the coil was located first over the left DLPFC area and after over the LTL area. In conjunction with the rTMS stimulation, all the patients underwent CT for up to 1h, in each session.

The study objectives consisted in assessing the patients' cognition, behavior, and metabolical changes after rTMS, and comparing them to the baseline results. The cognitive assessment showed a significant improvement in the real stimulation group, after the treatment and at the follow-up (4 weeks after the treatment). The primary outcome measure of the study, Alzheimer's Disease Assessment Scale-Cognitive (ADAS-cog), showed a significant improvement at the two time points after the treatment in the real group, but not in the sham group. The other cognitive examinations also showed a tendency towards a significant improvement in the real group, but not in the sham group. In terms of the neuropsychiatric behavior, substantially greater improvements in the Neuropsychiatric Inventory (NPI) total scores occurred for the real rTMS-CT group, rather than for the sham rTMS-CT group, both at the end of the treatment time-point, and at the follow-up time-point. The ADL scores, however, did not achieve a statistically significant difference between the real and the sham rTMS-CT groups.

The metabolic changes induced by the rTMS-CT treatment in the left DLPFC and the LTL showed a significant increase in the N-acetylaspartate/creatine (NAA/Cr) ratio in the real rTMS-CT group, compared to the sham rTMS-CT group, when the stimulation was over the left DLPFC, but not when it was over the LTL, at the first assessment time-point after treatment. The other evaluated metabolic changes were the choline/creatine (Cho/Cr) and myoinositol/creatine (mI/Cr) ratios in both

stimulated brain areas. In the left DLPFC, at the first assessment time-point, a significant difference in the ratios was observed between the real rTMS-CT group and the sham rTMS-CT group, with greater improvement (i.e., a decrease of the ratios after treatment) coming from the real rTMS-CT group. However, when the stimulation site was the LTL, statistically significant differences between the real rTMS-CT group and the sham rTMS-CT group were not observed. A statistically significant correlation was found between the change in the NAA/Cr ratios and the changes in the ADAS-cog scores, when the stimulation was over the left DLPFC area, but not when the stimulation site was the LTL. This correlation study was conducted since in other authors' research, a positive relationship between NAA levels and cognitive performance was found, as it was in this study, when the stimulation was applied over the left DLPFC. These metabolite levels and metabolic changes were evaluated since, in patients with AD, progressive neurodegeneration occurs with abnormal levels of brain metabolites (Zhang et al., 2019). Besides this, the normalization of the NAA levels in people with neurological disorders implies the recovery of neuronal function, given that this is a metabolite index that partially reflects neuronal function (Zhang et al., 2019).

The results of this study show improvement in cognitive function and neuropsychiatric symptoms, like agitation/aggression and apathy, when stimulation is applied over the left DLPFC. Improvement in metabolite levels in the left DLPFC, but not in the LTL, was also observed, with significant differences between the real and sham rTMS-CT groups. A carryover effect on cognitive improvement was observed in the AD patients enrolled in the study, since improvements in the ADAS-cog, and in other secondary outcomes' scales, particularly in the subscales of word recall memory in the ADAS-cog, and the domains of attention, memory and visual-spatial function in Addenbrooke's Cognitive Examination (ACE-III) maintained for, at least, 4 weeks after the treatment.

Even though in this study improvement in some ADAS-cog sub-domains related to memory and language, like word recognition, commands and naming did not achieve statistical significance, a tendency towards improvement was observed. This lack of statistically significant improvement might be related to the short treatment time of the study, compared to other studies' treatment time, in which these sub-domains achieved statistically significant improvement (Zhang et al., 2019).

The observed study's improvements in cognitive and neuropsychological scales, as well as in metabolite levels, when stimulation is applied over the left DLPFC, but not when it is applied over the LTL can, somewhat, be related to the fact that in the AD brain, temporal lobe atrophy appears earlier and is more severe than atrophy of

the frontal lobe, meaning that fewer neurons survive that can be stimulated by rTMS (Zhang et al., 2019). Concerning the ADL scores, a previous study has shown that 6 weeks of rTMS over the bilateral DLPFC significantly improved the Instrumental Daily Living Activity scale scores. Since in this study this assessment scale lacked statistically significant improvement, the shorter treatment course and observation time might justify the lack of significant results (Zhang et al., 2019).

Overall, these results allowed the authors to conclude that a treatment of 4 weeks with high-frequency rTMS-CT improves cognitive function, as well as behavioral symptoms, in patients with mild to moderate AD, with a positive correlation to metabolic changes, when stimulation is applied over the left DLPFC. Given the efficacy of pharmacological therapy in AD being modest and may come with adverse effects, rTMS-CT therapy emerges as a potentially safe and auxiliary treatment for AD, when stimulation is applied over the left DLPFC.

Yue et al. (2015) conducted a double-blind, randomized, sham-controlled study, to assess the effects of high-frequency rTMS, applied over the left DLPFC, on behavior and psychological symptoms of dementia (BPSD), and cognitive function in patients with AD. Just like in the study conducted by Zhang et al. (2019), the rTMS sessions were delivered five days a week, during four weeks. Two stimulation protocols divided the population of the study into two groups: one group received real 20-Hz rTMS, and the other sham rTMS. The groups consisted of 27 patients each, even though in both of them only 26 patients completed the study. All the patients that completed the study were taking conventional treatment (1 mg of risperidone per day), in addition to the rTMS stimulation. The assessment scales to which the study authors resorted to were the Behavioural Pathology in Alzheimer's Disease Rating Scale (BEHAVE-AD), as a primary outcome, and the ADAS-Cog, as a secondary outcome. The patients' scores in these assessment scales were rated at baseline, and after 4 weeks of treatment.

The results of the study show that, after 4 weeks, the total scores of the two assessment scales significantly improved, in both the real stimulation and the sham stimulation groups. However, the decrease in subscale scores was not statistically significant for all the subscales in the BEHAVE-AD, in both the real and sham stimulation groups, but was statistically significant, for both groups, in all the subscales of the ADAS-Cog. Even though the improvement in the total scores of the assessment scales was statistically significant for both the real and sham stimulation groups, the improvement in the total scores of both the assessment scales was significantly greater, after 4 weeks of treatment, for the group receiving 20-Hz stimulation.

The presented results show that 4 weeks of high-frequency rTMS to the left

DLPFC is an effective adjunctive treatment for the treatment of BPSD and cognitive functioning in patients with AD. However, some subscales scores, like the hallucinations subscale, in the BEHAVE-AD scale, achieved no significant improvement after the 4 weeks of treatment. This result has potential explanations for hallucinations being a marker of the severity of the AD psychopathology (being low-frequency stimulation a more effective treatment for auditory hallucinations), or even the period of time patients underwent rTMS sessions (Yue et al., 2015). Another important conclusion of the study is the correlation between the magnitude of improvement in cognitive symptoms and behavioral and psychological symptoms, as other studies have considered "BPSD in patients with AD a secondary cluster of symptoms directly resulting from the primary symptoms", and "BPSD and cognitive impairment two separate clusters of symptoms" (Yue et al., 2015). This study results, however, suggest that "BPSD and cognitive impairment are different, but related, pathological states", given that a modest correlation between the magnitude of improvement in cognitive and behavioral and psychological symptoms was observed, after the 4 weeks of treatment (Yue et al., 2015).

Overall, high-frequency used as an add-on treatment with low doses of risperidone significantly improved behavioral, psychological, and cognitive symptoms in patients with AD, being observed that better improvements came from the add-on treatment, rather than from the treatment with medication alone.

Both the previously mentioned studies have in common the DLPFC as the stimulation target. In both studies, this was a successful target of stimulation, since significant improvement in cognition, behavioral and psychological symptoms was achieved. The DLPFC is the most commonly targeted cortical region in studies exploring rTMS as a potential alternative therapy for AD symptoms. Experimental studies with stimulation over other regions that could prove to be effective for treating cognitive decline are lacking (Heath et al., 2018). The DLPFC is a brain area related to disorders like Major Depressive Disorder, or neuropsychiatric symptoms, like apathy. Both of these conditions have a high prevalence in patients with AD, and both are also highly associated with cognitive deficits. Given that several studies have reported, in AD patients with depression or apathy symptoms, an improvement in the cognitive deficits and in the depressive or apathy symptoms, and given the known correlation between these conditions, difficulties emerge in determining whether the improvements in cognitive deficits arise as a consequence of stimulating the DLPFC, or as a consequence of the improvement in the depressive and apathetic symptoms (Heath et al., 2018). Thus, it is important to understand how improvements in these symptoms influence cognitive functioning in patients with AD and

determine whether other brain areas may be more appropriate stimulation targets for improving the cognitive deficits (Heath et al., 2018).

A recent multisite rTMS approach, known as NeuroAD, alternates stimulation between several areas like the DLPFC, Broca's area, Wernicke's area, and the parietal somatosensory association cortex, in conjunction with cognitive training. Studies assessing this technique's effectiveness demonstrated significant improvements in cognition for months after stimulation, highlighting the potential of stimulating different brain areas, rather than just the DLPFC, for improvement of cognitive deficits in patients with AD (Heath et al., 2018). Other studies have examined potential alternative brain targets for cognitive function enhancement in patients with AD. Generalized and particular symptomatological improvements were obtained, thus emerging from these studies new brain areas to be considered for rTMS in patients with AD. In addition, a Brainsway treatment with resort to H2-coils, which positively affects spatial memory related to several standard tasks, has been approved by the European Union with a CE mark for the treatment of some of Alzheimer's symptoms (Brainsway, nda).

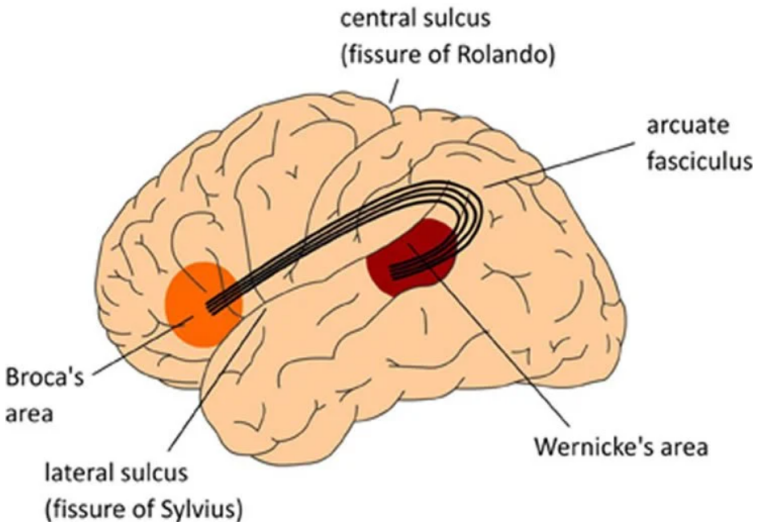

Figure 3.4: Representation of the Broca's and Wernicke's area in the brain, and respective connective tract between these regions, the arcuate fasciculus. These regions are commonly associated with language production and comprehension, although this model has been losing strength recently. Adapted from Jarrett (2016).

The main mechanisms of action regarding rTMS are the induction of plasticity and the potential strengthening of connections inside the brain. Identifying the areas that present a loss of functional connectivity in AD could provide potential targets for rTMS. In this investigation for potential accurate targets, neuronavigational techniques are of major importance, as well as the understanding of the disease

progression with concern to the affected areas, given that the stage of the disease influences the treatment outcomes. In addition, early identification of changes in specific brain areas over the progression of the disorder is important, as these areas could be targets to slow the development of AD (Heath et al., 2018).

3.3 Schizophrenia

Schizophrenia is a chronic and severe mental disorder affecting 24 million people worldwide (Schizophrenia, 2022). Schizophrenia is usually characterized by two types of symptoms: positive and negative. Positive symptoms are more related to abnormal experiences, like hallucinations and delusions, while negative symptoms are more related to abnormal behavior, like poverty of speech, flattening of affect, etc. (Frith, 2014). dTMS is being studied as a potential add-on or monotherapy for the various symptoms related to this condition, and promising studies concerning improvements of either negative, positive, or both symptoms were already conducted.

Kindler et al. (2013) conducted a study in which 30 patients with pharmacoresistant auditory hallucinations received active rTMS (15 patients) or standard Auditory Verbal Hallucinations (AVH) treatment (15 patients), for 10 consecutive days. The aim of the study was to assess neurobiological effects of TMS on AVH. AVH is a physical phenomenon in the human brain associated with increased neuronal activity in areas responsible for language production and perception. Activation of the primary auditory cortex (PAC), the Broca's and Wernicke's area, or their contralateral homologous areas, was reported during AVHs in other studies (Kindler et al., 2013). In addition, in the past, when TMS was studied as a potential treatment for AVH, the left temporoparietal was also, sometimes, considered the target region. However, for Kindler et al. (2013), a precise functional definition of the stimulation location was still missing.

The sylvian parietotemporal area (Area Spt) is a sensory interface between the sensorimotor and motor speech systems, strongly left dominant, and equally activated by the perception and reproduction of aurally or visually presented words. This area is connected to frontal and temporal language regions that are involved in the generation of AVH, and there is evidence of functional abnormalities within it, in patients with AD (Kindler et al., 2013). For these reasons, the study authors chose the Area Spt as the ideal target for TMS modulation of AVH.

The patients that participated in the study were randomly assigned to one of two TMS groups, or to the control group. The two TMS groups consisted of different TMS protocols: one group received low-frequency (1 Hz) TMS, and the

other received TBS, where each burst contained three pulses at 30 Hz. Both groups received stimulation for 10 consecutive days. For the low-frequency group, the protocol consisted of one session per day, whilst in the TBS group, from day 1 until day 3 of treatment, two double trains were applied, each session, and from day 3 until day 10, one double TBS train was applied each session. AVH assessment was performed using the Psychotic Symptom Rating Scale (PsyRats), at two different time points: before the first treatment, and 20±6 (mean, Standard deviation) hours after the last treatment session. The brain activity of the patients was the other assessment performed in the study, and it was performed using magnetic resonance arterial spin labeling (MR-ASL). This technique allows measuring the regional cerebral blood flow (rCBF) as a marker of neuronal activity (Kindler et al., 2013). The time points of this data acquisition were 20 ± 6 (mean, SD) hours before the first treatment session and 20 ± 6 (mean, SD) hours after the last treatment session.

The PsyRats scores in the control group indicate a nonsignificant decrease after treatment. For the TMS patients, the PsyRats scores indicate, in both groups, a significant decrease after treatment. Between the TMS groups, there were no statistically significant differences in the PsyRats scores. In terms of the rCBF assessment, in the TMS groups a significant decrease in the left PFC, Broca's area, and the cingulate gyrus was observed, whereas, for the control group, no significant decrease in the rCBF was found for any of these regions of interest. A significant difference between the TMS's and control group's CBF in all the regions of interest was also observed, whereas between the TMS groups there was no significant difference in the CBF in any of the regions of interest. A correlation between the clinical improvement and the CBF in the PAC was observed, but no correlation between Broca's area and cingulate gyrus clinical improvement and CBF was found. These results show that TMS over the area Spt improves AVH in schizophrenic patients, being this improvement connected to a reduction in neural activity in auditory and language systems, proving TMS as a potential alternative tool for AVH therapy in schizophrenic patients (Kindler et al., 2013).

A double-blind randomized controlled trial led by Li et al. (2016) aimed to study the effect of high-frequency (10 Hz) rTMS over the left DLPFC on schizophrenic patients' negative symptoms. Thus, 47 patients with schizophrenia were randomly assigned into two groups: 25 patients into an active rTMS stimulation group, and 22 patients into a sham rTMS stimulation group. The stimulation protocol consisted of five consecutive daily sessions throughout the week, during the course of four weeks, valid for both groups. The assessment scales for the negative symptoms of the study patients were the Scale for the Assessment of Negative Symptoms (SANS),

(a) **(b)**

Figure 3.5: Illustration and generalized 3D-image of the brain representing the location of the primary auditory cortex and the Area spt in the brain. **a)** Primary auditory cortex. **b)** Area spt. Adapted from (Reuell (2016), Hickok et al. (2009)).

and Positive and Negative Symptom Scale (PANSS). The assessment time points occurred at baseline, after 4 weeks of treatment, and at 4 weeks after the end of treatment.

A significant reduction of the SANS total score was observed in the rTMS group at the 4- and 8-week assessment time points. For the sham group, only scores of two subscales of the SANS dropped significantly after the four weeks of treatment. At the 4-week assessment time-point, no significant differences between the two groups in the total SANS scores and all of the SANS's subscales were observed. However, at the 8-week assessment, the total score in the SANS of patients in the active rTMS group significantly lowered, with a significant difference when compared to the SANS total scores in the sham group. The negative subscales of the PANSS, although, showed no significant differences between the two groups, neither at the 4-week nor at the 8-week assessment. This result might be a consequence of the lower sensitivity in detecting change of negative symptoms of the PANSS (Li et al., 2016).

The presented study results show a delayed response to rTMS treatment, but with positive outcomes and prospects of rTMS as a potential alternative therapy for negative symptoms in patients with schizophrenia. The delayed response, however, could be related to the elder age and lengthier illness duration of this study's patients. The therapeutic effect of rTMS in this study was only proved until 4 weeks after the treatment, but it could have lasted longer (Li et al., 2016). Moreover, A Brainsway's dTMS treatment for the negative symptoms of schizophrenia has been demonstrated to be safe and effective, thus leading to this treatment's CE approval.

3.4 Migraine

Migraine is a chronic lifelong disorder with quality-of-life impairing potential (Misra et al., 2013). Approximately 2% of the global population suffer from chronic migraine. Due to patients with chronic pain may not be responsive to standard drug treatment, and to the fact that prophylactic migraine drugs may trigger drug overuse, leading to drug overuse headache (Rapinesi et al., 2016), alternative therapies are sought.

Migraine is characterized by dysfunction of the trigeminovascular system, brainstem, and cerebral cortex. Experimental research has shown that a single-pulse of TMS was able to disrupt cortical spreading depression, which paved the way to study TMS as an abortive treatment of migraine (Misra et al., 2013). Misra et al. (2013) studied the outcomes of high-frequency rTMS in migraine prophylaxis. For this purpose, a randomized, placebo-controlled, double-blind study was conducted to assess the efficacy and safety of high-frequency rTMS on migraine prophylaxis. A hundred patients were then randomized to one of two groups: 50 patients to an active rTMS group, and the other 50 to a sham rTMS group. 93 patients had migraine with aura[1], whilst 7 had migraine without aura. 98 of these patients were taking migraine prophylaxis drugs, but these were withdrawn 1 month prior to enrolment for rTMS. The study consisted of 3 sessions of stimulation on alternate days, for both groups. The stimulation frequency of the active rTMS group was 10 Hz. The site of stimulation for this study was the hot spot of the right abductor *digiti minimi* (ADM). Assessment of the stimulation effect on patients was made in accordance with two groups of outcomes. The primary outcomes were a reduction in headache frequency and severity, as assessed by the VAS, bigger than 50%. The secondary outcomes were functional disability, rescue medication, and adverse events. The outcomes were assessed at baseline, after the third rTMS session and, thereafter, at weekly intervals until the 4^{th} week. All these weekly response parameters were reported from the patients' headache diary, when the patients came back for the follow-up session, 1 month after the rTMS treatment.

The primary outcomes' results showed a significant reduction in headache frequency and severity in both the active and sham rTMS groups, at 1-month follow-up. However, the improvement in both the parameters was more marked in the active rTMS group, with 78.7% of the active rTMS group's patients achieving a reduction in headache frequency bigger than 50%, whilst in the sham group, only 33.3% of

[1]Sensory disturbances that typically include vision changes (flashes of light, blind spots, among others) or tingling in the hand or face. These disturbances usually strike before the headaches.

the patients achieved this reduction, at 1-month follow-up. Regarding the headache severity, a significantly bigger improvement in this parameter was achieved in the active rTMS group, at 1-month follow-up, with 76.6% of the patients in the active group achieving a reduction bigger than 50%, compared to 27.1% of the patients in the sham group. Compared to baseline, for both parameters and groups, the maximum improvement achieved was at the first week after the rTMS treatment, with a progressive decline over the weeks until the last one (4^{th} week). Improvement in headache frequency and severity was more marked in the patients with chronic daily headaches, comparatively to those with episodic migraine.

The secondary outcomes, at the 1-month follow-up, came with similar generalized results to that of the primary outcomes, with a significant improvement in all the measures for both groups, but with a more marked improvement in the rTMS group. A maximum improvement was also attained in the first week after stimulation, for all the measures, and in both groups, with a progressive decline until the 4^{th} week.

Even though the sham rTMS group experienced significant improvements in all the parameters assessed in this study, at the 1-month follow-up, a more marked improvement in the rTMS group was obtained for all the assessed parameters. Compared to sham stimulation, significant improvements in the high-frequency rTMS group in migraine frequency and severity, assessed by VAS scores, and functional disability, were achieved at the 1-month follow-up, providing, overall, evidence of the efficacy and safety of 10-Hz rTMS over the hot spot of the right ADM in migraine prophylaxis.

Like Misra et al. (2013), Kumar et al. (2021) conducted a study where high-frequency rTMS was delivered to chronic migraine (CM) patients, following the literature results suggesting high-frequency rTMS as effective and "well tolerated" for CM therapy. Consequently, 20 right-handed CM patients were enrolled in the study. The group of patients enrolled was, thus, randomized either to a real rTMS group, or a sham rTMS group. For the real rTMS group, 10-Hz pulses were delivered over the left motor cortex. Ten rTMS sessions were delivered, 5 days per week, over the course of 2 weeks, to patients of both groups.

Kumar et al. (2021) aimed to assess improvements of several symptomatology related to CM with this study. Headache-intensity and headache-associated disability were the subjective pain-assessed symptomatology, using the VAS and the Migraine Disability Assessment (MIDAS), respectively. Headache intensity was assessed at three time points (pre-treatment, post-treatment, 3 months after treatment), and headache-associated disability was assessed before therapy and at the

3-month follow-up. Anxiety and depression were also assessed using the Trait anxiety inventory (STAI) and the Beck depression inventory (BDI), respectively. The assessment time points for both anxiety and depression were also pre-treatment (baseline), post-treatment, and a 3-month follow-up. Measurement of the corticomotor excitability parameters, with a figure-8 coil over the primary motor cortex (M1), aimed to map resting motor thresholds, and motor-evoked potentials. Given that "chronic migraine is a by-product of processes altering cortical excitability" (Kumar et al., 2021), and "the mechanisms of pain relief remain unexplored, accompanied by variations in the findings of sensory tests and corticomotor excitability" (Kumar et al., 2021), measurements of the corticomotor excitability, over the M1, were also studied to give some insight of the potential physical brain alterations, after rTMS treatment, related to symptomatology improvement. An objective pain measurement was also conducted in the study. Both these measurements were conducted at pre-treatment, post-treatment, and at a 3-month follow-up.

Headache intensity VAS scores showed a significant difference between baseline and post-treatment scores, and between baseline and follow-up scores, for the real rTMS group. No significant difference between post-treatment and follow-up was observed, for the real rTMS group, indicating maintenance of the treatment effect, until, at least, one month after treatment. No significant differences between any assessment time points were observed in the VAS scores for the sham rTMS group. Headache frequency significantly reduced between baseline and follow-up in the real rTMS group, but not in the sham group. Headache-associated disability, measured by the MIDAS scale, showed a significant difference between baseline and follow-up in both groups, but no significant differences at the follow-up between the groups' scores.

Regarding the anxiety and depression assessments, STAI scores showed no significant difference between real and sham rTMS in any assessment time-point. In addition, no significant changes when assessing real or sham rTMS groups were observed. The same results were observed for the depression assessments in both groups, using the BDI. The corticomotor excitability assessments showed no significant difference in neither the real nor the sham rTMS group for the resting motor threshold assessment. The motor-evoked assessments showed no significant difference between the baseline and post-treatment MEP amplitudes at 110, 120, 130, 140, and 150% RMT in real vs sham rTMS groups comparison. Additionally, the MEP latency showed no significant differences between the sham and real rTMS groups at any of the assessment time points.

Like the study from Misra et al. (2013), a significant improvement in headache

frequency, headache intensity/severity, and headache-associated disability was observed in the real rTMS group, when compared to the sham group, demonstrating the efficacy of rTMS over the motor cortex as a potential therapy for migraine-related symptoms. However, no significant improvements in anxiety and depression scales were reported. Significant changes in these psychological symptoms are typically related to rTMS over the DLPFC (Kumar et al., 2021). Additionally, no significant changes were observed in the neurophysiological parameters of corticomotor excitability in any of the stimulation groups.

3.5 Obesity

Obesity is a major risk factor for chronic diseases like diabetes, cardiovascular diseases, and cancer (Nutrition and team, 2021). However obesity is seen as a problem in high-incoming countries, in low and middle-incoming countries obesity is on the rise, making it a world health problem (Newman, 2020).

One of the main reasons why maintaining weight loss in obesity is so difficult is food craving. Neurophysiologically, this involves several brain areas, just like previously seen for drug-use disorders. Specifically, obese subjects tend to have an impaired function of PFC regarding inhibitory control and decision-making ability over appetite and eating, being the PFC integrated in the brain reward areas (Ferrulli et al., 2019a). Abnormal activation of central reward circuits, as in drug addiction, has also been reported in obese subjects (Ferrulli et al., 2019a). Dopaminergic neurons can potentially be reached by dTMS, and dopaminergic pathways can also possibly be indirectly modulated by stimulation of the PFC with rTMS, making this technique on the rise as a potential therapeutic solution for the obesity problem (Ferrulli et al., 2019a).

Ferrulli et al. (2019b) studied the effect of dTMS in reducing food craving and inducing weight loss in obese people. For this randomized, double-blind, sham-controlled study, 33 obese subjects were enrolled. The admitted subjects were randomized into one of three stimulation groups. Thirteen subjects underwent high-frequency dTMS (18 Hz) treatment, 10 underwent low-frequency (1 Hz) treatment, and 10 received sham stimulation, having been the stimulation delivered over the lateral PFC and insula, both possible to identify in Figures 3.3 and 3.2, respectively. All the study participants underwent a 5-week treatment. During this period, a total of 15 treatment sessions were delivered, with a distribution of 3 sessions per week. No drugs, psychological, or psychiatric therapy were administered throughout the study period (1 year), being dTMS the only treatment allowed. Additionally, during the

1-year period of the study, a hypocaloric diet was prescribed to all the participants, followed by instruction to engage in moderate-intensity physical activity.

The study objectives were to not only investigate the effect of 5-week dTMS treatment in food craving and bodyweight reduction in obese subjects, but also to explore the chronic effects on neuroendocrine pathways related to appetite/satiety balance, metabolic variables, and body energy homeostasis. The assessments of the treatment effects consisted of evaluating the patients' food craving, anthropometric values, blood pressure, metabolism analysis (measuring the resting energy expenditure (REE), the respiratory quotient (RQ), and the activity energy expenditure (AEE)), and laboratory measurements, to assess metabolite variations (glucose, glycated hemoglobin (HbA1c), cholesterol, and triglycerides), as well as hormonal and neuroendocrine markers (insulin, leptin, total ghrelin, -endorphins, epinephrine, and norepinephrine). Food craving was assessed at baseline, at the end of the 5-week treatment, and at the 1-month (follow-up 1), 6-month (follow-up 2), and 1-year (follow-up 3) follow-ups . Anthropometric values were measured at the same time points as food craving, and blood pressure was measured at each dTMS visit, and at the follow-up visits. REE and RQ were measured at baseline, at visit 15, and at follow-up 2. AEE was recorded with accelerometers during the 5-week treatment period, and at the follow-up monitored by phone calls. Laboratory measurements were carried out at baseline, after the last dTMS session, and at all the follow-ups. Of the 33 subjects who completed the dTMS treatment, 31 attended follow-up 1, 24 attended follow-up 2, and 17 attended follow-up 3.

Food craving scores showed a trend toward significant interaction between intervention group and time, with the HF group having the best improvement in the craving scores. Body weight and BMI measurements showed a significant interaction between time and group, with the high-frequency group having the bigger improvements. The HF group, at the last follow-up measurement, showed a significant decrease in body weight and BMI. For the metabolic variables, a trend toward significant interaction between intervention group and time was revealed for RQ, but not for REE. Systolic blood pressure (SBP) measurement showed no significant differences between treatment groups, whilst for diastolic blood pressure (DBP), a trend interaction between group and time was revealed. Compared to the other two groups, a significant increase in AEE was found in the HF group, and a trend towards an increase in the total energy expenditure and in the metabolic equivalent of tasks, steps, and traveled kilometers was observed in the same group. Metabolic and neuro-endocrine assessments showed a significant interaction between intervention group and time on logarithmized leptin, and on logarithmized epinephrine, with a

significant difference between the HF and the sham group. Mixed-model analysis of the β-endorphine neuroendocrine marker showed a trend effect of time by group interaction. For the metabolic variables, a borderline significant time-by-group interaction on logarithmized HbA1c was found.

The study results show a significant reduction of body weight in obese subjects submitted to HF dTMS treatment, with results improving over the course of 1 year, even after the dTMS treatment. Reduced craving for food and an increase in subjects' physical activity were the main inductors of this weight reduction. The main mechanism, in terms of brain functionality, responsible for these results, was the increased dopaminergic activity in the mesolimbic and mesostriatal pathways, but the study data indicating an increase in β-endorphins and epinephrine, during the HF dTMS treatment, suggests these alterations as potential additional mechanisms (Ferrulli et al., 2019b).

3.6 Obsessive Compulsive Disorder (OCD)

Obsessive compulsive disorder is a common chronic and highly debilitating disorder (Zaman and W Robbins, 2017) (Carmi et al., 2018). It is characterized by intrusive obsessive and repetitive compulsive symptoms ("repetitive ritualistic physical or mental actions performed to reduce obsession-provoked anxiety") (Hawken et al., 2016), leading to a detrimental effect on the quality of life of OCD patients (Lusicic et al., 2018). A high percentage of OCD sufferers are drug-resistant (40-60%), or cannot tolerate the drug's side effects (Zaman and W Robbins, 2017) (Carmi et al., 2018). Given this high percentage of drug-resistant OCD patients, alternative therapies have been studied, including TMS.

Hawken et al. (2016) studied the effect of rTMS over the sensory motor area (SMA), depicted in Figure 3.3, as an adjunctive treatment in patients with treatment-refractory OCD. The etiology and pathophysiology of OCD are unknown. According to Hawken et al. (2016), it has been hypothesized that OCD's clinical symptoms "are the result of a deficit in inhibition throughout the cortico-striato-thalamo-cortical circuits". Hyper-excitation within the network including the prefrontal and orbital frontal cortices, supplementary motor and premotor areas, the striatum, globus pallidus, and thalamus, is suggested by evidence as one of the potential OCD's symptomatology causes (Hawken et al., 2016). The hypothesis of the SMA as a potential target for OCD therapy emerges from other studies' results showing clinical utility of cortical excitation mitigation using rTMS over the SMA, being the ability to restore cortical inhibition and effective clinical response the main reasons (Hawken

et al., 2016). This hypothesis led Hawken et al. (2016) to conduct a randomized double-blind study to assess the effect of rTMS over the sensory motor area (SMA) as an adjunctive treatment for patients with treatment-refractory OCD. For this study, 23 patients were enrolled. Of these 23, 22 patients were randomly assigned either to a sham rTMS group or to an active rTMS group. The active treatment consisted of low-frequency (1 Hz) rTMS. Both groups underwent 25 rTMS sessions, over the course of 6 weeks. The stimulation target was the SMA, with stimulation being delivered bilaterally. The outcome measures used by the study authors to assess the improvements in OCD symptomatology were the Yale-Brown Obsessive-Compulsive Scale (Y-BOCS), the Clinical Global Impression Scale (CGI), and the Hamilton Depression Rating Scale (HDRS-21). This was a multi-center study, with patients coming from Bulgarian and Turkish mood disorder sites. However, only the Bulgarian patients completed all the treatment stages and assessments. The assessment scales were administered at baseline (pre-treatment), biweekly during the treatment phase, and at two and six weeks after the end of the treatment. The patients selected for the study were almost all on at least one medication, being only one patient drug free, six receiving only one medication, and the rest on polypharmacotherapy.

Y-BOCS scores showed a significant difference between groups, by the time of the last treatment session (session 25), with a prevalence of improvement in the active rTMS group. Moreover, at the two-week and six-week follow-ups, the scores in the active group continued to improve, but not significantly compared to the previous assessment session. These results demonstrate a sustained response to treatment. Regarding the sham group, at the two-week follow-up, the Y-BOCS scores improved compared to the assessment at the end of the treatment, but at the six-week follow-up, the scores worsened, being significantly different from the scores obtained in the active group. The HDRS-21 and CGI scores showed a significant difference between the active and sham rTMS groups, at the last treatment session, but at the two-week follow-up session, no significant difference between the groups was observed, even though they remained stable compared to the previous assessment session.

The study results show a clinically significant decrease in Y-BOCS scores in patients receiving active rTMS. These same patients, previous to the rTMS treatment, were on pharmacological treatment, and their symptomatology scores, in the Y-BOCS, were in the moderate to extreme range. However, after the rTMS treatment, the scores in the active group generally decreased to a less severe range, specifically, sub-clinical to moderate. This effect was sustained at both the two-week and six-week follow-ups. These results demonstrate that bilaterally SMA rTMS has

the potential to be an effective augmentative treatment in OCD (Hawken et al., 2016).

Another potential stimulation target for the treatment of OCD with rTMS is the DLPFC, above depicted in Figure 3.3. Given that the OCD pathophysiology is potentially related to hyperactivity in specific cortical-subcortical loops, that include the DLPFC, Seo et al. (2016) proposed to study low-frequency (1 Hz) rTMS over the right DLPFC as a potential treatment alternative for OCD. For this study, 28 patients were recruited, having one of the patients dropped out prior to the start of the treatment, making part of the final sample, 27 patients. These patients were randomly assigned to either an active rTMS group (1 Hz) or a sham rTMS group. The patients underwent 3 weeks of rTMS treatment, with daily sessions, 5 days a week. Patients' pharmacotherapies were continued in the same dosages for the whole duration of the study. The assessment scales considered by the study authors were the YBOCS (the main outcome measure), the CGI, the seven-item Hamilton Depression Rating Scale (HAMD), the Hamilton Anxiety Rating Scale (HAMA), and the Beck Depression Inventory (BDI). These assessment scales were delivered at baseline and every week during the treatment period. The third week of treatment assessment revealed a significant difference between the two groups in the YBOCS scores, with prevalence to the active group. The other assessment scales that showed a significant difference between the groups' scores were the HAMD, at the week 2 assessment, and the CGI, at week 3. No significant differences between the treatment groups' scores were ever achieved for the HAMA and BDI scores.

Albeit the good results from the previous studies, stimulation of the mPFC and the ACC with Brainsway's H7-coil got FDA clearance for the treatment of OCD's symptoms, particularly for patients who have not achieved sufficient improvement from traditional OCD treatments. A multicenter, randomized, double-blind, sham-controlled study demonstrated stimulation with the H7-coil to significantly alleviate OCD's symptoms after a six-week treatment, with improvement up until one month after treatment (Brainsway, ndd).

OCD's pathophysiology is related to several brain areas. Studies where improvements in OCD's symptoms were reported, as mentioned above, had as main targets the SMA and the DLPFC. Despite this, an FDA-approved treatment already exists, with main targets the mPFC and the ACC, where the stimulation coil that applied the magnetic field was Brainsway's H7-coil. Albeit this effective treatment already exists, and given that positive outcomes also arise from stimulating different areas, alternative treatment solutions for OCD's symptoms can continue to be studied, with deeper stimulation coils, capable of stimulating known affected areas

from this condition, like the globus pallidus and the thalamus, emerging as potential alternatives to achieve better, or similar results.

3.7 Post-Traumatic Stress Disorder (PTSD)

Post-traumatic stress disorder (PTSD) is a trauma and stress-related disorder characterized by intrusive, avoidance, and hyperarousal core symptoms, that may result in significant social or occupational dysfunction (Trevizol et al., 2016). Current therapies, like medications and psychotherapy, have been showing to help reduce symptoms and treat comorbid anxiety and depressive symptoms (Trevizol et al., 2016). However, in approximately one-third of patients, there is no improvement of symptoms, enhancing the need for novel therapies, like TMS, that might improve the disorder's induced symptoms.

In terms of rTMS delivery to PTSD patients, the right DLPFC is a brain target studied with positive outcomes (Watts et al., 2012), being the DLPFC location in the brain depicted in Figure 3.3. Watts et al. (2012) studied the effect of 10 rTMS sessions over the right DLPFC on PTSD patients. In this study, 20 PTSD patients were randomly assigned to a sham rTMS or an active rTMS group (1 Hz). PTSD symptoms, anxiety, depression, and cognition were assessed. At the end of the treatment, PTSD symptoms in patients of the active group achieved a statistically significant reduction, being this reduction also statistically significant, when compared to the PTSD scores of the sham group. Depression and anxiety also improved significantly at the end of the treatment, for the active group, but not for the sham group. The active group's depression improvement at this time point was significantly better than that of the sham group, but the anxiety improvement was not. No change in cognitive function was achieved at the end of the treatment, for neither of the groups. Follow-up assessments showed that symptoms' improvement was still observed 2 months after the end of the treatment, but with subtle signs of the rTMS effect starting to vanish. Thus, this study demonstrated a significant therapeutic effect of 1-Hz rTMS over the right DLPFC in subjects with PTSD, with sustained results even after the treatment.

Another TMS target with therapeutic potential for PTSD patients is the mPFC, illustrated above in Figure 3.3. PTSD is considered a fear circuitry stress-induced disorder, and "the ability to achieve and preserve extinction of the acquired fear response is severed due to functional impairment in the mPFC control over the amygdala" (Isserles et al., 2013), being the mPFC hyper-activation inversely correlated with the amygdala hyper-activation (Isserles et al., 2013). Therefore, Isserles

et al. (2013) proposed to study the effect of high-frequency (20 Hz) dTMS over the bilateral mPFC in 30 adults suffering from resistant PTSD. The study divided the patients into 3 groups, to which they were randomly allocated. One group received dTMS after script-driven imagery of the traumatic experience, immediately followed by script-driven imagery of a neutral event. Another group received dTMS after script-driven imagery of a positive experience, immediately followed by script-driven imagery of a neutral event. The last group received sham dTMS after script-driven imagery of a traumatic experience, immediately followed by script-driven imagery of a neutral event. The assessments of the study were related to PTSD and depression symptoms. An additional cross-over treatment was offered to patients of the control groups that did not meet the response criteria, consisting of active stimulation and traumatic exposure, being these patients, already, unblinded. Treatment sessions were delivered 3 days a week, over a 4-week period of time.

After the 4 weeks of treatment, the group receiving real dTMS stimulation and traumatic script-driven imagery was the only one that showed significant improvement in PTSD and depression symptoms. A significant improvement in the primary outcome of the PTSD symptoms was also observed for patients who crossed over to real treatment. These improvements in the PTSD symptoms, observed in both real dTMS groups (with traumatic script-driven imagery and the cross-over group) were also well preserved in both groups at the 2-week and 2-month follow-ups, with all the secondary scales also supporting this preserved effect.

Given the positive outcomes of the study, a potentially effective treatment of PTSD's symptoms might rely on HF dTMS over the mPFC, preceded by a brief exposure to a traumatic experience (Isserles et al., 2013). Although there already exists a safe and effective Brainsway's treatment approved by the CE (Brainsway, ndf), PTSD is a condition that potentially has several effective treatment targets, as the results of these two previously presented studies show. Other rTMS/dTMS treatment procedures might arise with the stimulation of new alternative targets with the help of coils capable of stimulating deeper in the brain, or the same targets, but with different stimulation patterns.

3.8 Stroke

Stroke is a common acute neurovascular disorder that causes long-term limitations to daily living activities (Fisicaro et al., 2019). Worldwide, stroke is the third leading cause of disability. Depending on the affected brain area by the stroke, several motor and non-motor deficits affect stroke victims' daily living. Stroke's

ischemic damage is associated with significant metabolic and electrophysiological changes in cells and neural networks involved in the affected area (Fisicaro et al., 2019). Beyond that, a local shift in the balance between the inhibition and excitation of both the affected and contralateral hemispheres is observed, consisting of increased excitability and disinhibition of the unaffected hemisphere. In addition, subcortical areas and spinal regions may be altered (Fisicaro et al., 2019). Generally, the consequent motor and non-motor deficits of a stroke can take many forms.

A recent review of the current evidence regarding rTMS's accuracy on stroke rehabilitation, by Fisicaro et al. (2019), concluded that there is a positive effect of rTMS in the rehabilitation of all the clinical stroke's manifestations (with the exception of spasticity and cognitive impairment): affected motor function, manual dexterity, affected walking and balance, dysphagia, aphasia, unilateral neglect, and depression. This review, by Fisicaro et al. (2019), has focused only on conventional high-frequency and low-frequency rTMS protocols.

A review of the most relevant articles, manuals, and clinical practice guidelines addressing not only, but also, TMS usefulness for stroke neurorehabilitation, published between 1985 and 2015, was conducted by Ruiz et al. (2018). This review focused on the rTMS role in improving post-stroke deficits, given that rTMS accelerates neuroplasticity, helping with the reorganization of brain networks, and increasing interneuronal connectivity in the damaged area (Ruiz et al., 2018). These interneuronal connectivity and reorganization of brain networks are important in stroke patients, given that strokes usually affect one brain hemisphere. This lesion leads to hyperactivity of the intact hemisphere, inhibiting neural activity in the damaged hemisphere. Low-frequency rTMS of the intact hemisphere and high-frequency rTMS of the affected hemisphere are usually the stimulation protocols applied to accelerate neuroplasticity, reorganize the brain networks, and increase interneuronal connectivity in the damaged area (Ruiz et al., 2018). This review by Ruiz et al. (2018) found several studies where improvement in patients with motor deficits, aphasia, dysarthria, dysphagia, perceptual disorders (specifically hemispatial neglect), and depression, following an rTMS treatment, was reported.

Both of the reviews previously mentioned concluded that rTMS is a feasible, safe, and effective tool for the treatment of several post-stroke motor and non-motor deficits, that integrated with other conventional treatment modalities might enhance the clinical recovery and the prognostic perspective of the stroke survivors (Fisicaro et al., 2019). In addition, Brainsway's treatments with resort to the dTMS H-coils have shown to be safe and effective for the treatment of symptoms like aphasia or lower limb deficient motor function, with this treatment having acquired

CE approval for post-stroke patients (Brainsway, nde). However, other important studies considering rTMS as a potential therapeutic alternative for symptoms that were not included in the previous reviews deserved our attention.

Central poststroke pain is a treatment-resistant problem difficult to control for some patients after a stroke. Kobayashi et al. (2015) proposed to study the effects of 5-Hz rTMS over the primary motor cortex affected side, an area of the brain illustrated in Figure 3.3, in 18 patients with central poststroke pain. Two studies were conducted, one to assess the short-term effect of rTMS, and the other the long-term. For the short-term effect study, 6 patients were enrolled and administered either real or sham stimulations in a pseudorandomized order. Three patients received real stimulation on the first day, and sham one week later, whereas the other three had an inverse order of treatment. Pain assessment showed a significant effect after real rTMS, but not after sham, even though no significant difference between the stimulation protocols was achieved. With regards to the long-term effect study, 18 patients completed a 12-week program, where rTMS was delivered once a week. Pain assessments were delivered previous to each rTMS session, also once a week, so that an evaluation of the sustained, and not the immediate rTMS effect, was made. This study had no sham rTMS group.

The study's weekly pain assessments showed a mean significant improvement, compared to the results at baseline, at week 3, reaching this improvement a plateau at about the 8^{th} or 9^{th} week. From the studied patients, 27.8% showed an excellent pain reduction (70% or more pain reduction), 33.3% showed a satisfactory pain reduction (40-69% pain reduction), and 38.9% of the patients showed a pain reduction less than 40%. This means that the rTMS treatment was effective for 61.1% of the patients that attended, which is a treatment efficacy similar to other invasive alternatives (Kobayashi et al., 2015). In addition, seven patients continued the treatment throughout the course of 1 year. The treatment protocol was maintained the same: one weekly stimulation session, and one weekly pain assessment, previous to the stimulation session. Only six of these seven patients completed this one-year treatment. No further improvements were observed behind the plateau already achieved during the 3-month program, and the pain-relief effect was kept approximately sustained throughout the course of this one-year treatment.

This study's results show a sustained long-term effect of 5-Hz rTMS over the affected primary motor cortex, as a treatment for poststroke pain, despite no sham group (Kobayashi et al., 2015). This way, game-changing conclusions cannot be addressed, but the positive outcomes should prompt other similar and more complete studies.

3.9 Depression

Depression, also referred to as major depressive disorder (MDD), is a highly prevalent and disabling mood disorder, that causes a persistent feeling of sadness and loss of interest, leading to several emotional and physical problems (Staff, 2018) (Levkovitz et al., 2009).

Regarding the response to pharmacological interventions, depression presents an inter-individual variability, meaning that there is a need for alternative therapeutic strategies. Historically, this is the first condition for which dTMS is FDA-approved. But not only in the United States of America is dTMS an official therapeutic alternative for MDD. In many other European countries, dTMS is a first-line treatment for depression.

When it comes to depression's neuropathophisiology, neuroimaging studies point to an imbalance hypothesis, where the left DLPFC is hypoactive, and the right DLPFC is hyperactive (Rapinesi et al., 2018). Considering this, the most prominent rTMS target area in MDD is the DLPFC (Baeken et al., 2019), with high-frequency stimulation over the left DLPFC showing therapeutic efficacy in several studies (Cao et al., 2018). Levkovitz et al. (2015) conducted a double-blind randomized placebo-controlled multicenter trial, in which 181 MDD patients participated. The patients were randomly assigned to either a sham dTMS group or an active dTMS group. The treatment target was the left DLPFC, and the treatment course was divided into two phases, an acute phase, and a maintenance phase. During the acute treatment phase, dTMS sessions were performed daily, 5 days per week, for 4 weeks, for both groups. The maintenance phase consisted of two dTMS sessions per week, with a time distance of, at least, 48 hours between sessions, for 12 weeks. The active dTMS group received 18-Hz stimulation, whereas, the control group received sham dTMS. This was a monotherapy study, and antidepressants, mood stabilizers, and antipsychotics were not allowed during the course of the study.

After the 4 weeks of acute treatment, and after the first week of the maintenance phase, a statistically significant difference in the depressive total scores was found between the active and the sham groups. Response and remission rates, at the 5-week assessment, were also significantly different between the active and the sham groups. At the 16-week assessment, after the maintenance phase, the difference in the depressive scores between the active and the sham groups remained statistically significant, as well as the difference between the groups' response rates, but not the remission rates. The study also demonstrated that patients with higher resistance to medications tend to be less responsive to dTMS. However, the effect of the treatment

was significant in patients who failed one or two medications, relative to the sham group, and marginally significant, also relative to the sham group, in patients who failed three or more medications.

The presented study's results provide awareness of the efficacy and safety of high-frequency dTMS over the left DLPFC in MDD patients who did not benefit from previous antidepressant treatment, thus, giving a good insight into why Brainsway's dTMS treatment with H1-coils over the left DLPFC is an FDA approved treatment for patients with MDD. Otherwise, this would not be the pioneer study that led to this approval (Brainsway, ndb).

Like the previously mentioned study, several studies showing significant improvements in MDD's symptoms after a treatment of high-frequency over the left DLPFC exist. This is already an approved treatment in several countries and is being considered a first-line treatment according to North American and European guidelines (Baeken et al., 2019). Nowadays, worldwide researchers' focus, regarding dTMS application for MDD's therapeutic improvement, is to optimize response and remission rates (Baeken et al., 2019). An opinion review study by Baeken et al. (2019) aimed to summarize the current knowledge considering the rTMS treatment for MDD patients, as well as to address the future direction of this therapy. According to Baeken et al. (2019), there are several different paths through which improvement in the response and remission rates can be achieved.

Accelerated rTMS (arTMS) is a stimulation protocol aiming at rapid antidepressant effects. This protocol consists of several daily sessions and fewer treatment days. Accelerated high-frequency (aHF) and accelerated intermittent theta-burst stimulation (aiTBS) are two protocols that were already proven capable of yielding similar remission and response rates to daily rTMS. Validation and optimization of this protocol parameters are the future challenge (Baeken et al., 2019).

Coil positioning is a very important feature of an rTMS application, with slight changes in the coil position leading to variations in the brain regions being stimulated, and, consequently, to potential undesired outcomes. The most precise coil positioning approach is TMS neuronavigation (Baeken et al., 2019). However, clinical efficacy increase due to neuronavigation is yet to be proved, when comparing this technique with others like the 5-cm rule[2]. Future large controlled studies comparing the different positioning methods and their correlation with superior clinical outcomes are needed to disclaim the possibility of coil localization methods as a

[2]Technic used to position the TMS coil on the scalp over the DLPFC area. It consists of evoking a motor response in the first dorsal interosseus muscle of the contralateral hand, and then moving the coil 5 cm in an anterior direction along a parasagittal line.

potential strategy to improve clinical rTMS results in MDD (Baeken et al., 2019).

Stimulation of deeper areas is now possible with coils like the double-cone and the H-coils. dTMS coils also seem to be a future scientific investment concerning response improvement of this alternative treatment strategy (Baeken et al., 2019), as is the aim of the present study and the whole project we are involved in.

Baeken et al. (2019) mentions combinatory treatments, like combining rTMS treatment with psychopharmacotherapy, psychotherapy, or cognitive training, as possible synergistic treatment alternatives with potential to increase antidepressant effects, but lacking research studies (although we mentioned some, regarding other diseases, that achieved positive outcomes).

Maintenance rTMS (mTMS) is used after a successful response to an acute rTMS treatment and has been suggested to prolong the acute treatment's positive effects, with most of the patients achieving remission throughout an interval between 3 months and 5 years (Baeken et al., 2019). However, given the heterogeneous designs of the studies, the small sample sizes, and the lack of placebo controls, future research should focus on mTMS's capacity to prevent relapses and its long-term safety and efficacy (Baeken et al., 2019).

Finally, Baeken et al. (2019) focuses on future personalized and stratified rTMS treatments, with a prediction of response to rTMS treatment based on machine learning approaches and other advanced statistics (e.g., baseline cognitive performance as a predictor of response to rTMS, or anxiety and anhedonia dimensions, and associated resting-state functional magnetic resonance imaging connectivity patterns, as means for depression stratification and so, a predictor of response to rTMS treatment).

The scientifical trend is to improve the response and remission rates of MDD patients. As seen previously, several paths can lead to this ending, with a lot of research yet to be done. Even though dTMS is already an FDA-approved therapy, for some specific coil designs and protocols, the response and remission rates still have potential to improve, being one of the potential paths related to the work being developed in our project.

3.10 Multiple Sclerosis

Multiple Sclerosis is a potentially disabling chronic autoimmune disease of the central nervous system (Staff, 2021) (Ayache and Chalah, 2017). It is characterized by causing damage in the nerve cells, given the demyelination of the neurons, dis-

rupting the ability of parts of the nervous system to transmit signals. This condition leads to a range of symptoms and signs, including physical, mental, and, sometimes, psychiatric problems (Staff, 2021). Although multiple sclerosis is a condition with no cure, treatments can modify the course of the disease and manage symptoms (Staff, 2021). TMS, in particular, seems to offer a variety of solutions in several aspects, including applications in diagnosis, prognostic, disease classification, and some symptoms treatment (Simpson and Macdonell, 2015). In this work, we are only going to focus on therapeutic applications' studies.

Some of the most common symptoms related to MS are cognitive impairment, motor impairment, and fatigue (Snow et al., 2019). More precisely, spasticity, lower urinary tract dysfunction, manual dexterity, gait impairment, balance, fatigue, and cognitive deficits related to working memory are some of the common MS symptoms. Studies where a TMS treatment is delivered to MS patients have been showing significant improvements in several domains of the MS symptomatology spectrum.

Korzhova et al. (2019) studied the effect of two rTMS protocols on the level of spasticity and concomitant symptoms in patients with secondary progressive MS. Thirty-four patients were enrolled and randomized to three distinct rTMS groups: HF-rTMS (20 Hz), iTBS, and a sham stimulation group. For all the groups, the treatment consisted of 5 daily sessions of rTMS, over the course of 2 weeks. iTBS consisted of bursts at a 5-Hz frequency, with each burst consisting of three stimuli, following a 35-Hz frequency, for a total of 10 bursts. The primary outcome measures of this study were the subjective and objective levels of spasticity. The objective level of spasticity was measured at baseline and after the 10 sessions treatment, whereas the subjective level was measured at the same two time-points, plus a 2-week and a 12-week follow-up. The secondary outcomes were pain and fatigue, assessed at the same time-points as the subjective levels of spasticity. Only the HF-rTMS and the iTBS groups showed a significant reduction in objective and subjective levels of spasticity, after the treatment, and at the 2-week follow-up, being the spasticity improvements kept at the 12-week follow-up only by the patients in the iTBS group. No spasticity improvements were observed in the sham group. Only in the HF-rTMS group significant pain and fatigue improvements, compared to baseline, were achieved, after treatment, and at the 2-week follow-up, showing the 12-week follow-up a return to baseline values, in both pain and fatigue assessments.

Both the HF-rTMS and the iTBS treatments were effective regarding their anti-spastic effects, with improvements kept for a longer period in the iTBS group. Only the HF-rTMS protocol was effective in pain and fatigue symptoms improvement. According to Korzhova et al. (2019), the significant antispastic effect of both the

HF-rTMS and the iTBS protocols are consistent with previous studies that showed the efficacy of these rTMS protocols regarding the treatment of spasticity in MS patients.

Manual dexterity (a common MS symptom) improvements were assessed following an iTBS treatment protocol, by Azin et al. (2016). In this study, 36 patients were non-randomly assigned either to a sham rTMS or an iTBS treatment group. The stimulation target was the primary motor cortex, depicted in Figure 3.3, and the treatment intervention consisted of daily rTMS sessions, five days a week, for two consecutive weeks. The study results show a significant improvement in the dexterity in both the patients' hands, after treatment, compared to the baseline and the sham group results. These positive results remained three days after the last session. The authors of the study mention this result was consistent with other similar studies' results.

A more general analysis of the therapeutical TMS efficacy, regarding several MS symptoms, was made by Ruiz et al. (2020), in a review article. The conclusions of the authors are that there is evidence of significant improvement, after a TMS treatment, for spasticity, fatigue, lower urinary tract dysfunction, manual dexterity, gait alterations, and cognitive disorders involving working memory. The TMS protocols used in those treatments, with evidence of significant improvement, were iTBS and standard rTMS. The application of dTMS treatments with resort to Brainsway's coils has revealed, in two double-blind sham-controlled different studies, improvements in fatigue, depressive symptoms (a very common symptom in MS patients), speed, and walking ability. Brainsway's treatment for MS symptoms is CE-approved, opening space for future research investment in therapeutic alternatives for MS patients with resort to dTMS coils (Brainsway, ndc). To achieve the goal of a standardized approved treatment, Ruiz et al. (2020) suggests future well-designed prospective studies including larger samples and longer follow-up periods than most of the research studies conducted to date, for a higher level of evidence.

4

The Orthogonal Configuration immersed in conducting liquid: A simulation work

4.1 Previous collaborative works simulations

One of the downsides of TMS is the rapid attenuation of the induced currents with depth in the brain. State-of-the-art dTMS and TMS coils (H-coils, figure-8, etc.) have a low or moderate relative current induction in deep brain regions relatively to the maximum induced current at the surface of the brain. To our knowledge, and as possible to conclude from Chapter 3, the abnormal functioning of several regions deeply located in the brain might be related to different psychological and neurological diseases. Thus, the interest in deep non-invasive stimulation as a potential therapeutic alternative for many of these conditions has been on the rise.

The orthogonal configuration is a built-in-house dTMS system of coils created with the purpose of attaining higher relative $\vec{J}$ induction (RI) values in deeply located regions when compared to state-of-the-art dTMS coils. This dTMS configuration results from previous collaborative work within the investigation group developing the current project, LIP. Along its development, the system has been going through changes, with new designs always bringing it closer to a more practical reality.

The orthogonal configuration is a system comprised of 5 coils positioned perpendicular to one another, around a head model, as depicted in Figure 4.2. The head model and the coils are immersed in a conductive liquid, a crucial feature for the unprecedented obtained RI results, as we will see in Section 4.2.1. The coils distribution of this dTMS system is one on each side of the head, one anteriorly located, and the remaining two placed posteriorly relative to the patient's head (Santos, 2015), as depicted in Figure 4.2. To understand the scope of the present

and future work, two designs of the orthogonal configuration must be considered. Sousa (2014) started developing an orthogonal configuration that suffered multiple changes along their project. At first, an optimal volume of 140x140x70 cm^3 was found for the conducting liquid, and, thus, for the container, as depicted in Figure 4.2. At this stage of the project, all the coils presented a rectangular shape, with the dimensions of the bigger coils having 32 and 50 cm of width and length, respectively. One smaller coil, placed posteriorly to the head of the patient, presented a 27.8 cm width and 49.5 cm length.

However, given that the process of validation of such a system requires experimental testing, cost and available space have to come into account. Thus, considering the limitations of the project regarding budget and space, a container with smaller dimensions had to be considered and simulated by Sousa (2014). The new simulated container volume was 100x100x70 cm^3. This reduction in the dimensions of the container implied a consequent reduction of the coils' dimensions, making the four bigger coils having a 45 cm length, and a 27 cm width, with the smaller coil having a 44.5 cm length and a 22.8 cm width (Sousa, 2014).

A new setback emerged when the container for the experimental testing was purchased. The dimensions of the container did not match the last simulated version, as depicted in Figure 4.1. Consequently, a new container had to be simulated by Sousa (2014). In order to match with the container available for the experimental testing, the container was set to have a volume of 94x94x70 cm^3. The coils' size did not suffer any changes. Considering this container volume, an unprecedented RI at the center of the brain of 56.2% was achieved by Sousa (2014) simulations.

This previous collaborative work by Sousa (2014) was thought to be in compliance with the patients' safety requirements. Later simulations by Santos (2015), however, found that this system was not capable of guaranteeing the patients' safety. The introduction of a spherical volume of air surrounding the whole system, by Santos (2015), in order to replicate, in an approximate way, the real-world conditions, brought up safety concerns. In addition, this configuration had not been tested regarding the operators' safety, an essential work concerning the academical and clinical practice validation of the proposed configuration. Safety requirements unfulfillment led to a rearrangement of the system, which was called "new orthogonal configuration", being this system illustrated in Figure 4.2 a). Nevertheless, the physical construction of the orthogonal configuration setup following Sousa (2014) coils' dimensions and shapes had already been done, and, for the scope of this and future works, it is a valid configuration, when it comes to experimental tests.

Concerning the rearrangement of the system conducted by Santos (2015), it

Figure 4.1: 1000 litres fiberglass container purchased by Sousa (2014) for experimental validations of the orthogonal configuration. Adapted from Sousa (2014).

started with changes in the design of the coils. In Sousa (2014) orthogonal configuration, 5 rectangular coils were considered. In Santos (2015) work, the coils were redesigned to three triangular and two rectangular coils. This was a first attempt to reduce the currents induced in the heart of the patient, by increasing the distance between coils and the patient's torso, as depicted in Figure 4.2 a). It was always considered in Santos (2015) work the best compromise between the currents induced at the center of the brain and in the heart. This modification of the system's physical layout has also led to alterations of another important feature of the orthogonal configuration: the ratio between the currents on each coil. Correlated with a specific ratio between the currents flowing the coils is a specific RI at the center of the brain and an E-field distribution in the brain.

With the new system geometry introduced by Santos (2015), the currents in the coils went from $I_A = 0.75I_0$, $I_B = -4I_0$, $I_C = I_0$, $I_D = I_E = -I_0$, to $I_A = 0.3I_0$, $I_B = -4I_0$, $I_C = I_0$, $I_D = I_E = -I_0$, where $I_0 = 3184$ A is the current delivered by the built-in-house magnetic stimulator (Santos, 2015). Santos (2015) conducted a study with an alternative distribution of currents in the coils, capable of being attained with the stimulator possessed by the research group. The experimental currents considered by Santos (2015) were $I_A = I_0$, $I_B = -12I_0$, $I_C = 3I_0$, $I_D = I_E = -3I_0$. Experimentally, this will imply coil A as having one wire turn, coil B having twelve wire turns, and coils C, D, and E comprised of three wire turns

each, as explained in Section 2.3.1. For the scope of our work, in Chapters 5 and 6 simulations, we will maintain the coils' current distribution defined by Santos (2015) in the optimization process previously mentioned. For future experimental tests, Santos (2015) study results, where all the currents crossing the coils were defined by an integer factor of the stimulator current, must be considered.

With regards to brain stimulation, the effect of this system on induced $\vec{J}$ distribution and penetration power with depth is assessed with resort to a spherical head model. This head model is comprised of four concentric layers: skin, skull, cerebrospinal fluid (CSF), and brain, as depicted in Figure 4.3. The total radius of the head model was set to 10 cm, with the thicknesses of the skin, skull, and CSF set to 6 mm, 5 mm, and 2 mm, respectively. The brain solution fills the rest of the head model volume, making up a sphere of 8.7-cm radius (Santos, 2015). The spheric geometry of the head model was thus chosen given it allows for the results of the simulations to be generalized over the universal population since the results are not strict to a specific patient's head anatomy.

Concerning the head layers, each is characterized in the simulation software by its dielectric properties, specifically, the electrical conductivity, σ, and the relative permittivity, ε_r. However, in typical TMS frequency ranges, up to 10 kHz, biological tissues can be considered mainly resistive, making the contribution of the electrical permittivity obsolete, and thus the current density mainly dependent on the electrical conductivity of the tissue (Santos, 2015).

The simulation results obtained by Santos (2015) demonstrate an unprecedented power with depth of the new orthogonal configuration, with a capacity of achieving more than 60% RI at the center of the brain, and 82% and 72% RI at brain depths of 6 cm and 8 cm, respectively. This stimulation with depth capacity of the new orthogonal configuration distinctively surpasses the capacity of standard coils such as the figure-8 and the H1-coil, as depicted in Figure 4.4 .

As demonstrated in Figure 4.5, the $\vec{J}$ distribution, and as expected given the presence of the conductive liquid, shows the presence of the minimum of induced $\vec{J}$ in an anterior-inferior position. The maximum induced $\vec{J}$ of 5.40 A/m^2 is in compliance with the 6 A/m^2 threshold for frequencies in the kHz range (Santos, 2015).

For the scope of our work, the only features of the system that will differ relatively to the simulations conducted by Santos (2015) will be, as depicted and explained in chapters 5 and 6, the dimensions of the containers and the increment of an insulating sheet around the wires that make the coils. A spherical world of

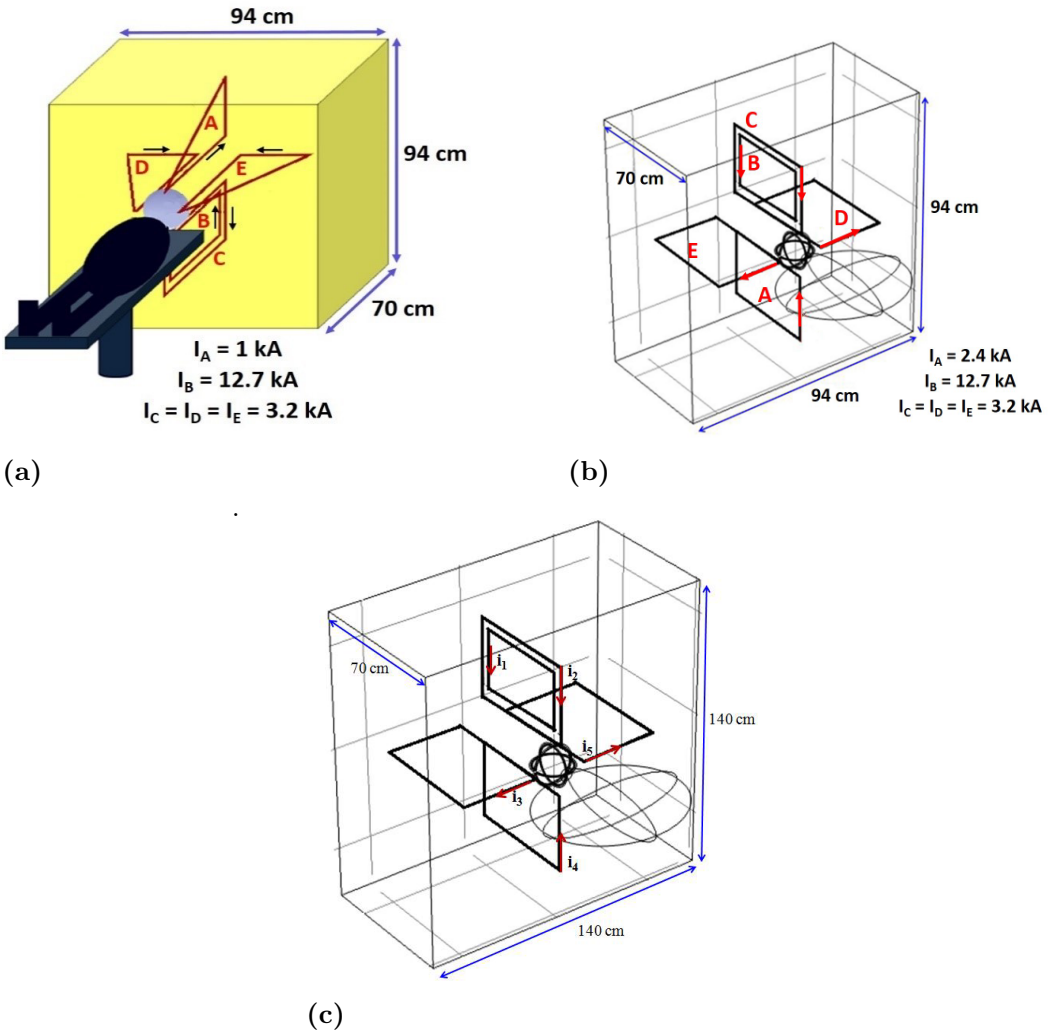

Figure 4.2: **a)** New orthogonal configuration by Santos (2015). The 3 triangular coils are placed anteriorly (A), and laterally (D and E). The rectangular coils are placed posteriorly, with the smaller coil (B) placed within the larger one (C). The black arrows represent the current direction flowing through the coils, while their respective intensity is indicated below the container, in kiloAmperes. The fiberglass container's dimensions are also represented. **b)** Simulated container by Sousa (2014) matching the dimensions of the experimental container. This configuration is composed of five rectangular coils with the same distribution in space as that of fig. **a)**. The coils' dimensions were approximately the same, except for coil B. The direction of the currents passing by the coils is indicated by the red arrows. The absolute maximum current values are indicated below in kA. **c)** First optimal container volume simulated by Sousa (2014). Five rectangular coils with similar dimensions (except for the coil where i1 current flows) were placed in anterior, posterior, and lateral positions. The direction of the currents passing by the coils is depicted by the red arrows. Adapted from (Santos (2015), Sousa (2014)).

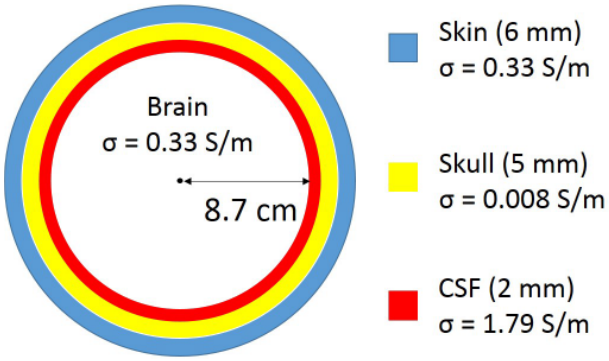

Figure 4.3: Representation of the layers constituting the simulations' head model. All the layers are spherical, being characterized electrically by their electrical conductivity, σ. The respective thicknesses and electrical conductivities are presented on the right side of the figure.

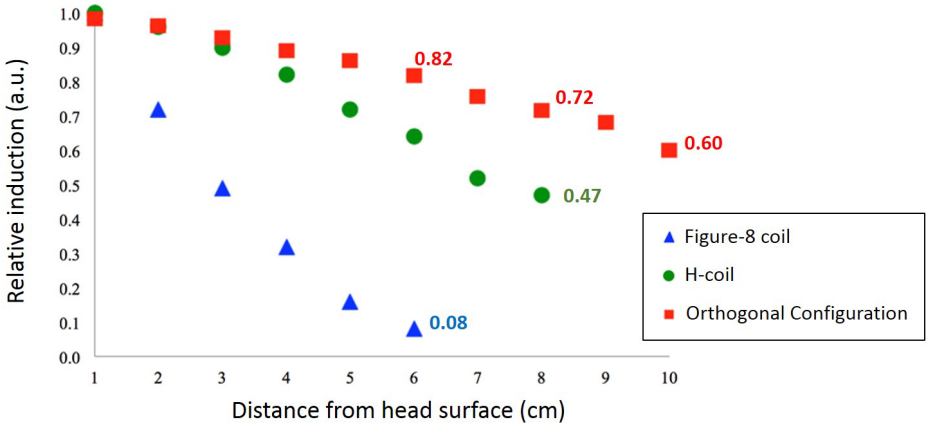

Figure 4.4: Power with depth of standard coils (Figure-8, H-coil) and the optimized orthogonal configuration model simulated by Santos (2015). Power with depth is represented by the current density, $\vec{J}$, induced with depth relatively to the surface maximum, in a spherical brain model. Adapted from Santos (2015).

air with a 2-m radius as depicted in Figure 4.6, will also be considered in all of the COMSOL Multiphysics® AC/DC simulations conducted in Chapters 5 and 6.

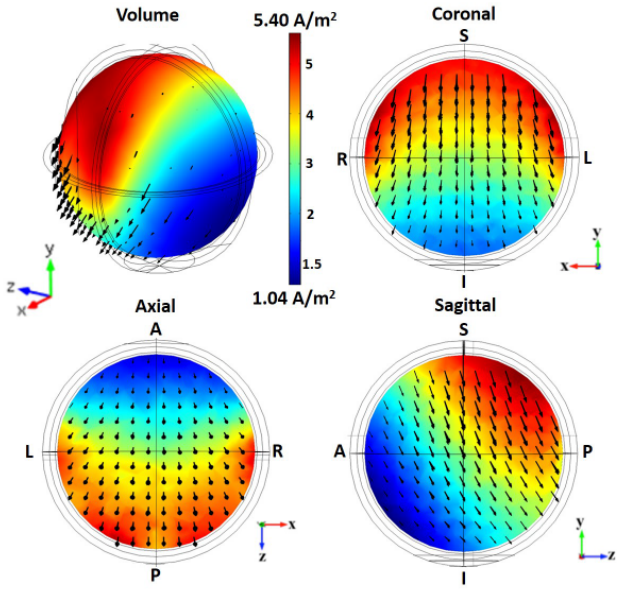

Figure 4.5: Color map of the current density, $\vec{J}$, distribution and respective directions in different views (three-dimensional, and the central-slices in the coronal, axial, sagittal planes), as a result of the simulations by Santos (2015) with the optimized orthogonal configuration. Both the head model and coils were surrounded by conductive liquid, and the whole system was surrounded by a 2-m radius spherical volume of air. S: superior. I: inferior. A: anterior. P: posterior. L: left. R: right. Adapted from Santos (2015).

4.2 Surface charge effect, conductive liquid, and skull contribution

4.2.1 Surface charge effect and conductive liquid

In previous studies concerning the dTMS project we are involved in, a conductive liquid surrounding the head model and the coils was introduced to this new configuration of stimulating coils. This liquid solution was included with the main purpose of mitigating one of the main factors of the rapid attenuation of the E-field with depth: the surface charge effect.

The surface charge effect arises from the electrical conductivity discontinuities at the surfaces separating the different head tissues. These different head tissues have different electrical properties, including the electrical conductivity, σ. In the presence of the induced electric field (E-field), ions accumulate at the interfaces between the different layers. These electric charges accumulate at these interfaces precisely as a consequence of the different electrical conductivities of the tissues.

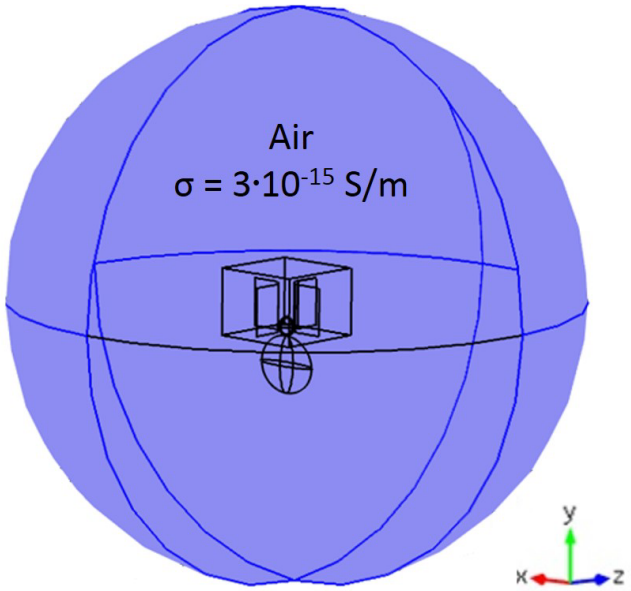

Figure 4.6: Spherical volume of air with a 3-m radius surrounding the whole experimental setup introduced by Santos (2015), and to be considered in all the simulations of the present work. The air volume electrical conductivity, σ, is also presented. Adapted from Santos (2015).

The different tissue conductivities lead to a higher normal component of the current density, $\vec{J}$, in the high conductivity tissues, as it is mathematically described in Section 2.3.1. This phenomenon leads to an accumulation of charge, due to the number of ions reaching the interface being higher than the ones leaving it. As a consequence of this charge accumulation effect, a discharge along the surface discontinuity occurs, as depicted in Figure 4.7. When several eddy-current paths reach the same portion of a discontinuity, this surface charge density grows, leading to a higher current density on the surface. The consequence of this charge accumulation on the surface discontinuity, also leading to a higher current density on this surface, is, thus, a decrease of the current density on the deeply located brain regions (Santos, 2015). Simulation works by Sousa (2014) have shown that this surface charge effect is, indeed, a direct consequence of the electrical conductivity discontinuities at the surface between the different layers.

A study by Sousa (2014), using the four-layer head model and a 5-cm radius circular coil located above the head model, analyzed three different cases. The first case consisted of the head model surrounded by air, and the three different layers surrounding the brain (skin, skull, CSF) with values equal to their real conductivities. In the second case, the head model and the coil were immersed in a conductive liquid with an electrical conductivity of about 120 times higher than the conductivity

of the brain. The three external layers of the head model were also considered with their respective conductivities. The third and final case consisted in a non-realistic situation, where all three external layers had the same conductivity, and the whole system was surrounded by the conductive liquid.

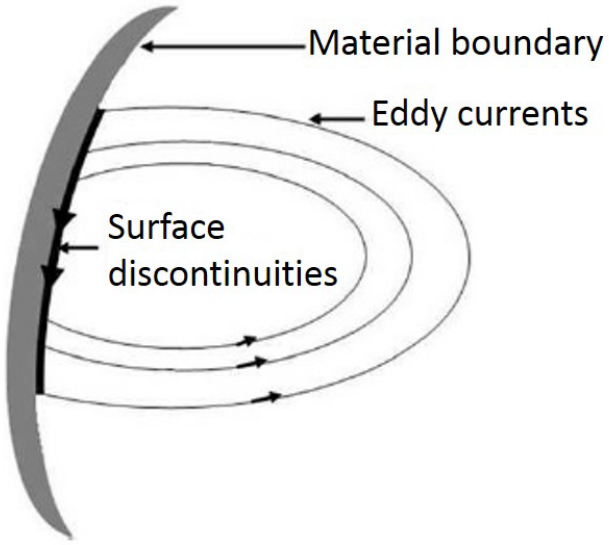

Figure 4.7: Representation of the surface charge effect. In a surface discontinuity, the eddy currents accumulate charge in the boundary, and an electrical discharge happens along the surface discontinuity. The bold black arrows represent the discharge along this surface discontinuity, and the thinner arrows the eddy currents' direction. Adapted from Oliveira et al. (2012).

The results of the study have shown that the surface charge effect is a consequence of the discontinuities of electrical conductivity present in the head. Figure 4.8 clearly supports this conclusion, as the head model with no discontinuities in electrical conductivity between its layers (Figure 4.8 - right) presents the highest RI at the center of the brain and the minimum induced $\vec{J}$ the furthest away from the center of the brain. This study is also important in understanding the important role of the conductive liquid, as the difference between having the brain surrounded by conductive liquid or air is reflected in RIs at the center of the brain of 13.8% or 3.3%, respectively.

Another study was conducted by Simões et al. (2013) with the purpose of demonstrating that this surface charge effect can be highly diminished by surrounding a brain-like solution ($\sigma = 0.11$ S/m), and the stimulating coils, with a conductive liquid. In Simões et al. (2013) work the brain-like solution was limited by a cylindrical container. This was a study conducted in the lab, where both the coil and the brain-like solution were immersed in a larger container filled with a saline solution

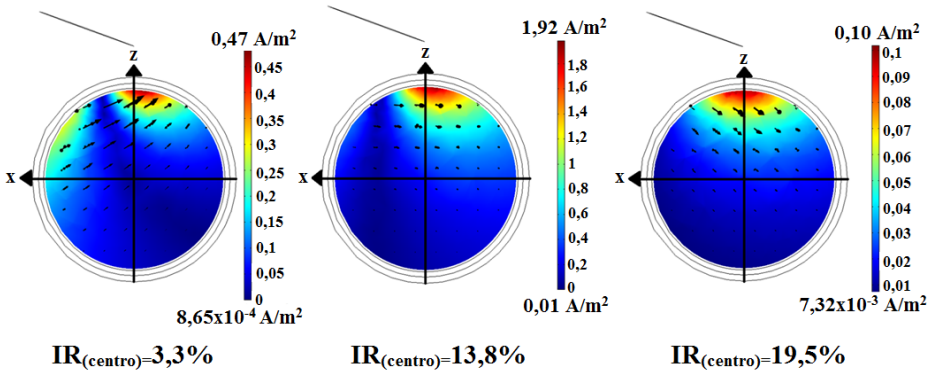

Figure 4.8: Representation of the color map distributions of the current density in the brain for three different cases. The color map distributions are the result of a study conducted by Sousa (2014), where the surface charge effect origin was studied. The left image represents the head model surrounded by air with all the layers having their respective electrical conductivities. The central image represents the head model surrounded by conductive liquid with all the layers having their respective electrical conductivities, and the image most to the right represents the head model surrounded by conductive liquid with all the head layers having the same electrical conductivity. It is possible to see the current density minimum getting further away from the brain center with the introduction of the conductive liquid, and the furthest away when all the layers have the same electrical conductivity. These results allow to conclude that the surface charge effect is a result of electrical conductivity discontinuities between the head layers. Adapted from Sousa (2014).

50 times more conductive than the brain solution. The experiment consisted of applying a TMS monophasic pulse, delivered by a built-in-house magnetic stimulator, and measuring the induced E-field in several points of the brain-like solution. This monophasic pulse was applied in two situations. In the first situation, the coil and the brain solution were surrounded by air, whereas, in the second situation, the coil and the brain solution were immersed in the conductive liquid.

As a result of the experience, it was observed a signal loss, from the center of the container to the surface maximum, of 84% and 24%, when the stimulator coil and the brain-like solution were surrounded by air and conductive liquid, respectively (Simões et al., 2013). The reduction in the signal loss was quite notorious, thus showing that by immersing the whole system involved in the stimulation (coil and brain model) in a conductive liquid, the signal intensity loss from the surface of the brain to its center can be highly diminished.

4.2.2 Effect of tissue conductivity

As mentioned in the previous sub-section, the presence of a conductive liquid surrounding the head model and the stimulating coil is crucial for the unprecedented results regarding the RI at the center of the brain. A simulation study, with the purpose of comprehending the physical origin of the deep stimulation achieved by the proposed configuration of this Deep-Brain TMS project, was conducted by Santos (2015). It was crucial to understand if there was an electrical contribution due to the presence of the conductive liquid, rather than just the magnetic stimulation, and, if so, the magnitude of this electrical stimulation concerning the neuromodulation capabilities of this dTMS configuration.

With this in mind, Santos (2015) conducted a simulation considering an insulating layer located specifically between the skin layer and the cerebrospinal fluid (CSF). The purpose of the study was to specifically understand the impact of the skull in the induced $\vec{J}$ in the brain. This simulation study was performed under the COMSOL Multiphysics® AC/DC software. The results and conclusions of the study are presented next, in Section 4.2.2.1.

4.2.2.1 Impact of the skull tissue conductivity and the new orthogonal configuration

The skull is known as the head layer surrounding the brain that has the lowest electrical conductivity, σ. To understand the impact of this layer on the induced $\vec{J}$ distribution by the new orthogonal configuration, Santos (2015) conducted two simulation studies. The first study consisted of three distinct cases. In this study, the impact of an insulating layer on the distribution of the induced $\vec{J}$ was analyzed. The coil used in the study was a 5-cm radius circular coil. In all of the cases, the coil was placed above the head model.

In the first case, a head model consisting of two layers having real electrical conductivity values and one insulating layer with an electrical conductivity of 1×10^{-15} S/m, was surrounded by air. In the second case, the same electrical conductivities of the previous case were considered for the same layers, but the medium surrounding the head model and the coil was the conductive liquid ($\sigma = 10$ S/m). The third case consisted of all three layers having the same insulating conductivity, 1×10^{-15} S/m, surrounded by the conducting liquid. The results are depicted in Figure 4.9.

The results obtained with this simulation demonstrated that the presence of the insulating layer hinders the reduction of the surface charge effect observed when considering a conductive solution around the head model. This means that the

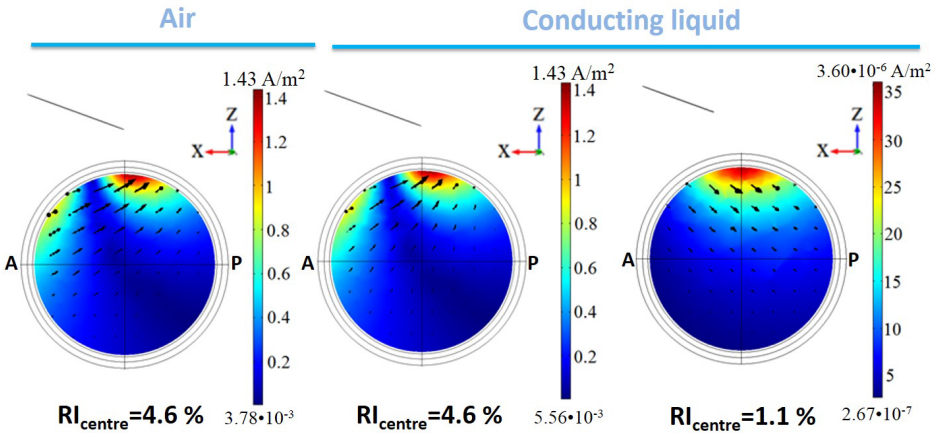

Figure 4.9: Color map of the current density, $\vec{J}$, distribution, and respective direction induced in the brain for three different cases, when stimulated by a circular coil positioned above the head model and tilted by 20^o. This study was conducted by Santos (2015) to understand the impact of the skull layer on the induced $\vec{J}$ in the brain by the new orthogonal configuration. The left image consists of the skull layer being replaced by an insulating material ($\sigma = 1 \times 10^{-15}$ S/m), while the head model and circular coil were surrounded by air. The central image consists of the same layers as in the previous case, with the circular coil and the head model being surrounded by the conductive liquid. In the right image, all of the layers are replaced by an insulating layer, and the head model and circular coil are surrounded by air. All the cases represent a sagittal view of the current density distribution in the brain, with the relative current density distribution at the center of the brain relative to the surface maximum (RI) being presented for each case. A: anterior. P: posterior. Adapted from Santos (2015).

presence of the insulating layer leads to charge accumulations at the interfaces of the skin/insulator and insulator/Cerebrospinal fluid (CSF) that cannot be avoided in spite of the presence of the conductive liquid. It can also be seen in Figure 4.9 that the $\vec{J}$ distribution and direction, and RI at the center of the brain are quite similar between the situations depicted in the middle and left images. According to the right image depicted in Figure 4.9, it can be seen that when all the external layers have the same electrical conductivity, the surface charge effect vanishes.

The second study conducted by Santos (2015) was similar to the first one, but instead of a circular coil, the new orthogonal configuration was considered. In the first case, the head model had all the different layers with their real electrical conductivities, and the whole system (head model and coils) was surrounded by air. In the second case, the skull layer was replaced by an insulating layer, with $\sigma = 1 \times 10^{-15}$ S/m, and the entire system was surrounded by the conductive liquid ($\sigma = 10$ S/m). The results of the two cases are depicted in Figures 4.10 and 4.11.

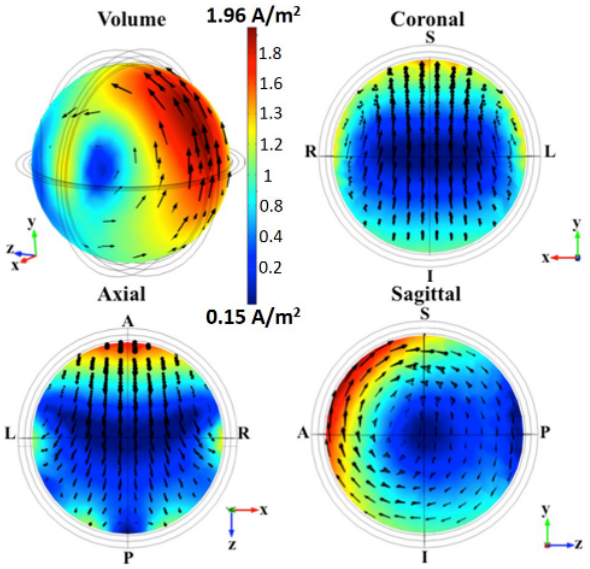

Figure 4.10: Color map of the current density distribution and respective current direction induced in the brain volume. A three-dimensional view and three different central slices (Coronal, Axial, Sagittal) are depicted. All the different head layers have their original electrical conductivity, and the head model and the orthogonal configuration coils were surrounded by air. The results depicted show the consequence of the surface charge effect, with the minimum RI located at the center of the brain. S: superior. I: inferior. A: anterior. P: posterior. L: left. R: right. Adapted from Santos (2015).

From the first case, it can be seen that, comparatively with the previous results obtained with the new orthogonal configuration surrounded by conductive liquid by Santos (2015) (mentioned in Section 4.1), changing the surrounding medium to air leads to drastic changes in the induced $\vec{J}$ distribution in the brain. These changes are reflected in the direction of the currents, the shift of the minimum $\vec{J}$ from the anterior-inferior region to the center of the brain, and also in the magnitude of the induced $\vec{J}$. The difference in magnitude, and the shift of the minimum $\vec{J}$ to the center of the brain, arise from the lack of attenuation of the surface charge effect, which was attained by surrounding the whole system with the conductive liquid.

The second case of this study allows observing the influence of adding an insulating layer to the head model, as well as to conclude about the meaningful contribution of the skull currents to the distribution of currents attained with the new orthogonal configuration. From Figure 4.11, it is possible to see that the direction of the induced currents and the position where the minimum $\vec{J}$ is induced inside the brain are practically the same as the ones depicted in Figure 4.10.

The values of the $\vec{J}$, as well as of the relative induction at the center of the

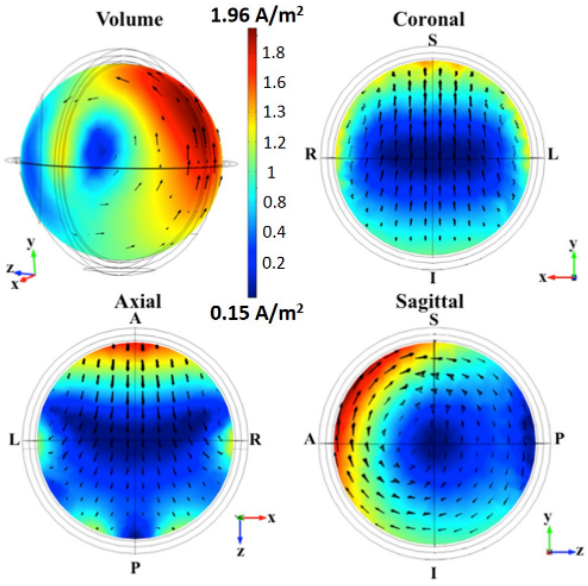

Figure 4.11: Color map of the current density distribution and respective current direction induced in the brain volume. A three-dimensional view and three different central slices (Coronal, Axial, Sagittal) are depicted. All the different head layers have their original electrical conductivity, except the skull layer. A highly insulating layer was considered instead in spite of the skull. The head model and the orthogonal configuration coils were surrounded by conductive liquid. The results depicted show the consequence of having an insulating layer. The surface charge effect attenuation by the conductive liquid is hindered by the presence of the insulating layer, with the minimum RI still located at the center of the brain. S: superior. I: inferior. A: anterior. P: posterior. L: left. R: right. Adapted from Santos (2015).

brain, for the two cases, were found by Santos (2015) to be extremely similar. Since the whole system, in the second case, is surrounded by conductive liquid, and having in mind all the similar results obtained from the two cases, it is possible to conclude from this study how significant is the skull currents' contribution to the distribution of currents obtained with the orthogonal configuration in the brain. More precisely, it is possible to conclude that the brain currents induced by the orthogonal configuration are strongly complemented by electrical currents existing in the skull (Santos, 2015).

This was also a major study concerning the objectives of our work since one of our main focuses was to find a material with a similar electrical conductivity to that simulated for the skull layer of the head model, in order to, in future collaborative works, try to achieve experimentally similar results to the ones obtained in this study by (Santos, 2015)

5

The Orthogonal configuration immersed in conductive liquid: towards a practical implementation

We focused our work on finding material solutions for the future experimental tests, on improving via simulation some of the new orthogonal configuration features, and also on getting our simulated system closer to some of the features of the future experimental stimulation tests. This work is described throughout the next sections. All the simulation work presented in this chapter was developed using the COMSOL Multiphysics® AC/DC software.

5.1 Head model with skull's physical properties and experimental setup progress

A very important conclusion of Santos (2015) previous work was that the electric currents induced in the skull play a major role in the unpreceded "high penetration power of this new 5-coil dTMS system". Being the skull the layer of the head model with the lowest electrical conductivity, Santos (2015) conducted a simulation study to understand if the currents induced in this layer had an important physical influence in the currents induced in the brain, as described in Section 4.2.2.1. This important conclusion by Santos (2015) simulation work was the main experimental test we were aiming to conduct in this project, but, in order to achieve this goal, some materials were still missing. Specifically, a material with a similar or equal electrical conductivity to the one used in Santos (2015) simulation works for the skull layer was still to be found. The value we were looking for was an electrical conductivity of ≈ 0.008 S/m.

Companies
Silicone Engineering Ltd. (UK)
Primasil Silicones Ltd.(UK)
Elastostar Rubber Corporation (USA)
Wacker Chemie AG (Ge)
Soliani EMC s.r.l. (Ita)
Specialty Silicone Products, Inc. (USA)
Simolex Rubber Corporation (USA)
Shin-Etsu Chemical Co., Ltd. (Jap)
OCSiAI - Tuball (Lux)
Stockwell Elastomerics, Ltd. (USA)
Avantor, Inc. (USA)

Table 5.1: Companies providing conductive silicone solutions that might fit the electrical properties needed for an experimental skull-model.

It was not easy to find a material with the specific physical and electrical properties this part of the project requires, but after analyzing the diversity of physical properties silicone materials can have, in a silicone solutions company catalogue about characteristic properties of silicone rubber components, some interesting results were found, as it is depicted in Figure 5.1. We found that conductive silicone rubbers can have electrical conductivities similar to the value determined for the skull layer in the simulation model ($\sigma = 0.008$ S/m $(=)$ $\rho = 125\ \Omega \cdot m$). After looking for companies working with silicone materials, we have identified many that might be able to provide the solution we are looking for, being all these companies identified in Table 5.1. Although, at the time, we have made already contact with Silicone Engineering Ltd., no agreement to a final solution was yet settled.

This finding of the silicone materials solution brought some other interesting future applications for the work yet to be done within the aim of our dTMS system project. Within the silicone solutions the companies presented in Table 5.1 offer, there are different types of silicone materials when it comes to the material rigidity. There are some silicone solutions in which the material is more rigid (solutions that fit for the skull model solution), and some solutions in which the material is more flexible, i.e., less rigid. Looking at silicone's range of electrical conductivities depicted in Figure 5.1, we notice that silicone materials can also have electrical conductivities equal or close to that of the conductive liquid ($\sigma \approx 10$ S/m). Thus, we realize that a cap-like solution that potentially would not harm the unprecedented stimulation results we are aiming at with this new project, since the electrical con-

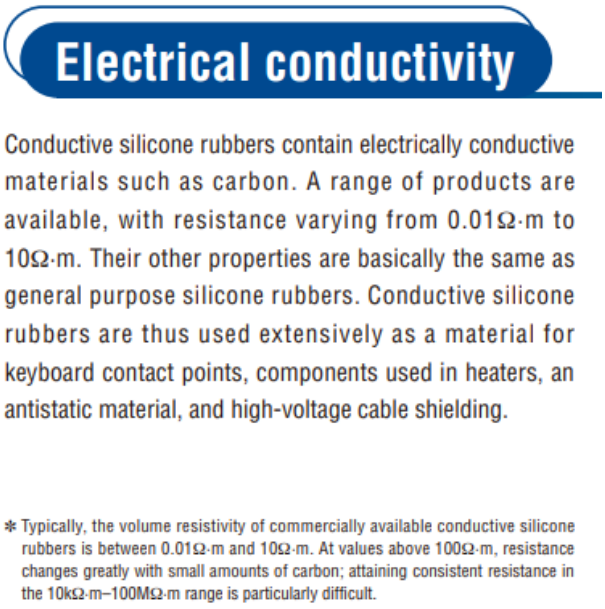

Electrical conductivity

Conductive silicone rubbers contain electrically conductive materials such as carbon. A range of products are available, with resistance varying from 0.01Ω·m to 10Ω·m. Their other properties are basically the same as general purpose silicone rubbers. Conductive silicone rubbers are thus used extensively as a material for keyboard contact points, components used in heaters, an antistatic material, and high-voltage cable shielding.

* Typically, the volume resistivity of commercially available conductive silicone rubbers is between 0.01Ω·m and 10Ω·m. At values above 100Ω·m, resistance changes greatly with small amounts of carbon; attaining consistent resistance in the 10kΩ·m–100MΩ·m range is particularly difficult.

Figure 5.1: Text script from Shin-Etsu (2020), a Shin-Etsu catalogue about their silicon rubber compounds products, regarding typical electrical conductivities of conductive silicone rubbers.

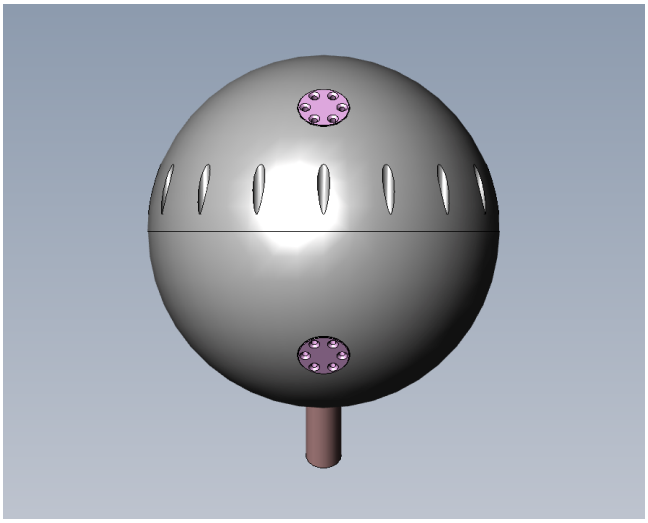

Figure 5.2: Spherical shape head model to be used in experimental tests.

ductivity of the cap would be the same as that of the liquid conductive solution, might also be possible to attain with resort to the silicone materials. In addition, a flexible solution for this silicone-based cap would be ideal, in order for it to fit different head shapes and sizes.

Furthermore, regarding works related to the experimental setup, a container and

a pump were also already acquired by LIP's high-precision mechanical workshop, in order to prepare the conductive solution outside the container where the coils will be placed, and pump this solution in and out the container that is part of the experimental setup. Another important step given throughout the development of this project was the development of two sensors (essentially made-up of a coil), to be placed inside the head model, at the top, and center of the sphere, so that, in future works, it is possible to measure the relative induction at the center of the brain, in order to try to validate the results obtained with the simulations.

5.2 Electric wires insulation

Santos (2015) simulation work did not include an insulating layer around the electric wires that make up the coils. This is an important feature to be added to the simulations yielded by Santos (2015) since in real conditions this insulation layer is going to be added to the system's electrical wires.

In this part of the project, we have conducted a simulation in the COMSOL Multiphysics® AC/DC software, considering an insulating material ($\sigma = 10^{-15}$ S/m) surrounding the electric wires, with a 5-mm radius, as depicted in Figure 5.3. The whole apparatus of the orthogonal configuration in this simulation was the same as that of Santos (2015) simulations. The only difference was the insulation sheet in what were previously bare wires.

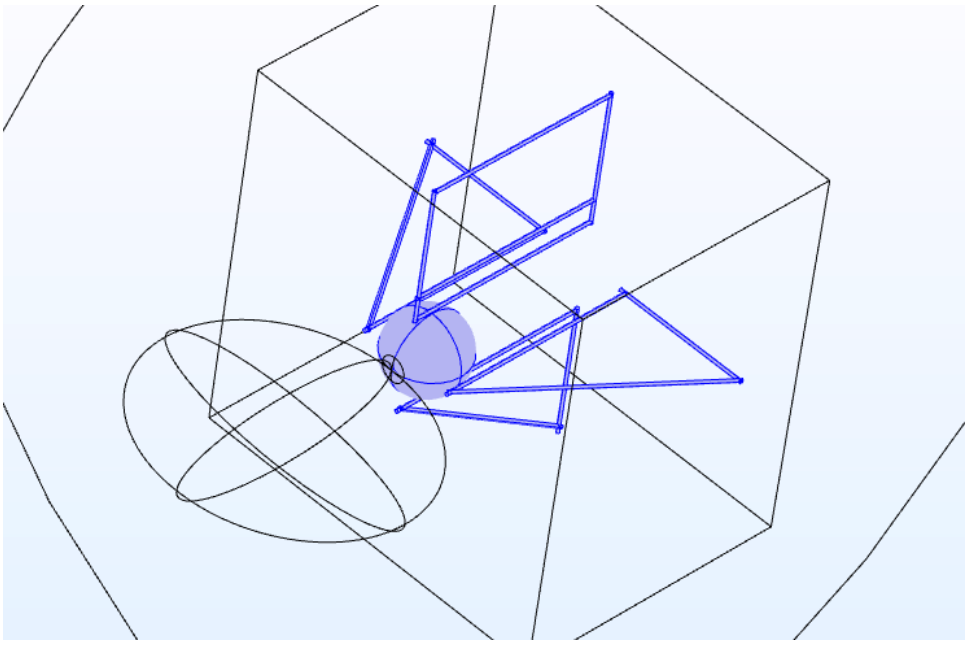

Figure 5.3: Orthogonal configuration with insulated wires.

The distribution of the induced $\vec{J}$ at the brain layer for these simulations is depicted in Figure 5.4. The results obtained are very similar to those obtained previously by Santos (2015), both in terms of the induced $\vec{J}$ intensity in the various brain areas, and of the $\vec{J}$ distribution. The maximum induced $\vec{J} = 5.7932$ A/m^2 is also in compliance with the cortical activation threshold value of 6 A/m^2, defined for frequencies in the kHz range. As mentioned by Santos (2015), in case it becomes necessary to increase the maximum current density in the brain to values equal to the cortical activation threshold, 6 A/m^2, it is possible to increase the value of I_0, the output current of the stimulator, to achieve that. Hence the output current of the stimulator is increased, the current in all the five coils will increase by the same amount, thus not affecting the $\vec{J}$ distribution.

In Santos (2015) work, an unprecedented value of 60% RI at the center of the brain (10-cm depth) relative to the surface maximum was achieved, as mentioned in Section 4.1. In this simulation, the induced RI at the center of the brain is even more promising, as we obtained an ever higher and unprecedented 71% RI at the center of the brain.

Comparatively to the state-of-the-art coils, namely, the figure-8 coil and the H1-coil, and even the previous simulated new orthogonal configuration with bared wires, the value of 71% RI at the center of the brain, achieved with the insulation layer surrounding the electric wires of the coils, represents an unprecedented stimulation power with depth. The mentioned state-of-the-art coils (figure-8 and H1-coil) cannot stimulate brain areas as deep as this new configuration. Comparing the RI at attainable stimulation depths for these coils and the new orthogonal configuration with insulated wires, it is noticeable that, at deep brain areas, this configuration RI distinctively surpasses the RI of these state-of-the-art coils, and even the new orthogonal configuration with bare wires, as it is depicted in Figure 5.5.

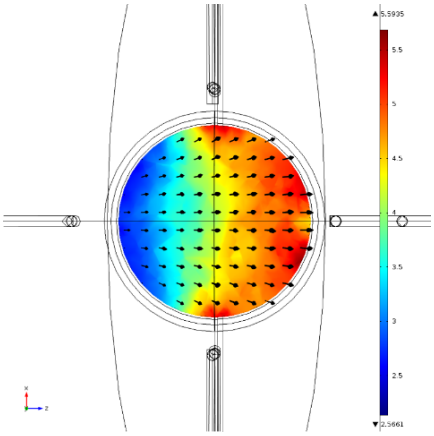

(a) Axial view: Max $\vec{J} = 5.59$ A/m^2. Min $\vec{J} = 2.57$ A/m^2.

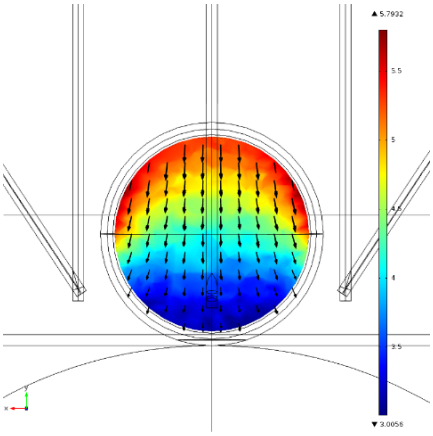

(b) Coronal view: Max $\vec{J} = 5.79$ A/m^2. Min $\vec{J} = 3.00$ A/m^2.

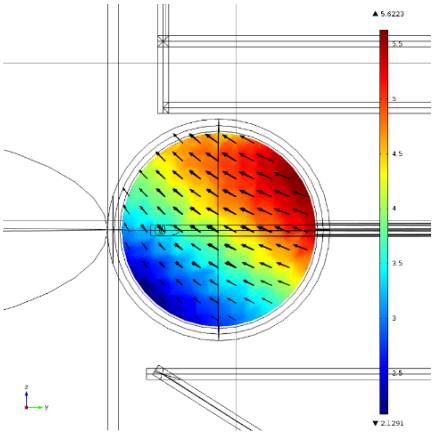

(c) Sagittal view: Max $\vec{J} = 5.62$ A/m^2. Min $\vec{J} = 2.13$ A/m^2.

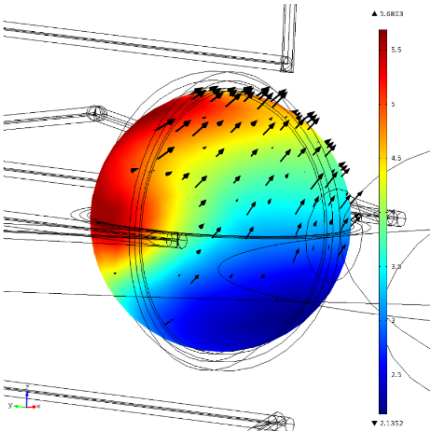

(d) Brain volume: Max $\vec{J} = 5.68$ A/m^2. Min $\vec{J} = 2.14$ A/m^2

Figure 5.4: Color map of the current density, $\vec{J}$, distribution in the brain when stimulated by the optimized orthogonal configuration with insulated wires. A three-dimensional view and three central slices (axial, coronal, sagittal) are depicted.

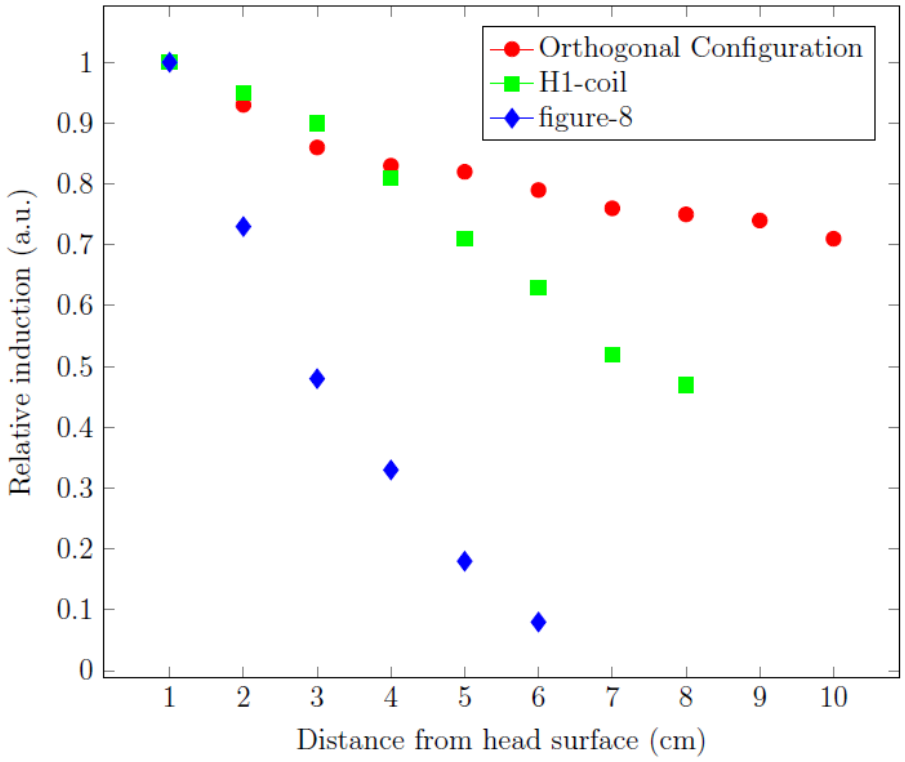

Figure 5.5: Current density, $\vec{J}$, induction relative to surface maximum, with brain depth, for the optimized orthogonal configuration with insulated wires, and state-of-the-art coils. Unprecedented power with depth observed. Data for the figure-8 and H1-coil obtained from Roth et al. (2007).

6

Optimizing the dimensions of the Orthogonal configuration's container

The new orthogonal configuration is a system of coils perpendicularly placed to one another, enclosed in a container that is made up of a volume of $70 \times 94 \times 94$ cm^3, being the coils immersed in a conductive liquid, as described in Chapter 4. This volume is approximately the same as that of the conductive liquid surrounding both the coils and the head model (less the volume of the head model and the coils' layout). Foreseeing the potential future application of this new dTMS system in a clinical/hospital environment, it is difficult not to picture the lack of practicality involved in and with the whole system and associated processes. The dimensions of the container make clear that the system will occupy a relevant amount of space, considering a clinical or hospital environment. As a consequence, the amount of water and NaCl to be used as solvent and solute of the conductive liquid will also be high. These questions led us, throughout this part of the project, to study the consequences of varying the dimensions of the container, while not varying the dimensions of the coils.

A similar study to this one was already conducted by Sousa (2014). It was from this previous work that resulted the dimensions of the simulated container by Santos (2015) depicted in Section 4.1. All the simulations by Sousa (2014) guaranteed that the coils were totally immersed in water. However, in the study presented in this dissertation, even though aware that the simulations' induced currents RI at the center of the brain had a high probability of not being as promising as the value already achieved with the coils totally immersed in water, we have decided to evaluate the results of varying the container's dimensions, while not varying the coils' dimensions. This means that, in the following presented studies, part of all the coils or just some particular coils will be outside of the container and not in

contact with the conductive liquid. With this study, we intend to understand if there are any promising results regarding the induced currents distribution in the brain considering this particular approach. Our aim is to achieve a more practical design of the whole system for a potential future real application.

With this in mind, this part of the project consisted of two different approaches concerning the changes we introduced to the system. In one of the studies, we focused on changing just one of the container's dimensions (width), while in the other we focused on changing all the dimensions by the same amount, while concurrently having all the container's dimensions the same size. Both studies were simulation-based, having been the simulations conducted with resort to COMSOL Multiphysics® AC/DC software. In all the simulations the container is only represented by the volume of conductive liquid, consequently meaning that we are varying the volume of conductive liquid, although it is referred throughout the text as the container.

6.1 Cubic container

This study consisted of four different simulations in COMSOL Multiphysics® AC/DC. In all the simulations we varied the container's dimensions by the same amount (10 cm). Only in the last simulation (container with the bigger dimensions), the depth of the container was kept equal to that of the container simulated by Santos (2015).

The approach behind this study consists in the increase of the container's dimensions by the same amount, with all dimensions having the same size. We can thus understand if having all the coils with part of their structure outside the conductive liquid affects significantly the $\vec{J}$ distribution in the brain, as well as the RI at the center of the brain. If the results diverge negatively from the results previously obtained in Section 5.2, there is no interest in further studying this particular approach.

From Figure 6.1 it is possible to see that in all the containers part of the coils are outside the container, i.e., in all the containers the coils are not totally immersed in the conductive liquid.

As we can see from Table 6.1, the value of the RI at the center of the brain increases with the enlargement of the conductive liquid volume. This increase in the dimensions of the container also leads to an increase of the surface maximum $\vec{J}$, and consequently, the $\vec{J}$ in the center of the brain. As the coils are almost totally immersed in the biggest simulated container, the RI at the center of the

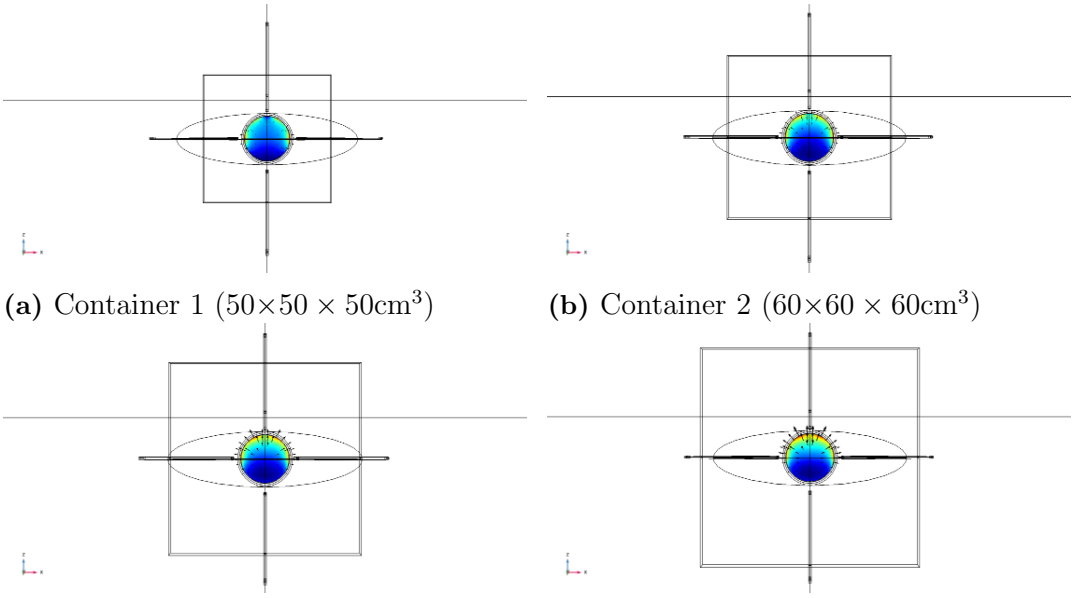

(a) Container 1 ($50\times50\times50\text{cm}^3$) **(b)** Container 2 ($60\times60\times60\text{cm}^3$)

(c) Container 3 ($70\times70\times70\text{cm}^3$) **(d)** Container 4 ($80\times70\times80\text{cm}^3$)

Figure 6.1: First study: cubic containers. All the simulated containers are depicted with the respective central brain slice current density, $\vec{J}$, distribution in a distanced axial view. Each container's dimensions are listed below each sub-figure.

brain (67%) becomes very close to the value obtained with the dimensions of the container simulated in Section 5.2 (71%).

Container	**Volume** (dm^3)	**Max** $\vec{\boldsymbol{J}}$ (A/m^2)	**Min** $\vec{\boldsymbol{J}}$ (A/m^2)	**RI**	**Central** $\vec{\boldsymbol{J}}$ (A/m^2)
1	125	3.28	0.567	48%	1.57
2	216	4.03	0.888	57%	2.29
3	343	4.71	1.33	64%	3.01
4	448	5.27	1.76	67%	3.53

Table 6.1: Dimensions and achieved simulations' results for four different cubic containers. Volume: Individual container's volume. Max $\vec{J}$: Maximum $\vec{J}$ recorded in the brain (at the surface). Min $\vec{J}$: Minimum $\vec{J}$ recorded in the brain. RI: Relative $\vec{J}$ induction at the center of the brain comparatively to the surface maximum. Central $\vec{J}$: Recorded $\vec{J}$ value at the center of the brain.

The maximum induced $\vec{J}$ value in the brain changes from container to container. Depending on the volume of conductive liquid surrounding the dTMS system, and, as a consequence, the proportion of the coils' volume immersed in it, this value tends to be higher for greater volumes.

Looking at the distribution of the induced $\vec{J}$ in the brain for all the particular cases studied, in Figure 6.2, we notice that the minimum $\vec{J}$ is not located at the center of the brain. This correction in the induced $\vec{J}$ distribution was accomplished

in previous works (Simões et al. (2013), Sousa (2014)) with the introduction of the conductive liquid surrounding the whole dTMS system and head model, and is a consequence of the mitigation of the surface charge effect, as seen in Section 4.2.1.

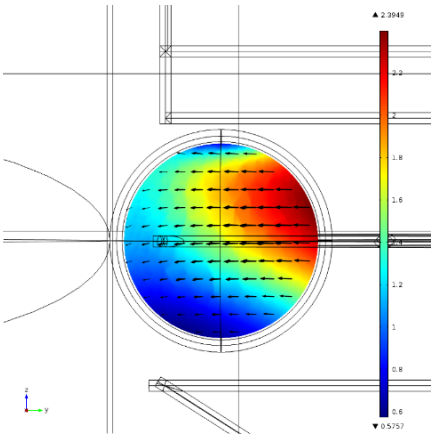

(a) $\vec{J}$ distribution in the brain for container 1. Max $\vec{J} = 2.40$ A/m^2. Min $\vec{J} = 0.58$ A/m^2.

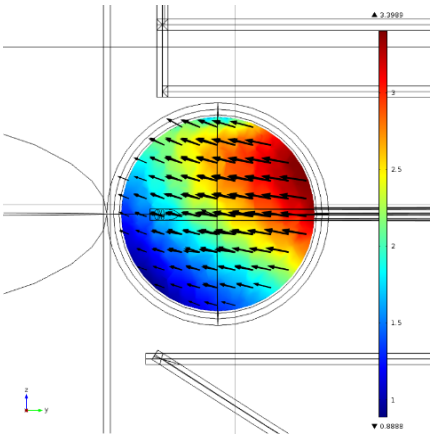

(b) $\vec{J}$ distribution in the brain for container 2. Max $\vec{J} = 3.40$ A/m^2. Min $\vec{J} = 0.89$ A/m^2.

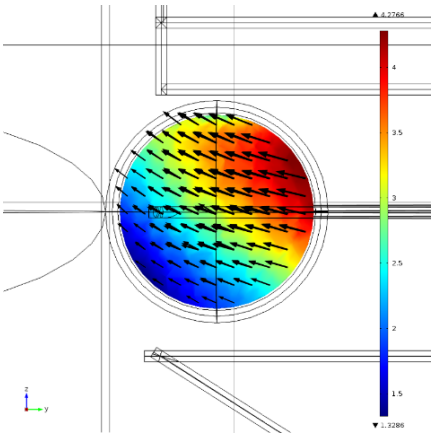

(c) $\vec{J}$ distribution in the brain for container 3. Max $\vec{J} = 4.28$ A/m^2. Min $\vec{J} = 1.33$ A/m^2.

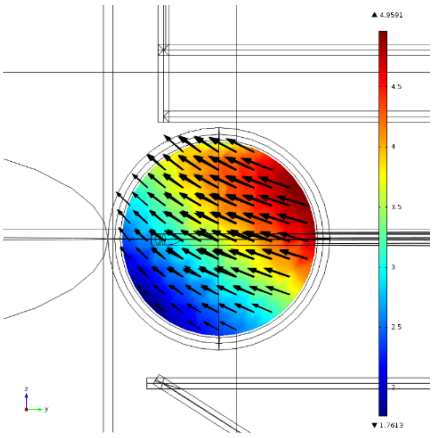

(d) $\vec{J}$ distribution in the brain for container 4. Max $\vec{J} = 4.96$ A/m^2. Min $\vec{J} = 1.76$ A/m^2.

Figure 6.2: Color map of the $\vec{J}$ distribution in a central sagittal view for the four simulated cubic containers.

The overall distribution of the induced $\vec{J}$ in the brain for all the different containers simulated in this study is also very similar to the distribution of the $\vec{J}$ obtained with the system configuration simulated in Section 5.2. This was an expected result since the relationship between the currents passing through each coil was kept equal to the original relationship, and constant throughout the different simulated systems.

Looking at the results obtained from this simulation study, and comparing them to those obtained with the simulation in Section 5.2, we can conclude that the solutions we arrived at are not the best fit for the goals we established. Our main goals with this study were to reach a more practical solution regarding the container's dimensions while maintaining some of the previous good results regarding current induction in the brain (RI at the center). With neither of the simulated containers we reached a value as good as the RI at the center of the brain achieved with the simulated layout in Section 5.2 (71%). The simulated containers with results closer to that of Section 5.2 were characterized by dimensions similar to the original ones, bringing no significant improvement in terms of practicality to the system and surrounding environment.

6.2 Varying the container's width

The second study we conducted to assess the effect of the container's dimensions on the induced $\vec{J}$ distribution in the brain was carried out with a different approach when it came to varying the container's dimensions. This was also a study based on COMSOL Multiphysics® AC/DC simulations, but in this case there was only one dimension of the container varying: the width. Just like the previous study in Section 6.1, this study was also made via four different simulations, as depicted in Figure 6.3, and from simulation to simulation, only the width of the containers varied.

As depicted in Figure 6.3, the coils located at the lateral positions are, in all cases, only partially immersed in the conductive liquid, while the anterior and posterior coils are always fully immersed in the conductive liquid. In Table 6.2 we present the values of the RI at the center of the brain, the maximum and minimum values of the induced $\vec{J}$ in the brain, and the values of the induced $\vec{J}$ in the center of the brain.

From Table 6.2, we see that the maximum induced $\vec{J}$ in the brain model increases with the expansion of the width of the container. However, from container to container these maximum values of induced $\vec{J}$ do not have significant alterations.

As seen in the previous study (Section 6.1), the distribution of the induced $\vec{J}$ throughout the brain is similar to the induced $\vec{J}$ distribution in Section 5.2 simulation, as it is depicted in Figure 6.4. Thus, we notice that the minimum induced $\vec{J}$ is also not located at the center of the brain. Although Figure 6.4 only depicts the $\vec{J}$ distribution in a central sagittal plane for all the containers, three-dimensional, central axial, and central coronal views of the $\vec{J}$ distribution for all of these containers

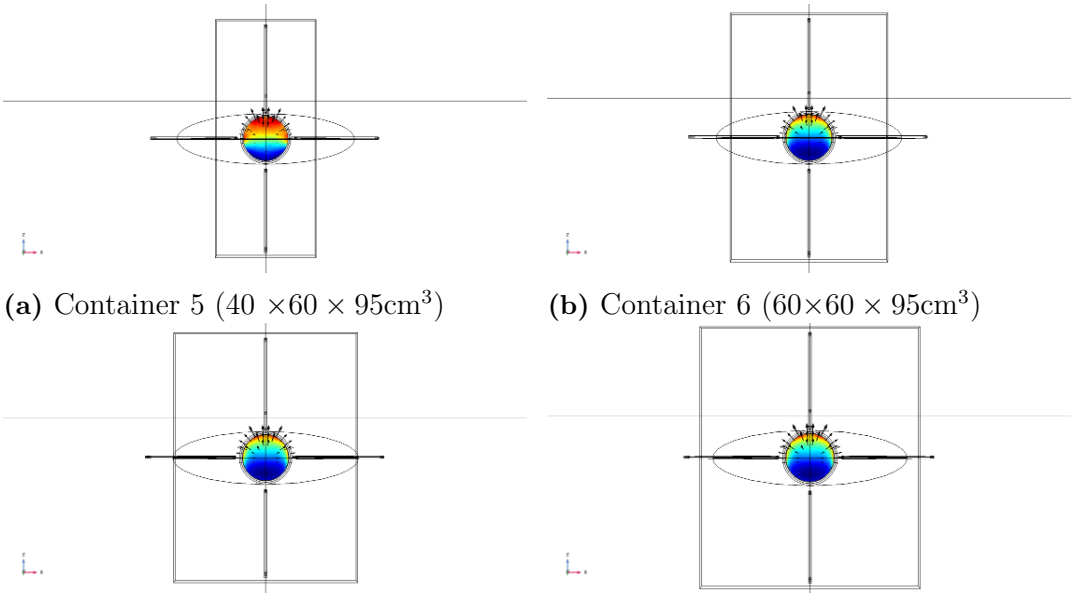

(a) Container 5 (40 ×60 × 95cm^3)

(b) Container 6 (60×60 × 95cm^3)

(c) Container 7 (70×60 × 95cm^3)

(d) Container 8 (80×60 × 95cm^3)

Figure 6.3: Second study: Only the width of the containers varied. All the simulated containers are depicted with the respective colored central brain slice current density, $\vec{J}$, distribution in a distanced axial view. Each container's dimensions are listed below each sub-figure.

are illustrated in Appendix A.1.

Regarding the RI at the center of the brain, this is the major accomplishment of our simulations. For all the containers simulated in this study, the RI at the center of the brain was kept approximately constant. Plus, the RI values obtained in all the simulations do not compromise the previous optimum stimulation results obtained in Section 5.2. As can be observed from Table 6.2, the RI at the center of the brain for all the containers was approximately 71%. Concerning the practicality of the system, the obtained results converge with what we were aiming for. However, and this subject was not evaluated in this study, these results might imply safety concerns, especially regarding magnetophosphenes induction and facial pain.

Analyzing the results provided by this simulation study conducted via COMSOL Multiphysics® AC/DC software, we notice some interesting results which might lead to future improvements of the dTMS device, as we were hoping for. The value of the RI at the center of the brain for all the simulated containers was approximately the same, and, more importantly, an approximate value to that of the simulations in Section 5.2 was achieved. Regarding our goals with this project, we see that the smaller simulated container has a volume of 228 dm^3, while the original simulated by Santos (2015) carries a volume of 618.52 dm^3. The obtained RI at the center of

Container	**Volume** (dm^3)	**Maximum** $\vec{J}$ (A/m^2)	**Minimum** $\vec{J}$ (A/m^2)	**RI**	**Central** $\vec{J}$ (A/m^2)
5	(228)	5.00	1.64	70.80%	3.54
6	(342)	5.33	1.92	70.73%	3.77
7	(399)	5.49	2.01	70.67%	3.88
8	(456)	5.60	2.07	70.71%	3.96

Table 6.2: Dimensions and achieved simulations' results for four different parallelepipedal containers. Volume: Individual container's volume. Max $\vec{J}$: Maximum $\vec{J}$ recorded in the brain (at the surface). Min $\vec{J}$: Minimum $\vec{J}$ recorded in the brain. RI: Relative $\vec{J}$ induction at the center of the brain comparatively to the surface maximum. Central $\vec{J}$: Recorded $\vec{J}$ value at the center of the brain.

the brain, however, is practically the same for both of these containers. This result indicates a potential reduction of 390 dm^3 (liters) of water and container volume without compromising the expected RI at the center of the brain. As we were aiming for with these simulations, this result might lead to an improved clinical/hospital practicality.

6.3 Skull currents

The conductive liquid surrounding this new dTMS system introduced an important paradigm in the performance of the orthogonal configuration system. It enabled the shifting of the minimum of $\vec{J}$ from the center of the brain to the anterior-inferior region, where the chin is located. Santos (2015) conducted a study that allowed to understand the physical origin behind these unprecedented results. This study led to the conclusion that the skull layer, even though it is the layer of the head with the lowest electrical conductivity, has a major role when it comes to achieving such a high deep-brain stimulation capability, as seen in Section 4.2.2.1. As a reinforcement to this very important conclusion from previous works, for all the simulations conducted in this project we have, for the first time, investigated the $\vec{J}$ distribution in the skull layer. All of the images depicting the various containers induced $\vec{J}$ distribution in the skull layer are depicted in Figure 6.5.

From Figure 6.5, we see that there are, indeed, induced currents in this layer. The induced $\vec{J}$ distribution is slightly different from that in the brain layer, but the currents' direction is the same. Moreover, looking at the magnitudes of the induced $\vec{J}$ values in the skull layer and the brain layer, for all the containers, we notice that these are of the same order of magnitude, even though, for the skull layer, the maximum $\vec{J}$s are slightly lower.

With this study, we have obtained the induced $\vec{J}$ distribution in the skull for

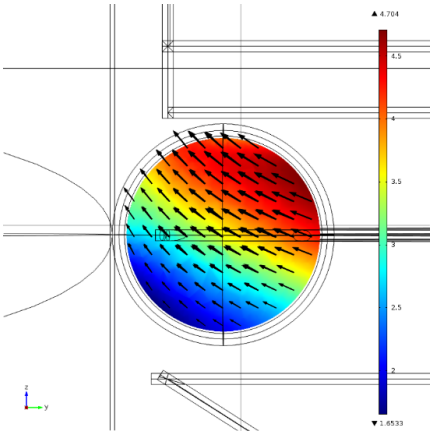

(a) $\vec{J}$ distribution in the brain for container 5. Max $\vec{J} = 4.70$ A/m^2. Min $\vec{J} = 1.65$ A/m^2.

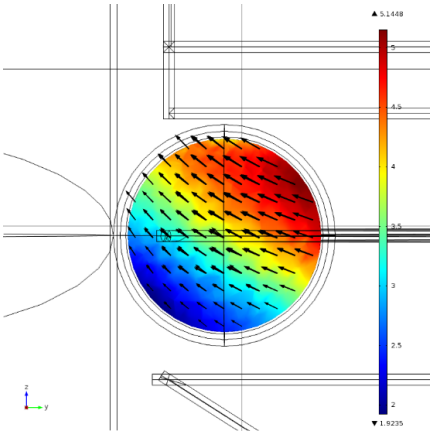

(b) $\vec{J}$ distribution in the brain for container 6. Max $\vec{J} = 5.14$ A/m^2. Min $\vec{J} = 1.92$ A/m^2.

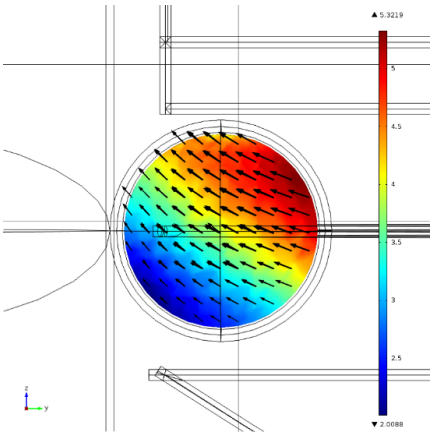

(c) $\vec{J}$ distribution in the brain for container 7. Max $\vec{J} = 5.32$ A/m^2. Min $\vec{J} = 2.00$ A/m^2.

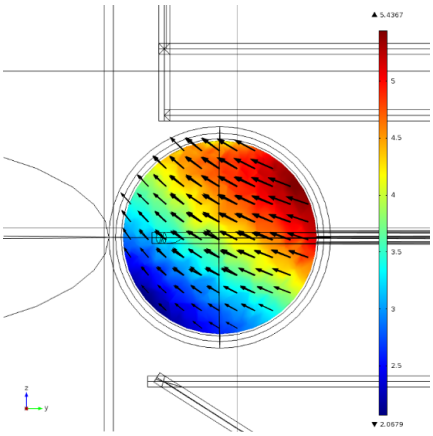

(d) $\vec{J}$ distribution in the brain for container 8. Max $\vec{J} = 5.44$ A/m^2. Min $\vec{J} = 2.07$ A/m^2.

Figure 6.4: Color map of the $\vec{J}$ distribution in a central sagittal view for all the simulated parallelepipedal containers.

all the containers and were able to show that this layer's induced $\vec{J}$ intensity is of the same order of magnitude as that of the brain. Even though the distribution of these induced currents is not exactly the same as for the brain currents, from Santos (2015), we know that these are the currents that strongly complement the currents induced in the brain and are of major importance for the high deep-brain stimulation capability of this new dTMS system. The direction of these induced currents being the same as that of the currents induced in the brain is also a potentially strong indicator of that conclusion.

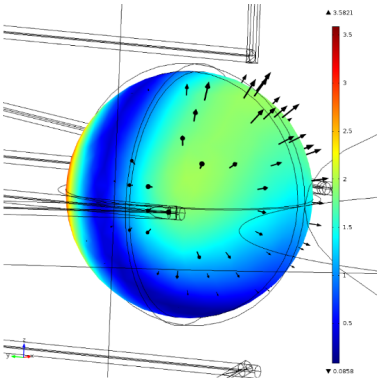

(a) $\vec{J}$ distribution in the skull for container 2. Max $\vec{J} = 3.58$ A/m^2. Min $\vec{J} = 0.09$ A/m^2.

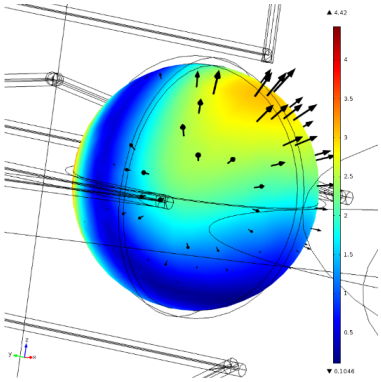

(b) $\vec{J}$ distribution in the skull for container 3. Max $\vec{J} = 4.42$ A/m^2. Min $\vec{J} = 0.10$ A/m^2.

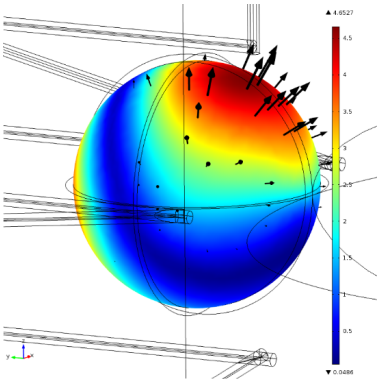

(c) $\vec{J}$ distribution in the skull for container 5. Max $\vec{J} = 4.65$ A/m^2. Min $\vec{J} = 0.05$ A/m^2.

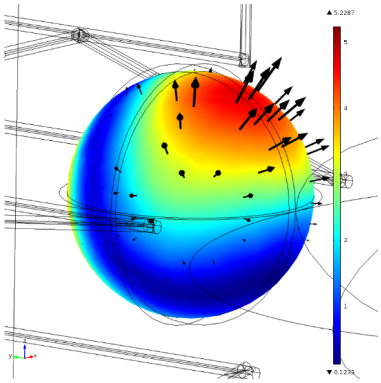

(d) $\vec{J}$ distribution in the skull for container 7. Max $\vec{J} = 5.23$ A/m^2. Min $\vec{J} = 0.12$ A/m^2.

Figure 6.5: Three-dimensional view of the $\vec{J}$ distribution (color map) in the skull layer surrounded by a cubic container (a) and b)) and a parallelepipedal container (c) and d)).

6.4 Patient's and TMS operator's safety

6.4.1 Heart-related concerns

The application of time-varying magnetic fields to stimulate brain tissue comes with some safety concerns, as we discussed in Section 2.6. One particular concern of the application of TMS is the stimulation of undesired biological tissues. When electrically stimulated, the cardiac muscle electrical activity can become disordered, leading to an unsynchronized contraction of the ventricles (ventricular fibrillation). A consequence of this unsynchronized contraction is that the heart will no longer be able to pump the required amount of blood for the entire organism, causing

collapse and cardiac arrest (Association, 2016). This phenomenon is more likely to be triggered when the electrical stimuli are applied during the portion of the cardiac cycle when the ventricles are recovering to their resting state.

In this work, we used 5 kHz pulsed B-fields, following the same frequency parameters as Santos (2015) and Sousa (2014). As a consequence, when it comes to the evaluation of the patient's heart safety, we will consider two safety references, one which follows the 1998 ICNIRP guidelines, that claimed stimulations with $\vec{J}$ above 1 A/m^2 can lead to adverse effects, such as cardiac fibrillation, and a more recent and conservative exposure limit of 0.45 A/m^2 for a stimulation frequency of 5 kHz, following the 2010 ICNIRP guidelines (ICNIRP, 1998)(ICNIRP, 2010). Santos (2015) considered that the safety of the patient was not endangered when the current density value in the heart laid below 4.5 mA/m^2, a very conservative value, 100 times inferior to the 2010 ICNIRP exposure limit and close to three orders of magnitude smaller than the 1998 ICNIRP exposure limit. We will consider, for our new orthogonal configuration with electrically insulated coils, the patients' safety to be ensured following this exposure limit of 4.5 mA/m^2 .

6.4.1.1 The problem

As previously studied by Santos (2015), the new orthogonal configuration without any metallic shielding structure did not ensure the patients' safety, following the exposure limit of 4.5 mA/m^2 adopted in Santos (2015) and in this project. The expected heart-safety results, given the physical layouts of our simulated containers, were also that the $\vec{J}$ in the heart was above the exposure limit. To calculate the induced $\vec{J}$ in the heart, via COMSOL Multiphysics® AC/DC, we averaged the $\vec{J}$ values of ten points taken from the central axis of the torso, between the two lines depicted in Figure 6.6 a), for the simulated containers in Section 6.2.

The induced $\vec{J}$ values in the heart for all the containers, as we can see in Table 6.3, surpass the exposure limit of 4.5 mA/m^2 defined for this project. The solution to this problem will be discussed in the next sub-section.

	Container 5	**Container 6**	**Container 7**	**Container 8**
Induced $\vec{J}$ at the heart (A/m^2)	0.332	0.370	0.392	0.379

Table 6.3: Induced $\vec{J}$ at the heart for all the parallelepipedal simulated containers.

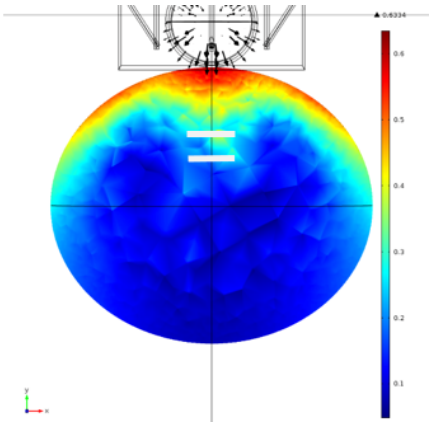

(a) $\vec{J}$ distribution in the patient's torso for container 5. Induced $\vec{J}$ (in the heart) = 0.332 A/m^2.

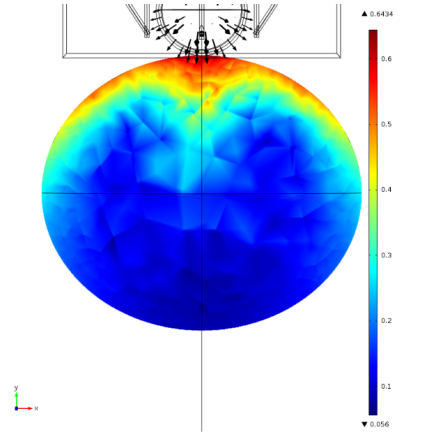

(b) $\vec{J}$ distribution in the patient's torso for container 6. Induced $\vec{J}$ (in the heart) = 0.370 A/m^2.

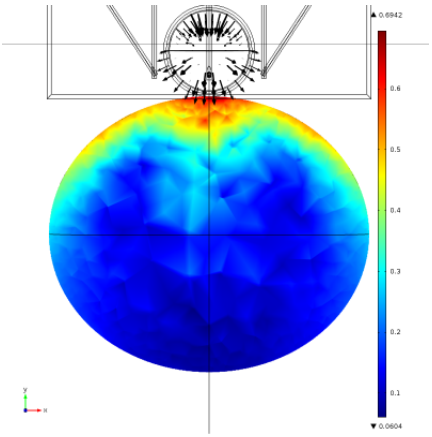

(c) $\vec{J}$ distribution in the patient's torso for container 7. Induced $\vec{J}$ (in the heart) = 0.392 A/m^2.

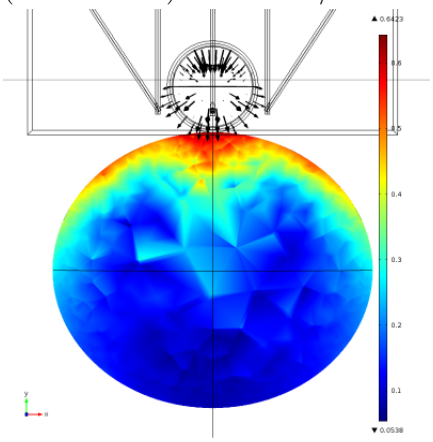

(d) $\vec{J}$ distribution in the skull for container 8. Induced $\vec{J}$ (in the heart) = 0.379 A/m^2.

Figure 6.6: $\vec{J}$ distribution in an ellipsoidal (patient's) torso for all the simulated parallelepipedal containers.

6.4.1.2 The solution

The solution consists of a metallic shielding structure around the fiberglass container (containing the conductive solution and the coils), as depicted in Figure 6.7.

With a highly conductive, 3-cm thick, iron or aluminum shielding structure, we are able to induce $\vec{J}$ values at the heart below the defined exposure limit of 4.5 mA/m^2, guaranteeing both the safety of the patient and of any system operator and/or nursing staff (Santos, 2015). To avoid contact between the skin and the highly conductive material, the minimum distance between the neck and the metal

was defined as 2 cm.

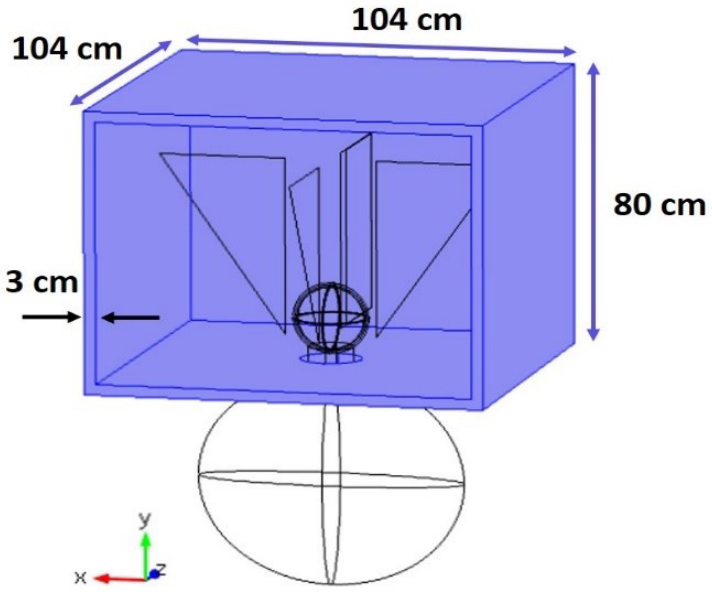

Figure 6.7: Metallic shielding structure proposed to reduce stimulations levels in the heart to two orders of magnitude below the fibrillation threshold. A 3-cm thickness structure ensured the patients' and operators' safety.

6.4.2 Ear-related concerns

6.4.2.1 The problem

As discussed in Section 2.6, the SPL produced by the TMS coil when it is energized can exceed the permissible noise exposure limit for impulsive noises. This condition requires caution from the operators/clinicians when administering a TMS session. As also mentioned in Section 2.6, when hearing protection was used, no reports of hearing sensitivity change after TMS were registered. We notice that, besides some patients with particular conditions, the use of hearing protection allows the patients to be stimulated with safety when it comes to potential hearing sensitivity changes. The technologies by which the sound of the coils' click can be cancelled or blocked are discussed in the next subsection.

6.4.2.2 The solution

In order to guarantee the hearing safety of the TMS patients, different methods of blocking or canceling the coils' sounds have been applied. Typical devices used for this purpose are earplugs and headphones. Earplugs are normally used alone, or

in combination with an earmuff, given that earplugs alone hardly attenuate even the airborne part of the "click" (Ter Braack et al., 2015) (Conde et al., 2019). The headphones, however, can be supported by more technology, in order to more effectively cancel the sound of the coils' click. With resort to noise-canceling technology, headphones are able to lower the volume of the sound waves that reach the patients' ears. Noise-canceling is a very common technology in nowadays commercial headphones and in-ear headphones. Putting it simple, it consists on an active monitoring of the external sounds by miniature microphones inserted in the headphones' earbuds, transmitting the sound information to internal electronics that is able to invert the received soundwaves and signal this information to speakers, which consequently will emitt these soundwaves in order to cancel the external incoming ones. An additional noise reduction can be achieved with the concurrent use of earplugs and noise-canceling headphones. In addition, it is recognized that sound not only travels through the air but also through bone conduction. Hence, a thin layer of foam can be placed between the coil and the head of the subject, in order to minimize the conduction through the bone medium (Ter Braack et al., 2015).

7

Conclusions

TMS therapeutic potential has now been observed for some years. Specifically, repetitive stimulation protocols have been demonstrated to be effective as adjunctive or monotherapies for several disorders. dTMS therapeutic applications have been increasing over the years, all over the world. In the United States, Brainsway's H-coils have received Food and Drug Administration (FDA) clearance for the treatment of disorders like major depressive disorder (MDD), smoking addiction, and obsessive compulsive disorder (OCD). In Europe, Brainsway's H-coils have even more therapeutic applications CE marked, including the aforementioned disorders, and others like post-traumatic stress disorder (PTSD), schizophrenia, Alzheimer's disease, Parkinson's disease, among others.

dTMS emerged as a therapeutic gap that over time has been filled with many solutions. The introduction of our system with such a power with depth capacity of stimulation as that demonstrated in this work can bring many interesting results regarding the therapeutic effect of stimulating deep brain areas. Given the unprecedented deep stimulation capacity of this system, some deep brain areas associated with some disorders may benefit from the possible direct stimulation this system can attain, meaning that, more than ever, given the already proven beneficial effect for many disorders of dTMS, it makes sense to keep investing on the development of a system with such potential.

In our work, we proposed to keep the development of the previously simulated 5-coil system, termed orthogonal configuration. Previous results had already achieved unprecedented deep stimulation results. On the experimental side, we managed to find some important material solutions required for the experimental realization of the project. At the beginning of our project, there was, already, a container where the coils would be inserted. In collaboration with LIP's high-precision mechanical workshop we managed to find another container and a pump, in order to create in this new container the electrical conditions required for the conductive solution, and with the help of the pump, introduce and take out the conductive solution

of the container with the coils. Another important step in our project was the construction of the coils that will be immersed in the head model and allow us to measure the RI at the center of the brain-model. Last, but not least, concerning the experimental setup, we were able to find that there are some silicone-based solutions that can potentially fulfill the electrical requirements for the skull model. Initial contacts were made with one company that provides silicone-based solutions, but other companies were also already identified, in order to increase our alternatives. The electrical properties required to get an experimental setup close to that of the simulations are an important demand in order to prove the unprecedented results of the simulations. A material with an electrical conductivity close to that of the skull model in the simulations was still lacking, and this might have been a major improvement. Future contacts with the company we initialized talks with are still required, in order to understand if they can provide the solution we are looking for, or if we have to resort to other of the identified companies.

In the previous work of our project, Santos (2015) made very important progresses towards the safety and functionality of the orthogonal configuration. However, in order to come close to real conditions, one important feature was lacking: the insulation of the electrical wires that make up the coils. We proposed to introduce a 5-mm radius insulating layer ($\sigma = 10^{-15}$ S/m). Our simulation study, via COMSOL Multiphysics® AC/DC software, of the $\vec{J}$ distribution in the brain, after the introduction of this layer, shows no significant differences with regards to Santos (2015) simulations' results, except for the RI at the center of the brain having increased from 60% to 71%. We believe this increase might be related to the extinction of electrical currents being directly conducted from the bared wires to the conductive liquid and the head model when introducing the insulating layer. These currents could have a detrimental effect on the deep stimulation power of the orthogonal configuration.

In this work, we proposed to try to improve the dimensions of the system, always keeping in mind the objective of maintaining the unprecedented deep power of stimulation. A first simulation study, via COMSOL Multiphysics® AC/DC, following an approach where the containers were essentially cubic showed no significant improvements regarding the relationship between volume occupied by the container and $\vec{J}$ distribution in the brain. The smaller containers were unable to maintain the stimulation power with depth achieved by the new orthogonal configuration with insulated wires, and only the containers with a volume similar to that of the original container enabled a RI at the center of the brain similar to that of the new orthogonal configuration with insulated wires. In the second study, also via COM-

SOL Multiphysics® AC/DC simulations, we focused on varying the width of the container. The coils positioned in the anterior and posterior positions were kept fully surrounded by the conductive liquid purposefully. One of the coils located in the posterior position is responsible for the highest current intensity present in the system. Looking at this study's results we notice that the RI at the center of the brain is kept very similar to that of the new orthogonal configuration with insulated wires ($\approx 71\%$). The $\vec{J}$ distribution throughout the brain was also kept very similar to that of the original orthogonal configuration, for all the simulated containers. However, the $\vec{J}$ intensity throughout the brain is smaller for all the simulated containers, comparatively to that of the new orthogonal configuration with insulated wires container. The smallest simulated container allows a reduction of 390 liters of water when compared to the original container, which also implies a reduction in NaCl. The space occupied by the container is also, obviously, smaller, and the necessity for a shielding structure, in order to ensure the safety of the patient and operator, even though not studied, might also imply a smaller volume of material. This way, even though at an early stage analysis, we can affirm we have accomplished one of the proposed objectives, which was to prove that changes in the dTMS system can still be implemented towards improved practicality.

In this project, we have started the development of the experimental setup of the orthogonal configuration. Many important parts of the system are already in the LIP high-precision mechanical workshop, such as the container, a pump to interchange the liquid solution between two containers, and we already made initial contacts with a company that might provide a solution for the experimental spherical skull model. It is important in future work to assemble all these integrant materials to start the experimental studies. A major step would be to find the best solution for the spherical skull model with the company offering silicone solutions we already made initial contacts with. With all these materials gathered it is possible to start the experimental testing of some of the simulations' results, with only the insulated wires being needed to be purchased.

Appendices

A

Appendices

A.1 Current density distribution in the brain for the simulated containers in Section 6.2 in axial, coronal, and three-dimensional perspectives

For practical reasons, in Section 6.2 we have only depicted the current density distribution for every container in a sagitall plane view. In this appendix, the current distribution for containers number 5, 6, 7, and 8, depicted in Figure 6.3, will be depicted in the Figures below, from axial, coronal, and three-dimensional views.

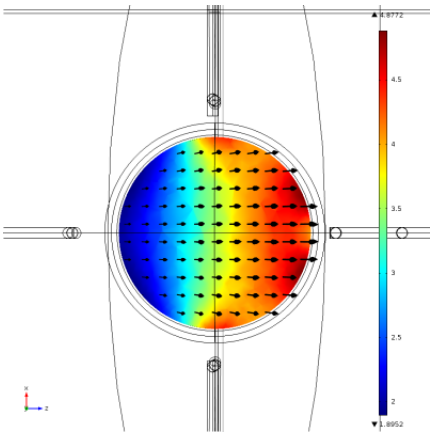

(a) Central axial view of the $\vec{J}$ distribution in the brain for container 5. Max $\vec{J} = 4.88$ A/m^2. Min $\vec{J} = 1.90$ A/m^2.

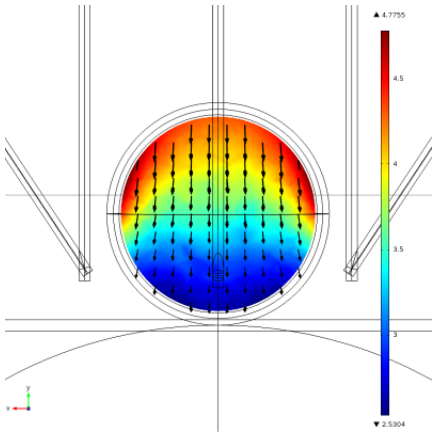

(b) Central coronal view of the $\vec{J}$ distribution in the brain for container 5. Max $\vec{J} = 4.78$ A/m^2. Min $\vec{J} = 2.53$ A/m^2.

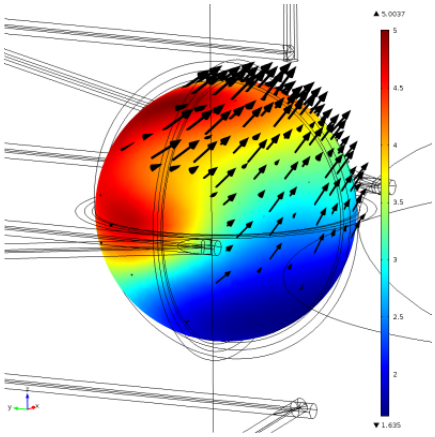

(c) Three-dimensional view of the $\vec{J}$ distribution in the brain for container 5. Max $\vec{J} = 5.00$ A/m^2. Min $\vec{J} = 1.64$ A/m^2.

Figure A.1: Color map of the $\vec{J}$ distribution in central brain planes (axial and coronal), and a three-dimensional view for simulated container number 5 in Section 6.2.

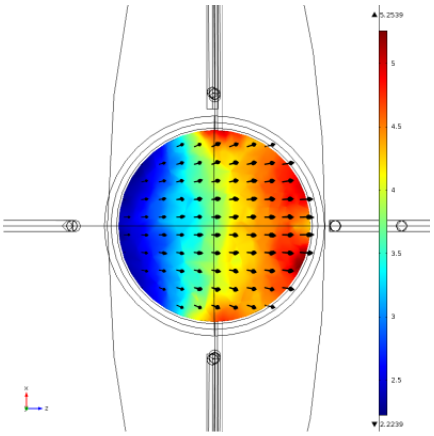

(a) Central axial view of the $\vec{J}$ distribution in the brain for container 6. Max $\vec{J} = 5.25$ A/m^2. Min $\vec{J} = 2.22$ A/m^2.

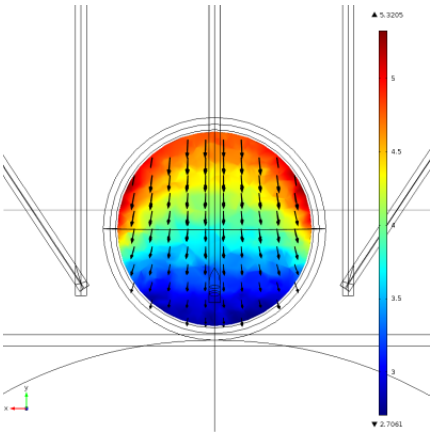

(b) Central coronal view of the $\vec{J}$ distribution in the brain for container 6. Max $\vec{J} = 5.32$ A/m^2. Min $\vec{J} = 2.71$ A/m^2.

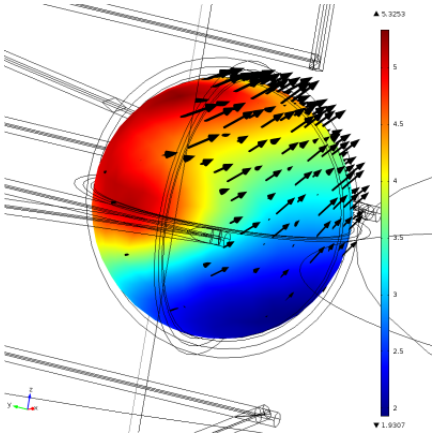

(c) Three-dimensional view of the $\vec{J}$ distribution in the brain for container 6. Max $\vec{J} = 5.33$ A/m^2. Min $\vec{J} = 1.93$ A/m^2.

Figure A.2: Color map of the $\vec{J}$ distribution in central brain planes (axial and coronal), and a three-dimensional view for simulated container number 6 in Section 6.2.

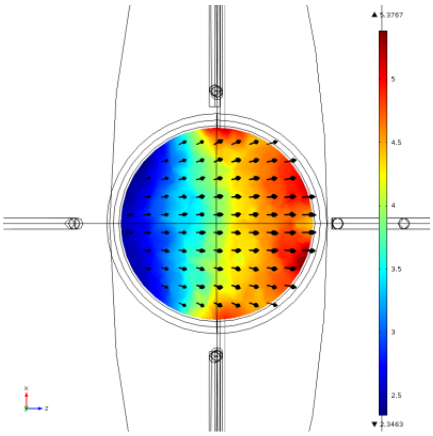

(a) Central axial view of the $\vec{J}$ distribution in the brain for container 7. Max $\vec{J} = 5.38$ A/m^2. Min $\vec{J} = 2.35$ A/m^2.

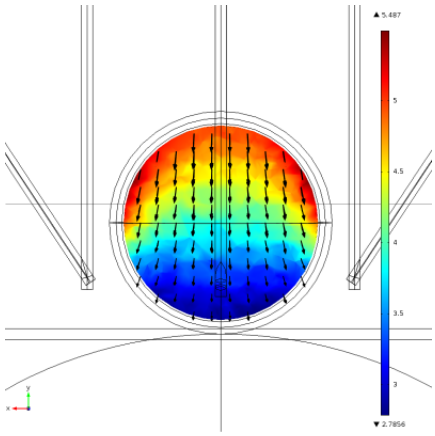

(b) Central coronal view of the $\vec{J}$ distribution in the brain for container 7. Max $\vec{J} = 5.49$ A/m^2. Min $\vec{J} = 2.79$ A/m^2.

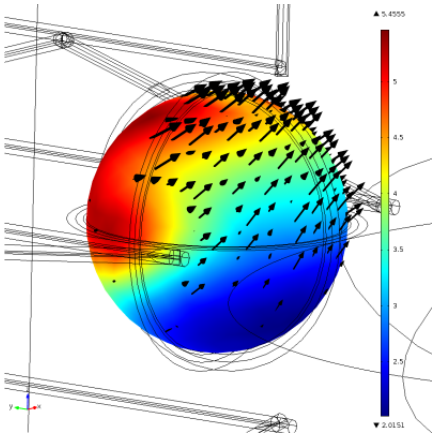

(c) Three-dimensional view of the $\vec{J}$ distribution in the brain for container 7. Max $\vec{J} = 5.46$ A/m^2. Min $\vec{J} = 2.02$ A/m^2.

Figure A.3: Color map of the $\vec{J}$ distribution in central brain planes (axial and coronal), and a three-dimensional view for simulated container number 7 in Section 6.2

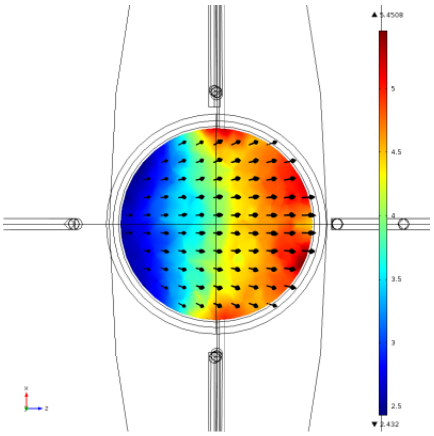

(a) Central axial view of the $\vec{J}$ distribution in the brain for container 8. Max $\vec{J} = 5.45$ A/m^2. Min $\vec{J} = 2.43$ A/m^2.

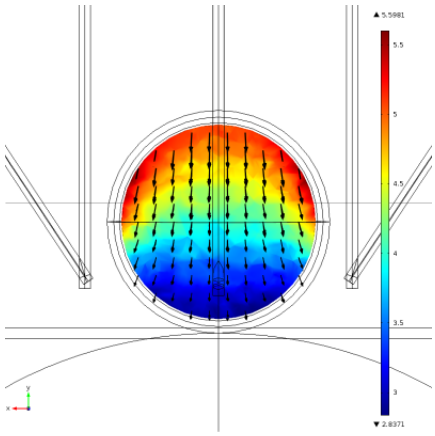

(b) Central coronal view of the $\vec{J}$ distribution in the brain for container 8. Max $\vec{J} = 5.60$ A/m^2. Min $\vec{J} = 2.84$ A/m^2.

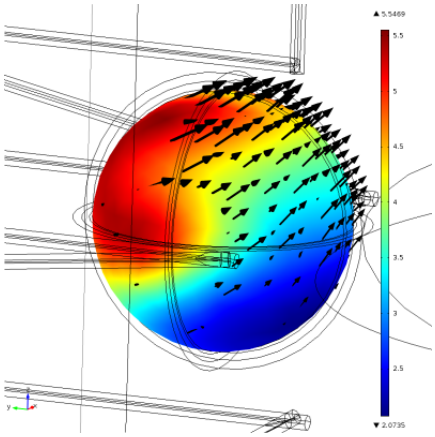

(c) Three-dimensional view of the $\vec{J}$ distribution in the brain for container 8. Max $\vec{J} = 5.55$ A/m^2. Min $\vec{J} = 2.07$ A/m^2.

Figure A.4: Color map of the $\vec{J}$ distribution in central brain planes (axial and coronal), and a three-dimensional view for simulated container number 8 in Section 6.2

Bibliography

Addolorato, G., Antonelli, M., Cocciolillo, F., Vassallo, G. A., Tarli, C., Sestito, L., Mirijello, A., Ferrulli, A., Pizzuto, D. A., Camardese, G., et al. (2017). Deep transcranial magnetic stimulation of the dorsolateral prefrontal cortex in alcohol use disorder patients: effects on dopamine transporter availability and alcohol intake. *European Neuropsychopharmacology*, 27(5):450–461.

Association, A. H. (2016). Ventricular fibrillation. Retrieved December 4, 2022, from `https://www.heart.org/en/health-topics/arrhythmia/about-arrhythmia/ventricular-fibrillation`.

Avirame, K., Stehberg, J., and Todder, D. (2016). Benefits of deep transcranial magnetic stimulation in alzheimer disease: case series. *The journal of ECT*, 32(2):127–133.

Ayache, S. S. and Chalah, M. A. (2017). Fatigue in multiple sclerosis–insights into evaluation and management. *Neurophysiologie Clinique/Clinical Neurophysiology*, 47(2):139–171.

Azin, M., Zangiabadi, N., Iranmanesh, F., Baneshi, M. R., and Banihashem, S. (2016). Effects of intermittent theta burst stimulation on manual dexterity and motor imagery in patients with multiple sclerosis: a quasi-experimental controlled study. *Iranian Red Crescent Medical Journal*, 18(10).

Baeken, C., Brem, A.-K., Arns, M., Brunoni, A. R., Filipčić, I., Ganho-Ávila, A., Langguth, B., Padberg, F., Poulet, E., Rachid, F., et al. (2019). Repetitive transcranial magnetic stimulation treatment for depressive disorders: current knowledge and future directions. *Current opinion in psychiatry*, 32(5):409.

Bagherzadeh, H. and Choa, F.-s. (2019). Effect of coil size on transcranial magnetic stimulation (tms) focality. In *Smart Biomedical and Physiological Sensor Technology XVI*, volume 11020, page 110200Z. International Society for Optics and Photonics.

Barker, A. T., Jalinous, R., and Freeston, I. L. (1985). Non-invasive magnetic stimulation of human motor cortex. *The Lancet*, 325(8437):1106–1107.

Bolloni, C., Panella, R., Pedetti, M., Frascella, A. G., Gambelunghe, C., Piccoli, T., Maniaci, G., Brancato, A., Cannizzaro, C., and Diana, M. (2016). Bilateral transcranial magnetic stimulation of the prefrontal cortex reduces cocaine intake: a pilot study. *Frontiers in psychiatry*, 7:133.

Brainsway (n.d.a). Alzheimer's disease treatment. Brainsway. Retrieved December 14, 2022, from `https://www.brainsway.com/treatments/alzheimers-disease/`.

Brainsway (n.d.b). Major depressive disorder treatment. Retrieved December 14, 2022, from `https://www.brainsway.com/treatments/major-depressive-disorder/`.

Brainsway (n.d.c). Multiple sclerosis (msc) treatment. Retrieved December 14, 2022, from `https://www.brainsway.com/treatments/multiple-sclerosis-msc/`.

Brainsway (n.d.d). Obsessive-compulsive disorder treatment. Retrieved December 14, 2022, from `https://www.brainsway.com/treatments/obsessive-compulsive-disorder/`.

Brainsway (n.d.e). Post stroke rehabilitation treatment. Retrieved December 14, 2022, from `https://www.brainsway.com/treatments/post-stroke-rehabilitation/`.

Brainsway (n.d.f). Post traumatic stress disorder treatment. Retrieved December 14, 2022, from `https://www.brainsway.com/treatments/post-traumatic-stress-disorder/`.

Brainsway (n.d.g). Smoking addiction treatment. Retrieved December 14, 2022, from `https://www.brainsway.com/treatments/smoking-addiction/`.

Brodal, P. (2010). *The central nervous system: structure and function*. oxford university Press.

Burke, M. J., Fried, P. J., and Pascual-Leone, A. (2019). Transcranial magnetic stimulation: Neurophysiological and clinical applications. *Handbook of clinical neurology*, 163:73–92.

Cao, X., Deng, C., Su, X., and Guo, Y. (2018). Response and remission rates following high-frequency vs. low-frequency repetitive transcranial magnetic stim-

ulation (rtms) over right dlpfc for treating major depressive disorder (mdd): a meta-analysis of randomized, double-blind trials. *Frontiers in psychiatry*, 9:413.

Carmi, L., Alyagon, U., Barnea-Ygael, N., Zohar, J., Dar, R., and Zangen, A. (2018). Clinical and electrophysiological outcomes of deep tms over the medial prefrontal and anterior cingulate cortices in ocd patients. *Brain stimulation*, 11(1):158–165.

Cocaine (2021). World Health Organization. `https://www.who.int/home/cms-decommissioning`.

Conde, V., Tomasevic, L., Akopian, I., Stanek, K., Saturnino, G. B., Thielscher, A., Bergmann, T. O., and Siebner, H. R. (2019). The non-transcranial tms-evoked potential is an inherent source of ambiguity in tms-eeg studies. *Neuroimage*, 185:300–312.

Davila-Pérez, P., Jannati, A., Fried, P. J., Mazaira, J. C., and Pascual-Leone, A. (2018). The effects of waveform and current direction on the efficacy and test–retest reliability of transcranial magnetic stimulation. *Neuroscience*, 393:97–109.

Deng, Z.-D., Lisanby, S. H., and Peterchev, A. V. (2014). Coil design considerations for deep transcranial magnetic stimulation. *Clinical Neurophysiology*, 125(6):1202–1212.

Di Lazzaro, V. and Rothwell, J. C. (2014). Corticospinal activity evoked and modulated by non-invasive stimulation of the intact human motor cortex. *The Journal of physiology*, 592(19):4115–4128.

Diana, M., Raij, T., Melis, M., Nummenmaa, A., Leggio, L., and Bonci, A. (2017). Rehabilitating the addicted brain with transcranial magnetic stimulation. *Nature Reviews Neuroscience*, 18(11):685–693.

Dinur-Klein, L., Dannon, P., Hadar, A., Rosenberg, O., Roth, Y., Kotler, M., and Zangen, A. (2014). Smoking cessation induced by deep repetitive transcranial magnetic stimulation of the prefrontal and insular cortices: a prospective, randomized controlled trial. *Biological psychiatry*, 76(9):742–749.

Ferrulli, A., Macrì, C., Terruzzi, I., Ambrogi, F., Milani, V., Adamo, M., and Luzi, L. (2019a). High frequency deep transcranial magnetic stimulation acutely increases β-endorphins in obese humans. *Endocrine*, 64(1):67–74.

Ferrulli, A., Macrì, C., Terruzzi, I., Massarini, S., Ambrogi, F., Adamo, M., Milani, V., and Luzi, L. (2019b). Weight loss induced by deep transcranial magnetic stim-

ulation in obesity: A randomized, double-blind, sham-controlled study. *Diabetes, obesity and metabolism*, 21(8):1849–1860.

Fiocchi, S., Chiaramello, E., Luzi, L., Ferrulli, A., Bonato, M., Roth, Y., Zangen, A., Ravazzani, P., and Parazzini, M. (2018). Deep transcranial magnetic stimulation for the addiction treatment: electric field distribution modeling. *IEEE Journal of Electromagnetics, RF and Microwaves in Medicine and Biology*, 2(4):242–248.

Fisicaro, F., Lanza, G., Grasso, A. A., Pennisi, G., Bella, R., Paulus, W., and Pennisi, M. (2019). Repetitive transcranial magnetic stimulation in stroke rehabilitation: review of the current evidence and pitfalls. *Therapeutic advances in neurological disorders*, 12:1756286419878317.

Frith, C. D. (2014). *The cognitive neuropsychology of schizophrenia*. Psychology press.

Girardi, P., Rapinesi, C., Chiarotti, F., Kotzalidis, G. D., Piacentino, D., Serata, D., Del Casale, A., Scatena, P., Mascioli, F., Raccah, R. N., et al. (2015). Add-on deep transcranial magnetic stimulation (dtms) in patients with dysthymic disorder comorbid with alcohol use disorder: a comparison with standard treatment. *The World Journal of Biological Psychiatry*, 16(1):66–73.

Gomez-Tames, J., Hamasaka, A., Hirata, A., Laakso, I., Lu, M., and Ueno, S. (2020). Group-level analysis of induced electric field in deep brain regions by different tms coils. *Physics in Medicine & Biology*, 65(2):025007.

Grossman, N., Bono, D., Dedic, N., Kodandaramaiah, S. B., Rudenko, A., Suk, H.-J., Cassara, A. M., Neufeld, E., Kuster, N., Tsai, L.-H., et al. (2017). Noninvasive deep brain stimulation via temporally interfering electric fields. *cell*, 169(6):1029–1041.

Hawken, E. R., Dilkov, D., Kaludiev, E., Simek, S., Zhang, F., and Milev, R. (2016). Transcranial magnetic stimulation of the supplementary motor area in the treatment of obsessive-compulsive disorder: a multi-site study. *International journal of molecular sciences*, 17(3):420.

Heath, A., Taylor, J., and McNerney, M. W. (2018). rtms for the treatment of alzheimer's disease: where should we be stimulating? *Expert review of neurotherapeutics*, 18(12):903–905.

Hickok, G., Okada, K., and Serences, J. T. (2009). Area spt in the human planum temporale supports sensory-motor integration for speech processing. *Journal of neurophysiology*, 101(5):2725–2732.

Hoogendam, J. M., Ramakers, G. M., and Di Lazzaro, V. (2010). Physiology of repetitive transcranial current file overview 10 magnetic stimulation of the human brain. *Brain stimulation*, 3(2):95–118.

Horvath, J. C., Perez, J. M., Forrow, L., Fregni, F., and Pascual-Leone, A. (2011). Transcranial magnetic stimulation: a historical evaluation and future prognosis of therapeutically relevant ethical concerns. *Journal of medical ethics*, 37(3):137–143.

Huang, Y.-Z., Lu, M.-K., Antal, A., Classen, J., Nitsche, M., Ziemann, U., Ridding, M., Hamada, M., Ugawa, Y., Jaberzadeh, S., et al. (2017). Plasticity induced by non-invasive transcranial brain stimulation: a position paper. *Clinical Neurophysiology*, 128(11):2318–2329.

ICNIRP (1998). Guidelines for limiting exposure to time-varying electric, magnetic, and electromagnetic fields (up to 300 ghz). *Health physics*, 74(4):494–522.

ICNIRP (2010). Guidelines for limiting exposure to time-varying electric and magnetic fields (1 hz to 100 khz). *Health physics*, 99(6):818–836.

Isserles, M., Shalev, A. Y., Roth, Y., Peri, T., Kutz, I., Zlotnick, E., and Zangen, A. (2013). Effectiveness of deep transcranial magnetic stimulation combined with a brief exposure procedure in post-traumatic stress disorder–a pilot study. *Brain stimulation*, 6(3):377–383.

Jafari, A. M. and Abdolali, A. (2019). A novel approach on dtms coil design based on tractography and neural cable theory. *bioRxiv*, page 683870.

Jarrett, C. (2016). Broca and wernicke are dead - it's time to rewrite the neurobiology of language. `https://www.bps.org.uk/research-digest/broca-and-wernicke-are-dead-its-time-rewrite-neurobiology-language`.

Kim, W.-S. and Paik, N.-J. (2020). Safety review for clinical application of repetitive transcranial magnetic stimulation. *Brain & Neurorehabilitation*, 14.

Kindler, J., Homan, P., Jann, K., Federspiel, A., Flury, R., Hauf, M., Strik, W., Dierks, T., and Hubl, D. (2013). Reduced neuronal activity in language-related regions after transcranial magnetic stimulation therapy for auditory verbal hallucinations. *Biological psychiatry*, 73(6):518–524.

Kobayashi, M., Fujimaki, T., Mihara, B., and Ohira, T. (2015). Repetitive transcranial magnetic stimulation once a week induces sustainable long-term relief of

central poststroke pain. *Neuromodulation: Technology at the Neural Interface*, 18(4):249–254.

Koponen, L. M., Nieminen, J. O., Mutanen, T. P., Stenroos, M., and Ilmoniemi, R. J. (2017). Coil optimisation for transcranial magnetic stimulation in realistic head geometry. *Brain stimulation*, 10(4):795–805.

Korzhova, J., Bakulin, I., Sinitsyn, D., Poydasheva, A., Suponeva, N., Zakharova, M., and Piradov, M. (2019). High-frequency repetitive transcranial magnetic stimulation and intermittent theta-burst stimulation for spasticity management in secondary progressive multiple sclerosis. *European journal of neurology*, 26(4):680–e44.

Kowalski, T., Silny, J., and Buchner, H. (2002). Current density threshold for the stimulation of neurons in the motor cortex area. *Bioelectromagnetics: Journal of the Bioelectromagnetics Society, The Society for Physical Regulation in Biology and Medicine, The European Bioelectromagnetics Association*, 23(6):421–428.

Kumar, A., Mattoo, B., Bhatia, R., Kumaran, S., and Bhatia, R. (2021). Neuronavigation based 10 sessions of repetitive transcranial magnetic stimulation therapy in chronic migraine: an exploratory study. *Neurological Sciences*, 42(1):131–139.

Lefaucheur, J.-P. (2019). Transcranial magnetic stimulation. *Handbook of clinical neurology*, 160:559–580.

Lerner, A. J., Wassermann, E. M., and Tamir, D. I. (2019). Seizures from transcranial magnetic stimulation 2012–2016: results of a survey of active laboratories and clinics. *Clinical Neurophysiology*, 130(8):1409–1416.

Levkovitz, Y., Harel, E. V., Roth, Y., Braw, Y., Most, D., Katz, L. N., Sheer, A., Gersner, R., and Zangen, A. (2009). Deep transcranial magnetic stimulation over the prefrontal cortex: evaluation of antidepressant and cognitive effects in depressive patients. *Brain stimulation*, 2(4):188–200.

Levkovitz, Y., Isserles, M., Padberg, F., Lisanby, S. H., Bystritsky, A., Xia, G., Tendler, A., Daskalakis, Z. J., Winston, J. L., Dannon, P., et al. (2015). Efficacy and safety of deep transcranial magnetic stimulation for major depression: a prospective multicenter randomized controlled trial. *World Psychiatry*, 14(1):64–73.

Li, Z., Yin, M., Lyu, X.-L., Zhang, L.-L., Du, X.-D., and Hung, G. C.-L. (2016). Delayed effect of repetitive transcranial magnetic stimulation (rtms) on negative

symptoms of schizophrenia: findings from a randomized controlled trial. *Psychiatry research*, 240:333–335.

Lu, M. and Ueno, S. (2015). Deep transcranial magnetic stimulation using figure-of-eight and halo coils. *IEEE Transactions on Magnetics*, 51(11):1–4.

Lu, M. and Ueno, S. (2017a). Comparison of the induced fields using different coil configurations during deep transcranial magnetic stimulation. *PloS one*, 12(6):e0178422.

Lu, M. and Ueno, S. (2017b). Deep transcranial magnetic stimulation with improved focality using figure-of-eight and halo coils. In *2017 XXXIInd General Assembly and Scientific Symposium of the International Union of Radio Science (URSI GASS)*, pages 1–4. IEEE.

Lusicic, A., Schruers, K. R., Pallanti, S., and Castle, D. J. (2018). Transcranial magnetic stimulation in the treatment of obsessive–compulsive disorder: current perspectives. *Neuropsychiatric disease and treatment*, 14:1721.

Maccabee, P., Nagarajan, S., Amassian, V., Durand, D., Szabo, A., Ahad, A., Cracco, R., Lai, K., and Eberle, L. (1998). Influence of pulse sequence, polarity and amplitude on magnetic stimulation of human and porcine peripheral nerve. *The Journal of Physiology*, 513(2):571–585.

Marcolin, M. A. and Padberg, F. (2007). *Transcranial brain stimulation for treatment of psychiatric disorders*, volume 23. Karger Medical and Scientific Publishers.

Martinez, D., Urban, N., Grassetti, A., Chang, D., Hu, M.-C., Zangen, A., Levin, F. R., Foltin, R., and Nunes, E. V. (2018). Transcranial magnetic stimulation of medial prefrontal and cingulate cortices reduces cocaine self-administration: a pilot study. *Frontiers in psychiatry*, 9:80.

Misra, U. K., Kalita, J., and Bhoi, S. K. (2013). High-rate repetitive transcranial magnetic stimulation in migraine prophylaxis: a randomized, placebo-controlled study. *Journal of neurology*, 260(11):2793–2801.

Newman, T. (2020). The numbers behind obesity. `https://www.medicalnewstoday.com/articles/319902`.

Noh, N. A. (2016). Exploring cortical plasticity and oscillatory brain dynamics via transcranial magnetic stimulation and resting-state electroencephalogram. *The Malaysian journal of medical sciences: MJMS*, 23(4):5.

Nutrition and team, F. S. W. (2021). Obesity. https://www.who.int/health-topics/obesity#tab=tab_1.

Oliveira, H., Silva, M. D., Ferreira, C. V., Fonte, P., Jesus, L., Salvador, R., Silvestre, J., and Crespo, P. (2012). Multiple coils in a conducting liquid for deep and whole-brain transcranial magnetic stimulation. i. single-frequency excitation. In *2012 IEEE 2nd Portuguese Meeting in Bioengineering (ENBENG)*, pages 1–4. IEEE.

O'Reardon, J. P., Solvason, H. B., Janicak, P. G., Sampson, S., Isenberg, K. E., Nahas, Z., McDonald, W. M., Avery, D., Fitzgerald, P. B., Loo, C., et al. (2007). Efficacy and safety of transcranial magnetic stimulation in the acute treatment of major depression: a multisite randomized controlled trial. *Biological psychiatry*, 62(11):1208–1216.

Pascual-Leone, A., Valls-Solé, J., Wassermann, E. M., and Hallett, M. (1994). Responses to rapid-rate transcranial magnetic stimulation of the human motor cortex. *Brain*, 117(4):847–858.

Perini, I., Kämpe, R., Arlestig, T., Karlsson, H., Löfberg, A., Pietrzak, M., Zangen, A., and Heilig, M. (2020). Repetitive transcranial magnetic stimulation targeting the insular cortex for reduction of heavy drinking in treatment-seeking alcohol-dependent subjects: a randomized controlled trial. *Neuropsychopharmacology*, 45(5):842–850.

Pitcher, J. B., Ogston, K. M., and Miles, T. S. (2003). Age and sex differences in human motor cortex input–output characteristics. *The Journal of physiology*, 546(2):605–613.

Quentin, R., Chanes, L., Vernet, M., and Valero-Cabré, A. (2015). Fronto-parietal anatomical connections influence the modulation of conscious visual perception by high-beta frontal oscillatory activity. *Cerebral cortex*, 25(8):2095–2101.

Rapinesi, C., Del Casale, A., Di Pietro, S., Ferri, V. R., Piacentino, D., Sani, G., Raccah, R. N., Zangen, A., Ferracuti, S., Vento, A. E., et al. (2016). Add-on high frequency deep transcranial magnetic stimulation (dtms) to bilateral prefrontal cortex reduces cocaine craving in patients with cocaine use disorder. *Neuroscience letters*, 629:43–47.

Rapinesi, C., Kotzalidis, G. D., Ferracuti, S., Girardi, N., Zangen, A., Sani, G., Raccah, R. N., Girardi, P., Pompili, M., Del Casale, A., et al. (2018). Add-on high frequency deep transcranial magnetic stimulation (dtms) to bilateral prefrontal

cortex in depressive episodes of patients with major depressive disorder, bipolar disorder i, and major depressive with alcohol use disorders. *Neuroscience letters*, 671:128–132.

Rastogi, P., Lee, E., Hadimani, R. L., and Jiles, D. C. (2017). Transcranial magnetic stimulation-coil design with improved focality. *Aip Advances*, 7(5):056705.

Reuell, P. (2016). The auditory cortex of hearing and deaf people are almost identical. `https://news.harvard.edu/gazette/story/2016/07/auditory-cortex-nearly-identical-in-hearing-and-deaf-people/`.

Rossi, S., Antal, A., Bestmann, S., Bikson, M., Brewer, C., Brockmöller, J., Carpenter, L. L., Cincotta, M., Chen, R., Daskalakis, J. D., et al. (2021). Safety and recommendations for tms use in healthy subjects and patient populations, with updates on training, ethical and regulatory issues: expert guidelines. *Clinical Neurophysiology*, 132(1):269–306.

Rossi, S., Hallett, M., Rossini, P. M., Pascual-Leone, A., of TMS Consensus Group, S., et al. (2009). Safety, ethical considerations, and application guidelines for the use of transcranial magnetic stimulation in clinical practice and research. *Clinical neurophysiology*, 120(12):2008–2039.

Roth, Y., Padberg, F., and Zangen, A. (2007). Transcranial magnetic stimulation of deep brain regions: principles and methods. In *Transcranial brain stimulation for treatment of psychiatric disorders*, volume 23, pages 204–224. Karger Publishers.

Roth, Y. and Zangen, A. (2012). 1 basic principles and methodological aspects of transcranial magnetic stimulation. *Transcranial Brain Stimulation*, page 1.

Roth, Y., Zangen, A., and Hallett, M. (2002). A coil design for transcranial magnetic stimulation of deep brain regions. *Journal of Clinical Neurophysiology*, 19(4):361–370.

Ruiz, M. L., Sarasa, M. R., Rodríguez, L. S., Benito-León, J., Ristol, E. G.-A., and Arce, S. A. (2018). Current evidence on transcranial magnetic stimulation and its potential usefulness in post-stroke neurorehabilitation: Opening new doors to the treatment of cerebrovascular disease. *Neurología (English Edition)*, 33(7):459–472.

Ruiz, M. L., Sospedra, M., Arce, S. A., Tejeiro-Martínez, J., and Benito-León, J. (2020). Current evidence on the potential therapeutic applications of transcranial magnetic stimulation in multiple sclerosis: a systematic review of the literature. *Neurología (English Edition)*.

Rutherford, G. A. (2018). Investigation of repetitive transcranial magnetic stimulation as a treatment for alzheimer's disease: treatment results and coil design considerations.

Santos, N. M. S. (2015). Development of a new, improved deep-brain transcranial magnetic stimulator (tms).

Schizophrenia (2022). World Health Organization. Retrieved November 29, 2022, from `https://www.who.int/news-room/fact-sheets/detail/schizophrenia`.

Schwalb, J. M. and Hamani, C. (2008). The history and future of deep brain stimulation. *Neurotherapeutics*, 5(1):3–13.

Seo, H.-J., Jung, Y.-E., Lim, H. K., Um, Y.-H., Lee, C. U., and Chae, J.-H. (2016). Adjunctive low-frequency repetitive transcranial magnetic stimulation over the right dorsolateral prefrontal cortex in patients with treatment-resistant obsessive-compulsive disorder: a randomized controlled trial. *Clinical Psychopharmacology and Neuroscience*, 14(2):153.

Shin-Etsu (2020). Characteristic properties of silicone rubber compounds. `https://www.shinetsusilicone-global.com/catalog/pdf/rubber_e.pdf`.

Siebner, H. R., Hartwigsen, G., Kassuba, T., and Rothwell, J. C. (2009). How does transcranial magnetic stimulation modify neuronal activity in the brain? implications for studies of cognition. *cortex*, 45(9):1035–1042.

Simões, H., Silva, M. D., Ferreira, C. V., Jesus, L., Oliveira, H., Miranda, P. C., Salvador, R., Crespo, P., and Silvestre, J. (2013). Experimental demonstration of induction by means of a transcranial magnetic stimulator coil immersed in a conducting liquid. In *2013 IEEE 3rd Portuguese Meeting in Bioengineering (ENBENG)*, pages 1–4. IEEE.

Simpson, M. and Macdonell, R. (2015). The use of transcranial magnetic stimulation in diagnosis, prognostication and treatment evaluation in multiple sclerosis. *Multiple sclerosis and related disorders*, 4(5):430–436.

Sironi, V. A. (2011). Origin and evolution of deep brain stimulation. *Frontiers in integrative neuroscience*, 5:42.

Snow, N. J., Wadden, K. P., Chaves, A. R., and Ploughman, M. (2019). Transcranial magnetic stimulation as a potential biomarker in multiple sclerosis: a systematic review with recommendations for future research. *Neural plasticity*, 2019.

Sommer, M., Alfaro, A., Rummel, M., Speck, S., Lang, N., Tings, T., and Paulus,

W. (2006). Half sine, monophasic and biphasic transcranial magnetic stimulation of the human motor cortex. *Clinical neurophysiology*, 117(4):838–844.

Sorkhabi, M. M., Wendt, K., and Denison, T. (2020). Temporally interfering tms: Focal and dynamic stimulation location. In *2020 42nd Annual International Conference of the IEEE Engineering in Medicine & Biology Society (EMBC)*, pages 3537–3543. IEEE.

Sousa, S. C. P. (2014). Otimização de um dispositivo de estimulação magnética transcraniana.

Staff, M. C. (2018). Depression (major depressive disorder). `https://www.mayoclinic.org/diseases-conditions/depression/symptoms-causes/syc-20356007`.

Staff, M. C. (2021). Multiple sclerosis. `https://www.mayoclinic.org/diseases-conditions/multiple-sclerosis/symptoms-causes/syc-20350269`.

Tang, A., Thickbroom, G., and Rodger, J. (2017). Repetitive transcranial magnetic stimulation of the brain: mechanisms from animal and experimental models. *The Neuroscientist*, 23(1):82–94.

Tendler, A., Barnea Ygael, N., Roth, Y., and Zangen, A. (2016). Deep transcranial magnetic stimulation (dtms)–beyond depression. *Expert review of medical devices*, 13(10):987–1000.

Ter Braack, E. M., de Vos, C. C., and van Putten, M. J. (2015). Masking the auditory evoked potential in tms–eeg: a comparison of various methods. *Brain topography*, 28(3):520–528.

Thomson, A. C., Kenis, G., Tielens, S., De Graaf, T. A., Schuhmann, T., Rutten, B. P., and Sack, A. T. (2020). Transcranial magnetic stimulation-induced plasticity mechanisms: Tms-related gene expression and morphology changes in a human neuron-like cell model. *Frontiers in molecular neuroscience*, 13:200.

Tobacco (2021). World Health Organization. `https://www.who.int/news-room/fact-sheets/detail/tobacco`.

Trevizol, A. P., Barros, M. D., Silva, P. O., Osuch, E., Cordeiro, Q., and Shiozawa, P. (2016). Transcranial magnetic stimulation for posttraumatic stress disorder: an updated systematic review and meta-analysis. *Trends in psychiatry and psychotherapy*, 38:50–55.

Tringali, S., Perrot, X., Collet, L., and Moulin, A. (2012). Repetitive transcranial magnetic stimulation (rtms) noise: A relevance for tinnitus treatment? *Brain stimulation*, 5(4):655–656.

Ueno, S., Tashiro, T., and Harada, K. (1988). Localized stimulation of neural tissues in the brain by means of a paired configuration of time-varying magnetic fields. *Journal of Applied Physics*, 64(10):5862–5864.

Valero-Cabré, A., Amengual, J. L., Stengel, C., Pascual-Leone, A., and Coubard, O. A. (2017). Transcranial magnetic stimulation in basic and clinical neuroscience: A comprehensive review of fundamental principles and novel insights. *Neuroscience & Biobehavioral Reviews*, 83:381–404.

Vidal-Dourado, M., Conforto, A. B., Caboclo, L. O. S. F., Scaff, M., Guilhoto, L. M. d. F. F., and Yacubian, E. M. T. (2014). Magnetic fields in noninvasive brain stimulation. *The Neuroscientist*, 20(2):112–121.

Ward, J. (2015). *The student's guide to cognitive neuroscience*. psychology press.

Wassermann, E. M. (1998). Risk and safety of repetitive transcranial magnetic stimulation: report and suggested guidelines from the international workshop on the safety of repetitive transcranial magnetic stimulation, june 5–7, 1996. *Electroencephalography and Clinical Neurophysiology/Evoked Potentials Section*, 108(1):1–16.

Watts, B. V., Landon, B., Groft, A., and Young-Xu, Y. (2012). A sham controlled study of repetitive transcranial magnetic stimulation for posttraumatic stress disorder. *Brain stimulation*, 5(1):38–43.

Wei, X., Li, Y., Yi, G., Lu, M., Wang, J., and Zhang, Z. (2017). The comparison of electric fields distribution applying various coil configurations in deep transcranial magnetic stimulation. In *2017 10th International Congress on Image and Signal Processing, BioMedical Engineering and Informatics (CISP-BMEI)*, pages 1–5. IEEE.

Wei, X., Shi, D., Lu, M., Yi, G., and Wang, J. (2019). Deep transcranial magnetic stimulation: Improved coil design and assessment of the induced fields using realistic head model. In *2019 Chinese Control Conference (CCC)*, pages 3727–3731. IEEE.

Wessel, M. J., Draaisma, L. R., Morishita, T., and Hummel, F. C. (2019). The effects of stimulator, waveform, and current direction on intracortical inhibition and facilitation: a tms comparison study. *Frontiers in neuroscience*, 13:703.

Young, H. D., Freedman, R. A., and Ford, A. L. (2004). *Sears and Zemansky's University Physics: With Modern Physics*. Addison-Wesley.

Yue, W., Wenwei, X., Xiaowei, L., Qing, X., Li, T., and Shuyan, W. (2015). Adjunctive treatment with high frequency repetitive transcranial magnetic stimulation for the behavioral and psychological symptoms of patients with alzheimer's disease: a randomized, double-blind, sham-controlled study. *Shanghai archives of psychiatry*, 27(5):280.

Zaman, R. and W Robbins, T. (2017). Is there potential for repetitive transcranial magnetic stimulation (rtms) as a treatment of ocd? *Psychiatria Danubina*, 29(suppl. 3):672–678.

Zangen, A., Moshe, H., Martinez, D., Barnea-Ygael, N., Vapnik, T., Bystritsky, A., Duffy, W., Toder, D., Casuto, L., Grosz, M. L., et al. (2021). Repetitive transcranial magnetic stimulation for smoking cessation: a pivotal multicenter double-blind randomized controlled trial. *World Psychiatry*, 20(3):397–404.

Zhang, F., Qin, Y., Xie, L., Zheng, C., Huang, X., and Zhang, M. (2019). High-frequency repetitive transcranial magnetic stimulation combined with cognitive training improves cognitive function and cortical metabolic ratios in alzheimer's disease. *Journal of Neural Transmission*, 126(8):1081–1094.

Zhen, J., Qian, Y., Weng, X., Su, W., Zhang, J., Cai, L., Dong, L., An, H., Su, R., Wang, J., et al. (2017). Gamma rhythm low field magnetic stimulation alleviates neuropathologic changes and rescues memory and cognitive impairments in a mouse model of alzheimer's disease. *Alzheimer's & Dementia: Translational Research & Clinical Interventions*, 3(4):487–497.